UNIVERSITY OF SOUTH BOHEMIA IN CESKE BUDEJOVICE
INSTITUTE OF PHYSICAL BIOLOGY

ACADEMY OF SCIENCES OF THE CZECH REPUBLIC
INSTITUTE OF NANOBIOLOGY AND STRUCTURAL BIOLOGY

Ph.D THESIS

Computational Investigations of Biomolecular Systems and Comparison with Experiments in Various Environmental Conditions

Morteza Khabiri

Supervisor: Assoc. Prof. RNDr. Rudiger Ettrich, PhD.
Institute of Nanobiology and Structural Biology of GCRC
Academy of Sciences of the Czech Republic, Nove Hrady

Nove Hrady, Czech Republic, 2011

Prohlášení (Declaration)

Prohlašuji, že svoji disertační práci jsem vypracoval samostatně pouze s použitím pramenů a literatury uvedených v seznamu citované literatury.

Prohlašuji, že v souladu s § 47b zákona č. 111/1998 Sb. v platném znění souhlasím se zveřejněním své disertační práce, a to v nezkrácené podobě elektronickou cestou ve veřejně přístupné části databáze STAG provozované Jihočeskou univerzitou v Českých Budějovicích na jejích internetových stránkách, a to se zachováním mého autorského práva k odevzdanému textu této kvalifikační práce. Souhlasím dále s tím, aby toutéž elektronickou cestou byly v souladu s uvedeným ustanovením zákona č. 111/1998 Sb. zveřejněny posudky školitele a oponentů práce i záznam o průběhu a výsledku obhajoby kvalifikační práce. Rovněž souhlasím s porovnáním textu mé kvalifikační práce s databází kvalifikačních prací Theses.cz provozovanou Národním registrem vysokoškolských kvalifikačních prací a systémem na odhalování plagiátů.

Date:

Morteza Khabiri

List of Publications

1. **Morteza Khabiri*** , Azadeh Nikouee* , Lukasz Cwiklik, Stephan Grissmer , and Rudiger Ettrich. **(2011)** Charybdotoxin Unbinding from the mKv1.3 Potassium Channel: A Combined Computational and Experimental Study. *J. Phys. Chem. B, DOI: 10.1021/jp2061909*

2. Azadeh Nikouee, **Morteza Khabiri**, Rudiger Ettrich and Stephan Grissmer . **(2011)** Peptide toxins prevent inactivation in a mutant K+ channel: implications for the C-type inactivated state. *Journal of General Physiology*, *submitted*

3. Veronika Štěpánková*, **Morteza Khabiri***, Jan Brezovský, Antonín Pavelka, Babak Minofar, Rudiger Ettrich, Radka Chaloupková, Jiří Damborský **(2011)** Molecular mechanisms of haloalkane dehalogenases activation and inhibition by water-miscible organic solvents *Proc. Natl. Acad. Sci. U.S.A. submitted*

4. Tana Koudelakova, Radka Chaloupkova, Jan Brezovsky, Zbynek Prokop, Martina Pavlova, Martin Hessler**, Morteza Khabiri**, Rudiger Ettrich, Uwe T Bornscheuer, Jiri Damborsky **(2011)** Engineering protein resistance to organic co-solvent and elevated temperature by access tunnel modification. *Nature Chemical Biology, submitted*

5. **Morteza Khabiri**, Babak Minofar, Jiri Damborsky, Rudiger Ettrich. **(2011)** Structural and Functional Effects of Organic Solvents on Haloalkane Dehalogenases. *J Mol Model. Submitted*

* Contributed equally.

Letter of declaration

Prohlašuji, že se Morteza Khabiri podílel na společných publikacích přibliženě v níže uvedeném rozsahu.

1. **Morteza Khabiri**, Azadeh Nikouee, Lukasz Cwiklik , Stephan Grissmer , and Rudiger Ettrich. **(2011)** Charybdotoxin Unbinding from the mKv1.3 Potassium Channel: A Combined Computational and Experimental Study. *J. Phys. Chem. B, DOI: 10.1021/jp2061909* ***(40 %)***

2. Azadeh Nikouee, **Morteza Khabiri**, Rudiger Ettrich and Stephan Grissmer . **(2011)** Peptide toxins prevent inactivation in a mutant K+ channel: implications for the C-type inactivated state. J*ournal of General Physiology*, *submitted* ***(40%)***

3. Veronika Štěpánková, **Morteza Khabiri**, Jan Brezovský, Antonín Pavelka, Babak Minofar, Rudiger Ettrich, Radka Chaloupková, Jiří Damborský **(2011)** Molecular mechanisms of haloalkane dehalogenases activation and inhibition by water-miscible organic solvents. *Proc. Natl. Acad. Sci. U.S.A. submitted* ***(25%)***

4. Tana Koudelakova, Radka Chaloupkova, Jan Brezovsky, Zbynek Prokop, Martina Pavlova, Martin Hessler**, Morteza Khabiri**, Rudiger Ettrich, Uwe T Bornscheuer, Jiri Damborsky **(2011)** Engineering protein resistance to organic co-solvent and elevated temperature by access tunnel modification. *Nature Chemical Biology, submitted* ***(5%)***

5. **Morteza Khabiri**, Babak Minofar, Jiri Damborsky, Rudiger Ettrich. **(2011)** Structural and Functional Effects of Organic Solvents on Haloalkane Dehalogenases. *J Mol Model. Submitted* ***(65%)***

doc. RNDr. Rudiger Ettrich, PhD

ACKNOWLEDGEMENTS

-I gratefully thank my supervisor, *assoc. Prof. RNDr. Rudiger Ettrich*, who introduced me to theoretical and computational biophysics. He is not only my scientific supervisor but also my great teacher in my life, from whom I learned how I can manage my life and science together. I appreciate his support to allow me to enter the scientific world, to visit great scientist either in Europe or USA, and also for his support to spent my last year in Prague.
-I gratefully thank *Babak Minofar*, who was my great help in abroad, as he was my scientific advisor, friend and brother.
-I would like to acknowledge *Professor Jannette Carey* for her advice, discussions and all her help regarding to my thesis, research and life. It is my great pleasure to have her met during my Ph.D education.
-I thank *Professor Jiri Damborsky* and *Professor Stephan Grissmer* for their collaboration and advice in the specific projects.
-I wish to thank *Professor Pavel Jungwirth* to accept me in his group for one year to increase my knowledge and also my scientific expertise in his excellent cooperative group.
-I acknowledge *Dr. Martina Roeselová* and *Dr. Lukasz Cwiklik* for their scientific advice and for introducing me into a new world of fatty acids and membranes.
-I wish to express my deep sense of gratitude to all the persons in the Institute of Nanobiology and Structural Biology of GCRC, Nove Hrady, my friends and colleagues for their scientific and moral support: *Dr, Milan Melicherčik*, *Dr. Abdul Samad*, *Dr. Natallia Kulik*, *Vasilina Zayats* and *Žofie Sovová*, *Anamika Mishra*, *Balasubramanian Harish*, *Petr Hamberger* (administrator) and *Daniela Hambergerová* (secretary).
-My profound gratitude also goes to all my friends and colleagues in the Institute of Organic Chemistry and Biochemistry, in the Canon building in Prague and to all people from the Castle: its stuff, students.

And from IRAN, I would like to appreciate and acknowledge all my family, parents, sister and brothers, and my family in law, specifically my sister in law, *Maryam*, who was supporting me during the time even though she had a crisis in that time herself. And also my brother and sister in law, *Ali* and *Hormat* for their constant support. And my close friends, *Mohammad Reza*, *Amir* and *Hassan* to remember me and for their moral support.

Lastly and most importantly, I am deeply grateful to

my love *Azadeh,*

who has provided me with love and scientific support

This thesis dedicated to whom that made me everything i am because they Loved me:

To my Mom and Dad

To my sister, Farzaneh

and

To my Brothers, Farhad and Farzad

Preface

The advantage of computer simulations as a complement to conventional experiments has been widely seen in the possibility for understanding the functional components of biomolecules such as proteins, DNA, RNA, membranes and small solutes that are difficult to address experimentally. However, in order to perform reliable computational studies, a high atomic resolution of the biomolecule structure is a necessary prerequisite. Although the molecular structure determination of membrane proteins in particular is still a generally unsolved problem, a few structures became available during the last decade. In the absence of an experimentally determined crystal structure, homology modeling could provide a rational opportunity to obtain a reasonable 3D model. It is generally recognized that homology modeling of proteins is currently the most accurate method for 3D structure prediction, yielding models suitable for a wide spectrum of applications, such as structure-based molecular design and mechanism investigation. This thesis addresses this problem in two parts.

1- Globular proteins

The main objective of this part is to provide an improved understanding of the behaviour of enzymes, and proteins in general, in nonaqueous media (organic solvents), and by this way extend our fundamental knowledge about the structure and function of enzymes as a whole. The understanding of the functional mechanism of enzymes in nonaqueous media is also particularly important in biotechnological applications where this type of system is employed. In this part structural and functional properties of haloalkane dehalogenases are studied as a globular protein in organic solvents. The aim is to understand the role of the organic solvents on the activity of wild type and mutations of these proteins at a molecular level. The long-term goal of dehalogenase research, and this projects tries to contribute a small part of understanding, is the development of bioremediation by engineering of the solvent medium. A better structural and functional understanding will also be helpful to improve the catalytic efficiency of these enzymes.These proteins are very important to protect the environment, e.g., in bioremediation of areas contaminated by chemical weapons like mustard gas, fuel combustions like oils, etc.

2- Membrane proteins

The second part of the thesis focuses on the human voltage-gated potassium channel Kv1.3. Potassium channels are complex integral membrane proteins with high selectivity for K^+ ions. Human Kv1.3 has been suggested to be an excellent target for potent blockers in the therapeutic management of stroke, epilepsy, and cardiac arrhythmias. In this part the importance of beta-branched residues on the structure and dynamics of the selectivity filter and the pore region is studied and the the effect of point mutations of these on the function, the channel structure, on toxin interactions with the channel, and the mechanism of unbinding of toxins from the channel is explored. Scorpion toxins hereby are powerful inhibitors of ion channels. Moreover, the binding free energy of toxin to the channel was studied in high and low KCl concentrations and confronted with exerimental data.

LIST OF ABBREVIATIONS

Asp (Aspartate), **Asn** (Asparagine), **Trp** (Tryptophan), **His** (Histidin), **Lys** (Lysine), **Thr** (Threonine)
AMBER- Assisted Model Building with Energy Refinement
CHARMM- Chemistry at HARvard Macromolecular Mechanics
ChTX- Charybdotoxin
DMSO- Dimethyl Sulfoxide
GROMACS- (GROningen MAchine for Chemical Simulations)
hKv1.3- human Kv1.3
Imp- improper dihedral
ISPN- isopropanol
IKCa1- Ca^{2}+ activated K^{+} channel
Kv- Voltage gated potassium channel
KTX- Kaliotoxin
MMFF- Merck Molecular Force Field
Lj- Lennard-Jones
LINCS- Linear Constraint Solver Algorithm
mKv1.3- mouse Kv1.3
MgTX- Margatoxin
MD- Molecular Dynamic
MKTOP- Make Topology
NMR- Nuclear Magnetic resonance
nM- nano Molar
OPLS-AA- Optimized Potentials for Liquid Simulations – All Atoms
PEG- Poly Ethylene Glycol
POPC- Palmitoyl oleoyl phosphatidyl choline
PMF- Potential Mean Force
2D-RMSD- 2 Dimensional-Root Mean Square Deviation
RDF- Radial Distribution Function
SPCE- extended simple point-charge
Str- stretch bond
SF- selectivity filter
Tor-torsion angle
THF- Tetra Hydro Furan
VMD- Visual Molecular Dynamics
VS-SFG- Vibrational Sum-Frequency Generation

HLDs- Haloalkane Dehalogenases
YASARA- Yet Another Scientific Artificial Reality Application
WHAM- Weighted Histogram Analysis Method

LIST OF FIGURES

LIST OF TABLES

TABLE OF CONTENTS

Summary

In the last few decades, computer simulation became a potent tool to study experimental systems such as chemical reactions and biological systems in more detail. Developments in computers and computational software increases the computational power every day to study more complex systems including biological molecules and structures like proteins, DNA, enzyme-substrate interactions, cell membranes, etc. In this thesis computational methods were used to study two different types of biological systems. The first study is related to the effect of three different organic solvents (formamide, acetone and isopropanol) on the structure and behavior of three globular proteins. These enzymes belong to the haloalkane dehalogenase family: DhaA, LinB, and DbjA. Moreover, the effect of mutation in the presence of DMSO was also investigated in two variants of DhaA; DhaA57 (L95V+A172V) and DhaA80 (Thr148Leu+Gly171Gln+Ala172Val+Cys176Phe). Previously, experiments had shown that these enzymes are more thermostabile and in some cases show higher activity in organic solvents compared to physiological conditions. Hence, different computational systems were constructed the same as experimental systems. The simulation results showed that except for DhaA80, organic solvents entered the active site and influence its hydration. Except for formamide which is able to penetrate deep to the active site, the organic molecules are trapped by a His residue of the catalytic pentad, and could not go further to the active site. Not only the active site but also the enzyme's hydration shell is influenced by organic molecules. The results showed that the water molecules are stripped out from the enzyme surfaces. It seems that the dual nature of organic molecules makes them favorable to solvate the enzymes. Since they are amphipathic, from one side they are able to interact with the enzyme's hydrophobic surface whereas from the other side they can have hydrophilic interactions with water or other organic molecules. Radial Distribution Function (RDF) of the different parts of each organic molecule reveals that the behavior of each organic solvent in the vicinity of hydrophobic surfaces is similar to their behavior at the air-water interface. Structural analysis of root-mean-square-deviations (RMSD) and B-factors reveals that the flexibility of the enzymes decreased in the presence of most organic solvents, mainly in the CAP domain. Changes of other structural properties like radius of gyration and total solvent accessible surface areas are minimal. DbjA exists as a dimer and is more influenced by organic molecules. They penetrate to the amino acid network between monomers and influence their motion. There is a very good agreement between experimental data and computational analysis.

The second study is the interaction of voltage-gated potassium channel Kv1.3 wild type and its mutants (Kv1.3_V388C, Kv1.3_V388C_H399T) with scorpion toxin (ChTX). Since there is no structure for Kv1.3, 94% sequence identity with Kv1.2 structure was used to make a homology model based on the Kv1.2 structure. The RMSD value of the model structure during MD simulation was stable and this model was used to derive the mutations and for docking of ChTX

to the wild type and mutants. MD structural analyses reveal that mutation of V388C changes the stability of selectivity filter by interrupting the amino acid network interactions behind the selectivity filter. The interaction of ChTX is also affected by the single mutant. ChTX is able to block wild type and double mutant channels but cannot occlude the pore entirely. Breaking the network behind the selectivity filter causes a conformational change that makes ChTX sit slightly higher than in wild type, titled toward one side of the channel. Introducing the second point mutation H399T in the pore region reverts the structural changes back to the wild type. These results are entirely consistent with experimental results. Additionally, the binding energy of ChTX with the wild type mKv1.3 was investigated by the potential of mean force method, in the presence and absence of KCl solution. The results both in experiment and simulation show that, even though the unbinding process and dissociation rate is changing in the present of K^+ ions, the binding energy is independent of K^+ concentration. All together, the combination of computer simulations together with experiments provides new knowledge about channel-toxin interactions which could be helpful for drug design.

Souhrn

Počítačové simulace se během posledních několika let staly výkonným nástrojem, který umožňuje studium systémů jako jsou chemické reakce a děje v biologických systémech detailněji než experiment. Vývoj počítačů a počítačových programů zvyšuje výpočetní kapacitu, což umožňuje studovat komplexnější systémy včetně biologicky významných molekul a struktur jako jsou bílkoviny, DNA, interakce enzymů se substráty, buněčné membrány atd. V předkládané práci se počítačové metody používají na studium dvou rozdílných typů biologických systémů. V prvním případě se jedná o studium vlivu tří organických roztoků (formamidu, acetonu a isopropanolu) na stukturu a chování tří globulárních bílkovin. Tyto enzymy patří do rodiny haloalkán dehalogenáz: DhaA, LinB a DbjA. Dále se zabývám vlivem mutací v přítomnosti DMSO na dva mutanty DhaA; DhaA57 (L95V+A172V) a DhaA80 (Thr148Leu+Gly171Gln+Ala172Val+Cys176Phe). Předchozí experimenty ukázaly, že struktura těchto mutantů je více odolná vůči vysokým teplotám a v některých případech jsou mutanty více aktivní v organických rozpouštědlech než ve fyziologických podmínkách. Proto jsem se snažili našimi simulacemi zopakovat experiment. Výsledky simulací ukázaly, že s výjimkou DhaA80, vstupují organická rozpouštědla do aktivního místa enzymu a ovlivňují jeho hydrataci. Kromě formamidu, který je schopen proniknout hluboko do aktivního místa, jsou organické molekuly zachyceny aminokyselinou histidin katalytické pentády a nemohou postupovat dále do aktivního místa. Organické molekuly ovlivňují nejen aktivní místo enzymu, ale i jeho hydratační obal. Výsledky ukazují, že molekuly vody jsou odpuzovány z povrchu enzymu. Zdá se, že amfipatická povaha organických molekul z nich činní oblíbené solváty zkoumaných enzymů. Protože používané organické molekuly jsou amfipatické, jsou schopny z jedné strany interagovat s hydrofóbním povrchem enzymu a z druhé strany mohou mít hydrofylní interakce s vodou nebo různými organickými molekulami. Radiální distribuční funkce (RDF) rozdíloných částí organické molekuly ukazuje, že chování jednotlivých organických rozpouštědel v blízkosti hydrofóbního povrchu a na rozhraní voda-vzduch je podobné. Strukturní analýza středních kvadratických odchylek (RMSD) a B-faktorů ukazuje, že flexibilita enzymů hlavně v oblasti CAP domény klesá v přítomnosti většiny organických roztoků. Změny ostatních strukturních vlastností jako poloměru rotace a celkového povrchu přístuponému solventu jsou minimální. DbjA se v roztoku vyskytuje jako dimer a je více ovlivněn organickými molekulami. Ty pronikají do oblasti vzájemného kontaktu monomerů a ovlivňují pohyb aminokyselin z této oblasti. Chování systémů modelovaných počítačovými simulacemi je ve velmi dobré shodě s experimentálními daty.

Druhá studie se zabývá interakcemi napěťově řízeného draselného kanálu Kv1.3 ve standardní formě a s mutacemi (Kv1.3_V388C, Kv1.3_V388C_H399T) se štířím toxinem (ChTX). Protože neexistuje krystalová struktura pro Kv1.3, vytvořili jsme její homologní model na základě Kv1.2, se kterým má s Kv1.3 sekvenční identitu 94%. Hodnota RMSD modelu je během molekulárně dynamických (MD) simulací stabilní a tentobyl tento model použit pro modelování mutací a “docking” ChTX ve standardní a mutované formě. MD strukturální analýza ukazuje, že mutace V388C mění stabilitu selektivního filtru přerušením vzájemných interakcí aminokyselin za selektivním filtrem. Přítomnost jedné mutace rovněž ovlivňuje interakci ChTX s kanálem. Toxin částečně blokuje standardní a dvakrát mutovaný pór kanálu. Rozbití sítě vzájemných interakcí za selektivním filtrem způsobuje konformační změnu v jejímž důsledku ChTX sedí trochu výš než u standardního typu a je nakloněn ke straně kanálu. Druhá

bodová mutace H399T v oblasti póru vrátí strukturu na pozici jako ve standardním typu. Tyto výsledky jsou naprosto v souladu s experimentem. Dále se zkoumala vazebná energie ChTX se standardním mKv1.3 pomocí výpočtu potenciálu průměrné síly, buď s přidáním KCl do roztoku nebo bez něj. Výsledky shodně v simulaci i v experimentu ukazují, že přestože se v přítomnosti draselných iontů mění nevazebný proces a disociační konstanta, je vazebná energie nezávislá na koncentraci K^+. Kombinace počítačových simulací s experimenty získává nové informace o interakcích kanálu s toxinem, které mohou být užitečné při navrhování léků.

Chapter 1

Molecular modeling theory and methods

1.1 Computer simulation

Computer simulation is a new tool for resolving scientific problems that complements experiments. One of the goals of computer simulation is to mimic experiments to light up the invisible microscopic details and thus explain the results. In parallel, simulations can be a useful tool to predict experimental results. There are two common methods for simulation of molecular systems, Monte Carlo and molecular dynamics simulation.

The Monte Carlo method is a simple and straightforward technique, based on stochastic approaches that rely on probabilities (Sadus et al., 1999). This method produces large numbers of microstates or configurations of equilibrated systems from one microstate to the next one in a particular statistical ensemble. For every configuration random changes are made together with their orientations and conformations and at the end the quantities are averaged over all produced microstates. Simplicity, flexibility in the choice of sampling, and simulating of different ensembles can be mentioned as major advantages of using Monte Carlo simulation (Allen and Tildesley., 1987).

Molecular dynamics simulations solve the equations of motion based on the force between atoms in an initial configuration in order to find out the next configuration (Allen and Tildesley., 1987). MD computes the movement of atoms in light of the new positions, velocities, and orientations with respect to time. Thus MD produces a series of configurations based on the initial configuration and velocities. Several numerical integration algorithms can be used to calculate the equations of motion. There are two categories of MD simulations: one for non-equilibrium and the other one for equilibrium systems. Most of systems are simulated in the equilibrium state which is defined as an isolated system with a constant volume (V) and fixed number of particles (N). Since the system is isolated, the total energy E is constant. Therefore, by knowing E, V, and N values of an isolated system, we can easily define its thermodynamic properties (Alder and Wainwright et al., 1950).

The advantage of using molecular dynamics compared to Monte Carlo simulation is that molecular dynamics by calculating the ensemble average evaluates different properties and quantities that cannot normally be achieved by the Monte Carlo technique (Haile., 1997). As a

result of this, the whole phase space is probed. Since the molecular dynamics simulation can calculate several properties of biomolecular systems that cannot be evaluated by experiments, it has become important in chemical, biological and biophysical research. In this thesis classical molecular dynamics simulation and the program GROMACS (GROningen MAchine for Chemical Simulations) is used to simulate biomolecular systems (Berendsen et al., 1995).

1.2 Classical molecular dynamics simulation

The molecular dynamics simulation method is based on Newton's second law. In this method it is assumed that every particle in the system behaves like a Newtonian particle and the quantum behavior is completely ignored. This means that electronic motions are not considered and electrons are assumed to remain in their ground state and adjust their dynamics instantly when atomic positions change (the Born-Oppenheimer approximation). Indeed, only classical mechanics are used to describe the motion of the particles. Hence, the equation of motion, **F = ma**, applies on the particles where **F** is the force, **m** is mass and **a** is the particle's acceleration. Once the positions and velocities of each atom are known, the state of the system can be predicted, and new positions and velocities can be calculated. The procedure can be repeated over and over again, and in this way a trajectory of atomic motions is obtained.

As mentioned before, there are several algorithms to solve Newton's equations of motion by integration. The verlet integrator and the leap-frog integrator are two common algorithms that are used by GROMACS software (Rapaport et al., 2004; Allen and Tildesley., 1987; Haile., 1997).

1.3 The verlet and velocity verlet algorithm

The Verlet algorithm (Verlet., 1967) uses positions and accelerations at time t and the positions from time (t-Δt) to calculate new positions at time (t + Δt). The Verlet algorithm uses no explicit velocities. This algorithm is a two-step method because it estimates x (t + Δt) from the current position x(t) and the previous position x(t - Δt). Therefore it is not self-starting: initial positions x (0) and velocities v (0) are not sufficient to begin a calculation, and a backward Euler method must be done at t = 0 to get x (-Δt).

$$x(t + \Delta t) = \frac{1}{2}a\Delta t^2 + V(t)\Delta t + x(t) \qquad (1.1)$$

$$x(t - \Delta t) = \frac{1}{2}a(t)\Delta t^2 - V(t)\Delta t + x(t) \quad (1.2)$$

$$x(t + \Delta t) = a(t)\Delta t^2 - x(t - \Delta t)\Delta t + 2x(t) \quad (1.3)$$

Velocity verlet algorithm (Swope et al., 1982) is the complete form of verlet algorithm. In this algorithm both the atomic positions and velocities are calculated at the same time. Positions and velocities at time t are used to integrate the equations of motion. In other words, positions, velocities and accelerations at time t + Δt are obtained from the same quantities at time t.

$$x(t + \Delta t) = \frac{\Delta t^2}{2m}F(t) + V(t)\Delta t + x(t) \quad (1.4)$$

$$v(t + \Delta t) = \frac{\Delta t}{2m}[F(t) + F(t + \Delta t)] + v(t) \quad (1.5)$$

1.4 Leap-frog algorithm

Similar to verlet algorithm, the leap-frog algorithm is also made from two steps (Gunsteren., 1988). In this algorithm, first the velocities are calculated at time ($t + \frac{1}{2}\Delta t$). By using this velocity as an initial velocity we can calculate the positions, x, at time (x + Δt). In this way, the velocities leap over the positions, and then the positions leap over the velocities.

$$x(t + \Delta t) = v(t + \frac{1}{2}\Delta t)\Delta t + x(t) \quad (1.6)$$

$$v\left(t + \frac{1}{2}\Delta t\right) = v\left(t - \frac{1}{2}\Delta t\right) + a(t)\Delta t \quad (1.7)$$

$$v(t) = \frac{1}{2}[v\left(t - \frac{1}{2}\Delta t\right) + v\left(t + \frac{1}{2}\Delta t\right)] \quad (1.8)$$

1.5 Empirical force field

The crucial step in molecular dynamics simulation is to describe the atomic interactions of a molecular system, called the force field (Ponder et al., 2003). The force field is built in order to cover all relevant molecular interactions that will model the important degrees of freedom. The first step to build a realistic atomistic model is to evaluate the forces. As described above the force $\mathbf{F_i}$ at time t is determined by the gradient of the potential energy **V** with respect to the position coordinates of particle i according to:

$$F_i = -\nabla_i V \quad (1.9)$$

The potential energy **V** can be calculated as bonded (intra-molecular) and non-bonded (inter-molecular) interactions:

$$E(R) = \sum_{bonded} E_i(R) + \sum_{non-bonded} E_i(R) \quad (1.10)$$

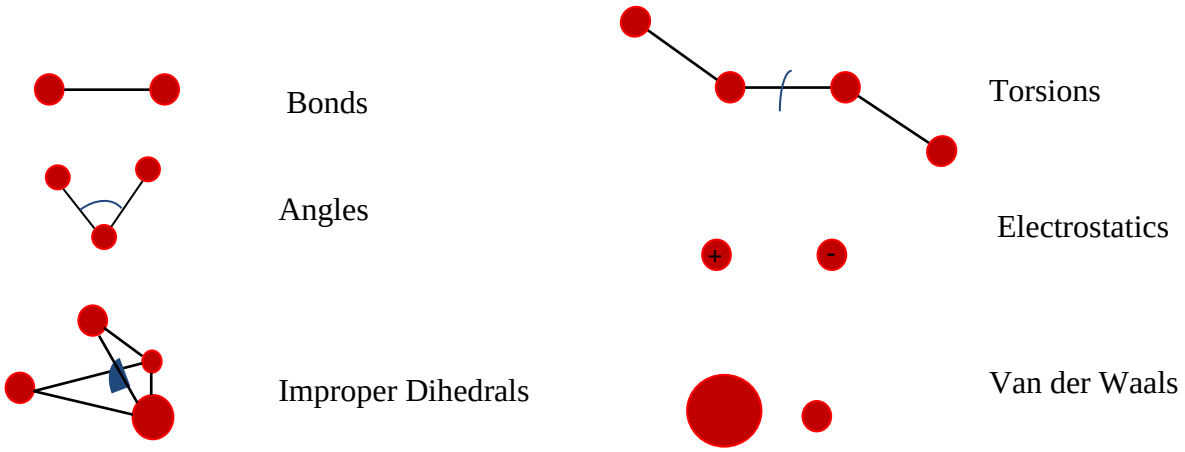

Figure 1.1. Graphic illustrations of energy terms described in the force-field terms.

1.6 Non-bonded interactions

There are two potential functions to be concerned about between non-bonded atoms:

Columbic interactions between electrostatic charges and Lennard-Jones interaction energy that reflects the van der Waals interaction between atoms. In van der Waals interaction, atoms with no net electrostatic charge will still tend to attract each other at short distances or tend to repel each other when they get too close. This potential is defined as:

$$E_{vdw} = \sum_{\substack{nonbonded \\ pairs}} \left(\frac{A_{ik}}{r_{ik}^{12}} - \frac{C_{ik}}{r_{ik}^{6}} \right) \quad (1.11)$$

Where the constants A and C depend on the atom types, and are derived from experimental data.

In electrostatic interactions atom charges are involved in interactions. Opposite atom charges attract and like atom charges repel each other. In this potential, the force of the attraction is inversely proportional to the square of the distance:

$$F = \frac{q_1 q_2}{4\pi\varepsilon_0 r^2} \quad (1.12)$$

1.7 Bonded interactions

There are four types of interaction of bonded atoms: stretching along the bond (E_{str}), bending between bonds (E_b), planar distortion ($E_{improper}$), and torsion (E_t). E_{str} represents the energy required to stretch or compress a covalent bond. A bond can be thought of as a spring having its own equilibrium length, r_o, and the energy required to stretch or compress it can be approximated by Hooke's law for an ideal spring:

$$E_{str} = \frac{1}{2} k_{s,ij} (r_{ij} - r_{ij})^2 \quad (1.13)$$

E_{bend} is the energy required to bend a bond from its equilibrium angle, θ_o. Bending can also be modeled by a spring and the energy is given by Hooke's law with respect to angle:

$$E_{bend} = \frac{1}{2} k_{b,ijk} (q_{ijk} - q_0)^2 \quad (1.14)$$

$E_{improper}$ is the energy required to deform a planar group of atoms from its equilibrium angle, ω_o, usually equal to zero. This system also can be modeled by a spring, and the energy is given by Hooke's law with respect to planar angle:

$$E_{improper} = \frac{1}{2} k_{o,ijkl} (\omega_{ijkl} - \omega_0)^2 \quad (1.15)$$

E_{tor} is the energy needed to rotate around the bonds. Torsional interactions are modeled by the potential:

$$E_{tor} = \sum_{1.4\ pairs} K_{\emptyset} \ (1 - \cos(n\emptyset)) \quad (1.16)$$

Most of the force field parameters are taken from experimental data on small molecules and others are taken from theoretical calculations. In general, reference bond lengths and angles are taken from crystallographic data for small molecules. Bonds, angles and improper dihedral force constants that model the molecular vibrations are obtained from spectroscopic data on small molecules. Dihedral parameters are usually derived from quantum chemical calculations of torsional angle rotational profiles. Partial atomic charges are also obtained from quantum chemical calculations. Parameters for the Lennard-Jones function are usually derived from knowledge of diffusion, viscosity and heats of vaporization of small molecules in the condensed phase and refined by molecular dynamics simulations. All these parameters have to be derived for all atom types involved in bonded and non-bonded interactions typically present in a bimolecular system. There are several reliable force fields developed for simulation of macromolecules. Currently, force fields widely used for bimolecular simulations are: Chemistry at HARvard Macromolecular Mechanics (CHARMM), Assisted

Model Building with Energy Refinement (AMBER), Optimized Potentials for Liquid Simulations (OPLS-AA), and Merck Molecular Force Field (MMFF).

1.8 Reference

- Allen M.P. and Tildesley D.J. (1987) Computer Simulation of Liquids, Clarendon, Oxford
- Alder B. J. and Wainwright T. E. (1957) Phase Transition for a Hard Sphere System. J. Chem. Phys. 27:1208-1209
- Alder B.J.; Wainwright T.E. (1959) Studies in Molecular Dynamics. I. General Method. J. Chem. Phys. 31(2): 459-466
- Berendsen H.J.C, Vander Spoel D, et al. (1995) GROMACS: A message passing parallel molecular dynamics implementation. Comp.phys.Comm. 91:43-56
- Haile J.M., (1997) Molecular Dynamics Simulation. Wiley-Interscience, 1 edition,
- Ponder J.W. and Case D.A. (2003) Force fields for protein simulations. Adv. Prot. Chem. 66:27-85
- New York, N.Y
- Rapaport D. C., (2004) The art of molecular dynamics simulation, Cambridge University Press, Cambridge
- Sadus R.J. (1999) Molecular Simulation of Fluids. Applications to Physical Systems. Second Edition, Elsevier, Amsterdam
- Swope W.C., Andersen H.C., Berens P.H., Wilson K.R. (1982) A computer-simulation method for the calculation of equilibrium-constants for the formation of physical clusters of molecules: Application to small water clusters. J. Chem. Phys. 76:637–649
- Verlet L. (1967) Computer experiments on classical fluids. I. Thermodynamical properties of Lennard-Jones molecules. Phys. Rev. 159:98–103
- van Gunsteren W.F., Berendsen H.J.C. (1988) A leap-frog algorithm for stochastic dynamics. Mol. Sim. 1:173–185

Part I

Haloalkane Dehalogenases and Organic Solvents

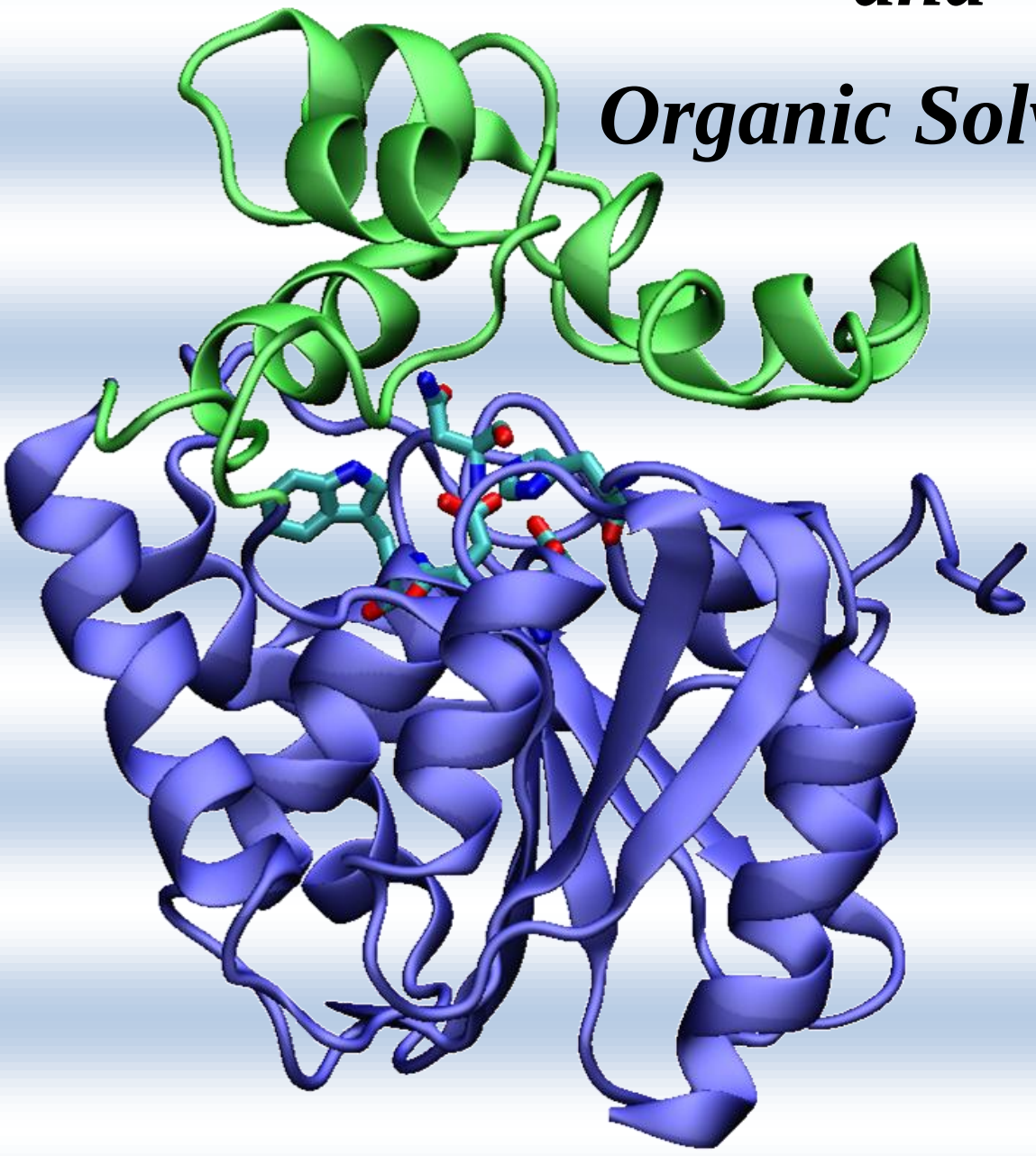

Chapter 2

Effect of organic solvents on haloalkane dehalogenases

2.1 Introduction

Life originated in water and could not exist in its absence. The importance of water's exclusive physical properties and of its distinctive solvent power particularly for ions discussed regularly; however, the importance of its unique lack of solvent power for many nonpolar substances has less attention (Ruth et al., 2010; Ben-Naim et al 1980). Molecules soluble in organic solvents but not in water, and dual nature molecules with one part soluble in water and another part expelled from water are important in biology. Molecules in the latter category were called amphipathic because they contain one part that has sympathy and another that has antipathy for water (Tanford 1980). Because of their special properties, they are forced to accept unique orientations with respect to the aqueous medium and to form properly organized structures. Nonpolar organic solvents such as tetrachlorocarbon (CCl_4) are close to hydrocarbons in their solvent properties. However, organic solvents that contain polar will have some structural organization and may prevent the interruption of nonpolar solute molecules.

2.1.2 Medium engineering

During the last decade, enzymatic catalysis under non-aqueous conditions has become a new important field in enzymology, and up to now many of the factors influencing catalysis in non-aqueous solvents (mostly organic solvents) are known (Bell et al., 1995; Halling, 2000; Klibanov, 2001). In an organic reaction, medium enzymes show several remarkable properties such as stereo specificities, enhanced stability (thermal) and different substrate (klibanova., 2001). In addition to their practical importance, these new reaction circumstances offer the possibility to study several mechanistic aspects of enzyme catalysis in more detail, like the role of solvation shell surrounding the enzyme. In organic solvents, the enzyme is not completely hydrated. Based on studies with enzyme powders with different humidities, less hydrated enzymes are expected to be more rigid. A decreased intramolecular motion of enzymes in non-aqueous organic solvents is used to explain increased thermal stability and the protection of conformations induced by high concentrations of ligands in aqueous solution. Moreover, the lower activity of enzymes in non-aqueous media might be also the result of the rigidity (Bross et al., 1995).

2.1.3 Water-miscible organic solvents

The solubility of poorly water-soluble substrates will increase by adding organic solvents to the medium. The enzyme does not dissolve in the organic solvent. Organic solvents shift the thermodynamic reaction equilibrium to favor catalysis, either by altering the partitioning of the substrate/product between the phases of interest, or by reducing the water activity (Goto et al., 1994). The last one can be reached by adding water-miscible organic solvents to the reaction mixture. Several studies show that using low-boiling organic solvents can make recovery of the products and enzymes from the reaction mixture easier. Using organic solvents in biocatalysis also has some disadvantages, e.g. the organic solvent may denature or inhibit the biocatalyst (Vermue and Tramer., 1995).

Four categories of organic solvent for biocatalysis can be distinguished (Figure 2.1.1). (A) The water/organic-solvent solution may consist mainly of water with a relatively small amount of a water-miscible solvent. (B) The solution with two-phase system of a water-immiscible organic solvent and an aqueous buffer. (C) The micro-aqueous organic-solvent mixture, which dry biocatalyst, is suspended in an organic solvent. In this case, the water is located mostly on the solid enzyme particles. (D) Reversed micelles, which consist of tiny droplets of aqueous medium (radii in the range of 1-50 nm) and stabilized by surfactant in a bulk of water immiscible organic solvent (Carrea., 2000).

The addition of water-miscible solvents like acetone, isopropanol, formamide, DMSO, ethanol, acetonitrile or dioxane has often used to increase the solubility of apolar reactants. Usually, addition of small amounts of a water-miscible solvent has little effect on the enzyme activity and stability. In some cases, small concentrations of these solvents show an enhanced enzyme activity and stability (Butler., 1979; Guargliardi et al., 1989; Vazquez-Duhalt et al., 1993). However, most water-miscible solvents have an inhibitory effect on the enzyme reaction in high concentration (O'Daly et al., 1990; Freeman and Lilly., 1987; Fernandez et al., 1991; Vazquez-Duhalt et al., 1993; Granot et al., 1988; Chatterjee and Russell., 1992). In reactions where hydrophobic interactions are involved in the complex formation between enzyme and substrate, decreasing of the enzyme activity at a high concentration of water-miscible organic solvent is mainly attributable to changes in the affinity of the enzyme for the substrate (Maurel., 1978).

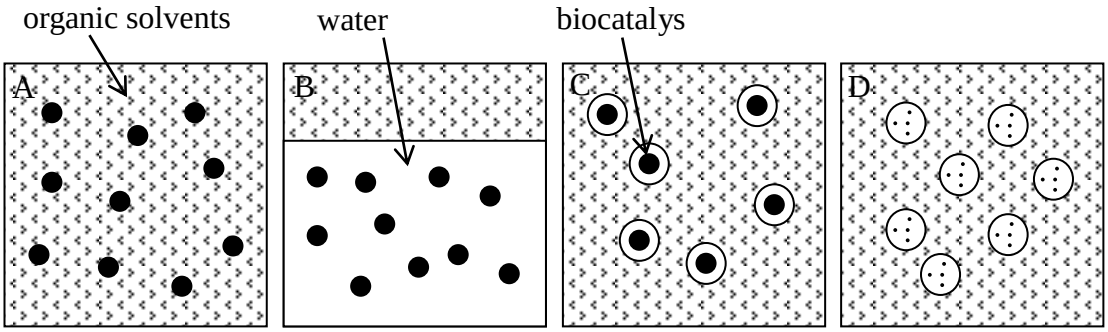

Figure 2.1.1. Representations of various organic solvent systems. Organic solvent system (A), Two phase system of a water-immiscible organic solvent (B), Micro aqueous organic-solvent mixtures (C), Reversed micelles (D). Black point resemble as biocatalyst.

2.1.4 Haloalkane dehalogenases

2.1.4.1 Biological function

Haloalkane dehalogenases are microbial enzymes that cleave a carbon-halogen bond in halogenated alkanes, cycloalkanes, alkenes, selected ethers, and alcohols (Damborsky et al., 2001). These enzymes act by a hydrolytic mechanism involving use of a water molecule as the only co-substrate (Janssen., 2004; Damborsky and kocka., 1999). The enzymes can be used for the protection of the environment, e.g., in bioremediation of contaminated areas, in removal of intermediates of chemical syntheses, and in biosensors (Prokop et al., 2006; Damborsky et al., 2001; Janssen., 2004; Campbell et al., 2006; Pieters et al., 2001). However, since haloalkane dehalogenases show low or no activity toward some significant industrially substrates, they are also objects for protein engineering studies to expand their applications. According to substrate specificity, three different groups of haloalkane dehalogenases can be distinguished: DhaA from Rhodococcus rhodochrous NCIMB 13064 (Newman et al., 1999), LinB from Sphingomonas paucimobilis UT26 (Marek et al., 2000), DbjA from Bradyrhizobium japonicum USDA110 (Sato et al., 2005).

2.1.4.2 General structure

Haloalkane dehalogenases structurally belong to the alpha-beta hydrolase superfamily (Ollis et al., 1992). The core of each enzyme is similar and consists of two different domains: the alpha-beta-fold (main) domain, which is conserved in all alpha-beta-hydrolases, and the so-called cap domain (Figure 2.1.2B). The main domain is composed of a B-sheet made up of eight B-strands surrounded by six alpha helices. The cap domain is composed of an additional five alpha-beta-helices connected by loops. There are two linkers, which connect the CAP domain to the main domain. These two linkers are

located between β6-α4 and α8-α9. The active site is located between these two domains in an internal, predominantly hydrophobic cavity and can be reached from the solvent through a tunnel (Ollis et al., 1992; Chovancova et al., 2007; Janssen et al., 2004). The substrate specificities for the classes of haloalkane dehalogenases are mainly due to differences in the geometry and the composition of the active site and the entrance tunnel connecting the active site to the protein surface (Tejo et al., 2004). The tunnel in LinB, DhaA and DbjA is U shaped and it is considerably wide. The size of the tunnel opening corresponds well with the preference of enzymes for larger substrates, with optimum activity reached with halogenated compounds containing five, six, or seven carbon atoms (Damborský and Koca., 1999; Sato et al., 2005). The power of haloalkane dehalogenases to decontaminate organic halide environmental pollutants in nature makes them interesting targets for engineering of the solvent

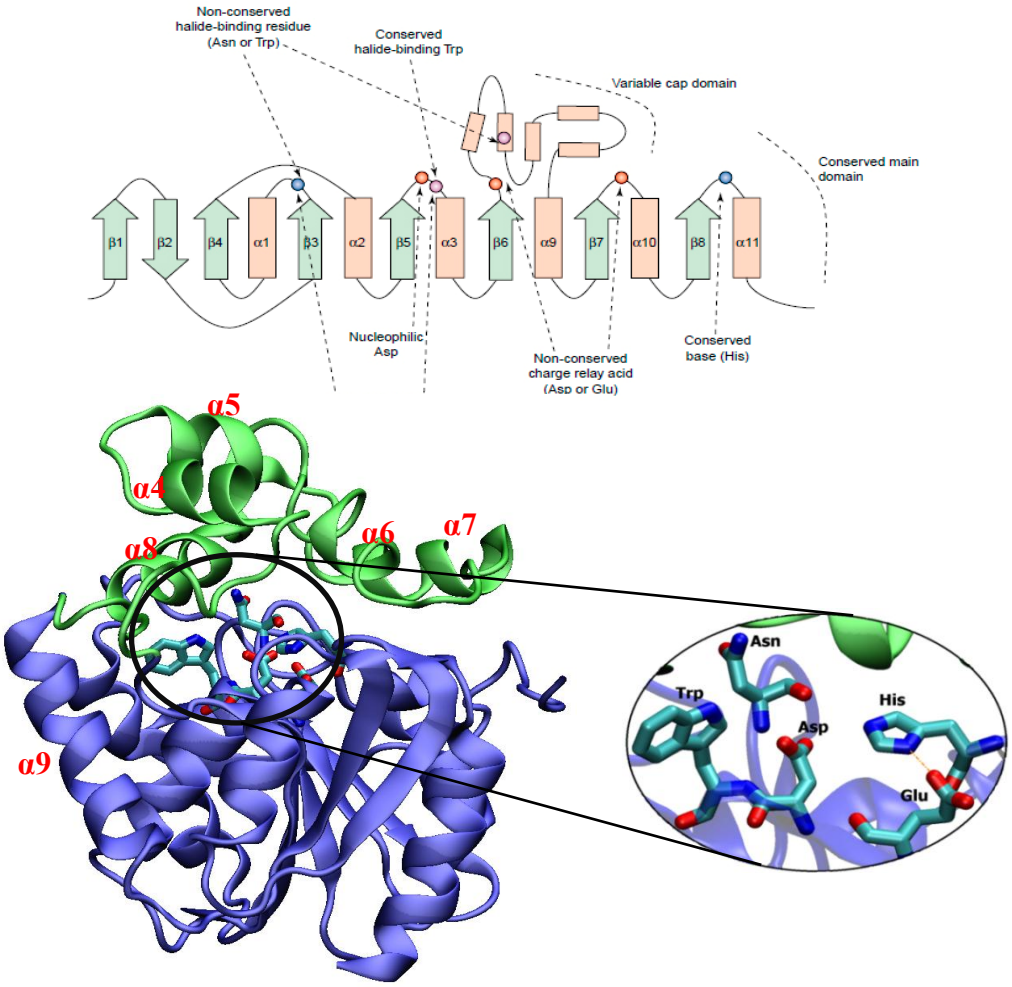

Figure 2.1.2. Secondary structure (from Janssen et al., 2004) (A), and 3-D structure of haloalkane dehalogenases (B). The active site, which consists of catalytic pentad residues (black circle), is located between Core (blue) and Cap (green) domain. medium to improve catalytic efficiency (Kaur et al., 2006).

2.1.4.3 Active site structure

In all these three haloalkane dehalogenases, the active site is located between the cap domain and main domain. The size of the active site is 246 $Å^3$ for DhaA, 264 $Å^3$ for DbjA and 276 $Å^3$ for LinB (Sato et al., 2005; Damborský and Koca., 1999). The active site is highly conserved among haloalkane dehalogenases family. It is formed mainly by five catalytic residues: Aspartic acid (nucleophile), Histidine (base), Glutamic acid (catalytic acid), Asparagine and Tryptophan (halide-stabilizing residues). The nucleophile is always located after strand β5, the base is always after strand β8, and the catalytic acid is after strand β6 (Chovancova et al., 2007).

2.1.4.4 Reaction mechanism

The overall reaction is a two-step S_N2 reaction. The amide groups of the Trp and Asn side chains hold the halogen group of the halogenated substrate. Oxygen from the nucleophile carboxylic acid (Asp) attacks the carbon of the halogen-carbon bond. This leads to a covalently bound ester intermediate, which is stabilized in the oxyanion hole (Figure 1) (Damborský and Koča., 1999). In the following nucleophilic addition, a histidine-activated water molecule acting as the catalytic base hydrolyzes the alkyl-enzyme intermediate. The positive charge that develops on histidine during hydrolysis is stabilized by glutamic acid. In the last step, elimination, the ester bond is cleaved and the three reaction products are released: a proton, the halide, and the corresponding alcohol.

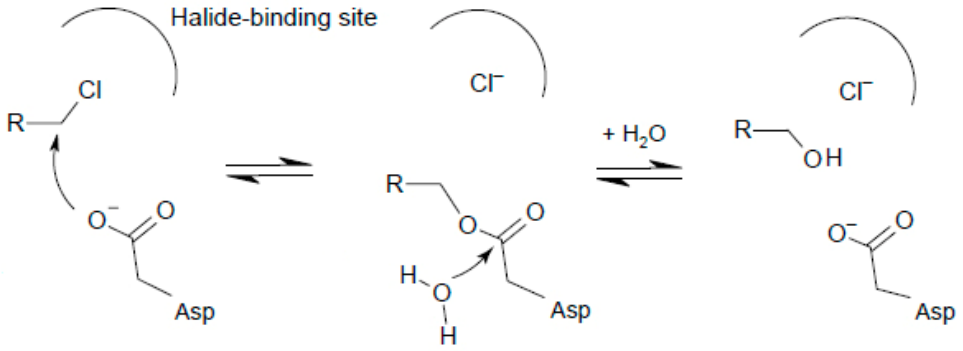

Figure 2.1.3. Schematic view of S_N2 reaction that takes place in the haloalkane dehalogenase active site (from de Jong and Dijkstra., 2003).

2.1.4.5 Properties of selected haloalkane dehalogenases

In this study, three haloalkane dehalogenases, DhaA from Rhodococcus rhodochrous NCIMB13064, LinB from Sphingomonas paucimobilis UT26 and DbjA from Bradyrhizobium japonicum USDA110,

were chosen for investigation that is more detailed. DhaA and LinB are strictly monomeric in solution whereas DbjA can occur in oligomeric form (Figure 2.1.4). DhaA (UniProtKB: P59336) and LinB (UniProtKB: P51698) have 48% sequence identity; DbjA (UniProtKB: P59337) has 39% sequence identity to LinB, and 50% identity to DhaA. A sequence comparison between DbjA and other haloalkane dehalogenases revealed that DbjA contains extra residues that prolong alpha-helix 4 of the cap domain and extend the loop between β-6 and α-4 (Sato et al., 2005). The volume of the active site cavity and the opening tunnel is wider than in LinB and DhaA (Damborsky and koca., 1999; Sato et al., 2005). Despite these differences, the position of the catalytic residues (Asp103, His280, Glu127) and halide-binding residues (Trp104, Asn38) (Sato et al., 2005) correspond to those of DhaA (Asp117, His283, Glu141, Trp107, Asn41) (Poelarends et al., 2000) and LinB (Asp108, His272, Glu132, Trp109, Asn38) (Nagata et al., 1999).

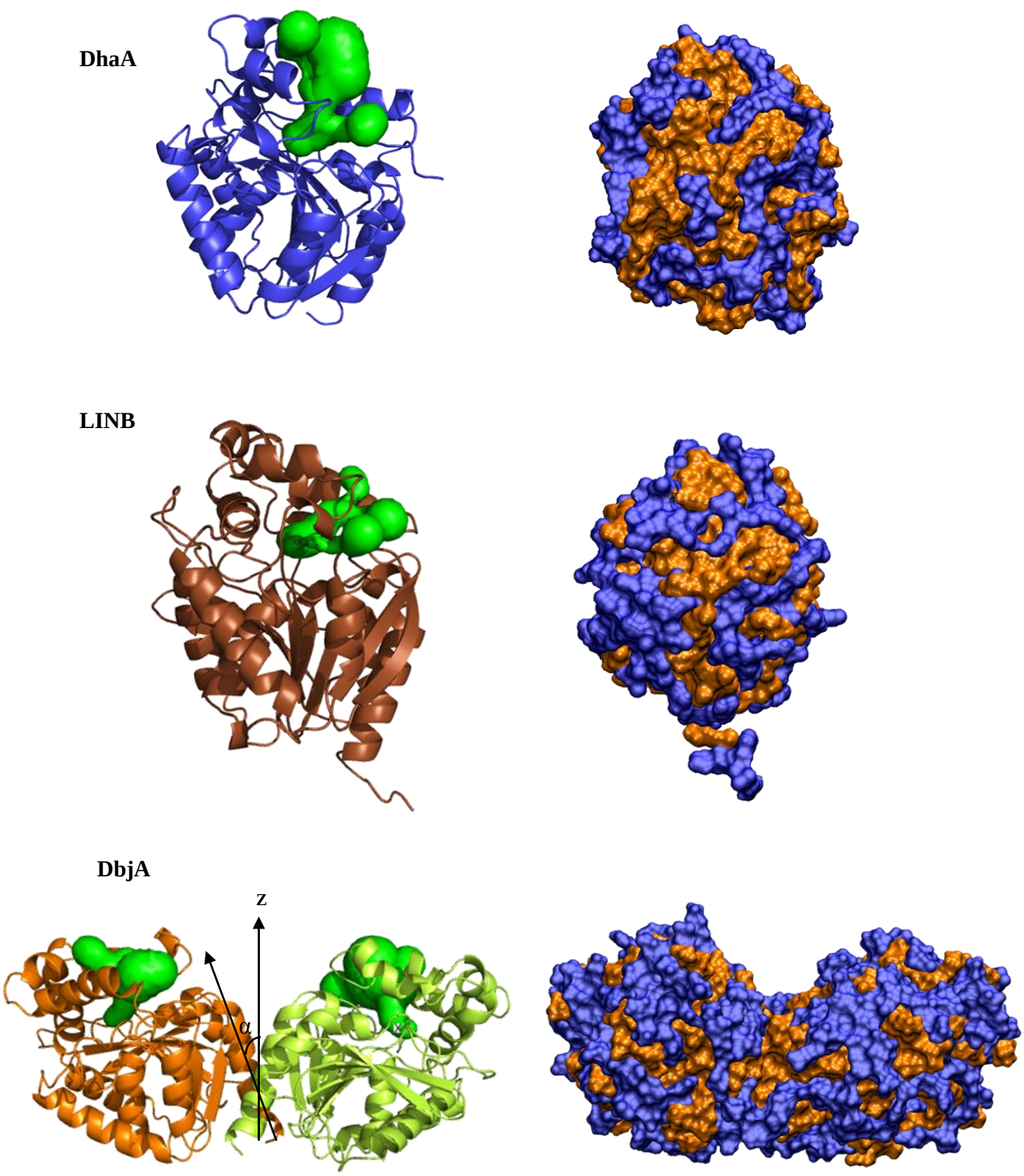

Figure 2.1.4. 3-D structures of DhaA, LinB, and DbjA. In each enzyme, the tunnel surface is shown in green. In DbjA the angle of contact between the helix axis of each monomer and the z axis is defined as α (left). The hydrophobic (brown) and hydrophilic (blue) surfaces of each enzyme are shown.

2.1.4.6 Aim of the present work

The effects of various concentrations of 14 water-miscible organic solvents on activity of three haloalkane dehalogenases DbjA, DhaA, and LinB were investigated at *Doc. Mgr. Jirí Damborský* group in *Loschmidt Laboratories, Masaryk University in BRNO,* by *Veronika Štepánková, PhD student*. They have been shown that although all three enzymes belong to the same family of enzymes they exhibited different solvent-resistance. Catalytic efficiency of DbjA was well preserved in most tested solvents up to a concentration of 20% (v/v). Furthermore, this enzyme was activated up to twofold by glycerol 30% (v/v), PEG1000 30% (v/v), ethylene glycol 30% (v/v), DMF 10% (v/v), methanol 20% (v/v), 1,4-dioxane 10% (v/v), acetone 10% (v/v), isopropanol 10% (v/v) and THF 5% (v/v). The only solvent negatively influencing DbjA activity at all tested concentrations was formamide. On the contrary, the activities of the other two tested enzymes DhaA and LinB sharply decreased with increasing solvent concentration. LinB was inactivated by the majority of tested solvents even at low concentrations (less than 10% v/v). The most rapid inhibition of LinB was detected in the presence of 1,4-dioxane. Similar behavior was observed for DhaA; however this enzyme exhibited also activation (1.3 fold) in the presence of formamide 5% (v/v) and methanol 5% (v/v).

Although the experiments clearly show the different behaviors of these enzymes, it is difficult to interpret the effects of these solvents at the molecular level. For this reason, molecular dynamics simulations were conducted to complement this weakness, focusing on those solvents showing significantly altered activities of the enzymes even at low and non-denaturing concentrations. Hence, formamide 5%, isopropanol 10%, and acetone 20% were chosen for study by molecular dynamics simulations. In addition, the effect of mutation on haloalkane dehalogenases DhaA structure and activity was investigated by *Tana Koudelakova, PhD student,* at the same laboratory. She made different mutations in the tunnel and CAP domain of DhaA and observed the effect of DMSO in the presence of these mutations. Corresponding to these experiments the effect of DMSO 40% also was investigated by molecular dynamics simulation.

Therefore, to put it briefly, the main goal of this part of the thesis is to make a detailed analysis of the molecular interactions on the protein surface, the behaviors of organic solvents near the protein surface and the effects of selected organic solvents on protein structure and dynamics.

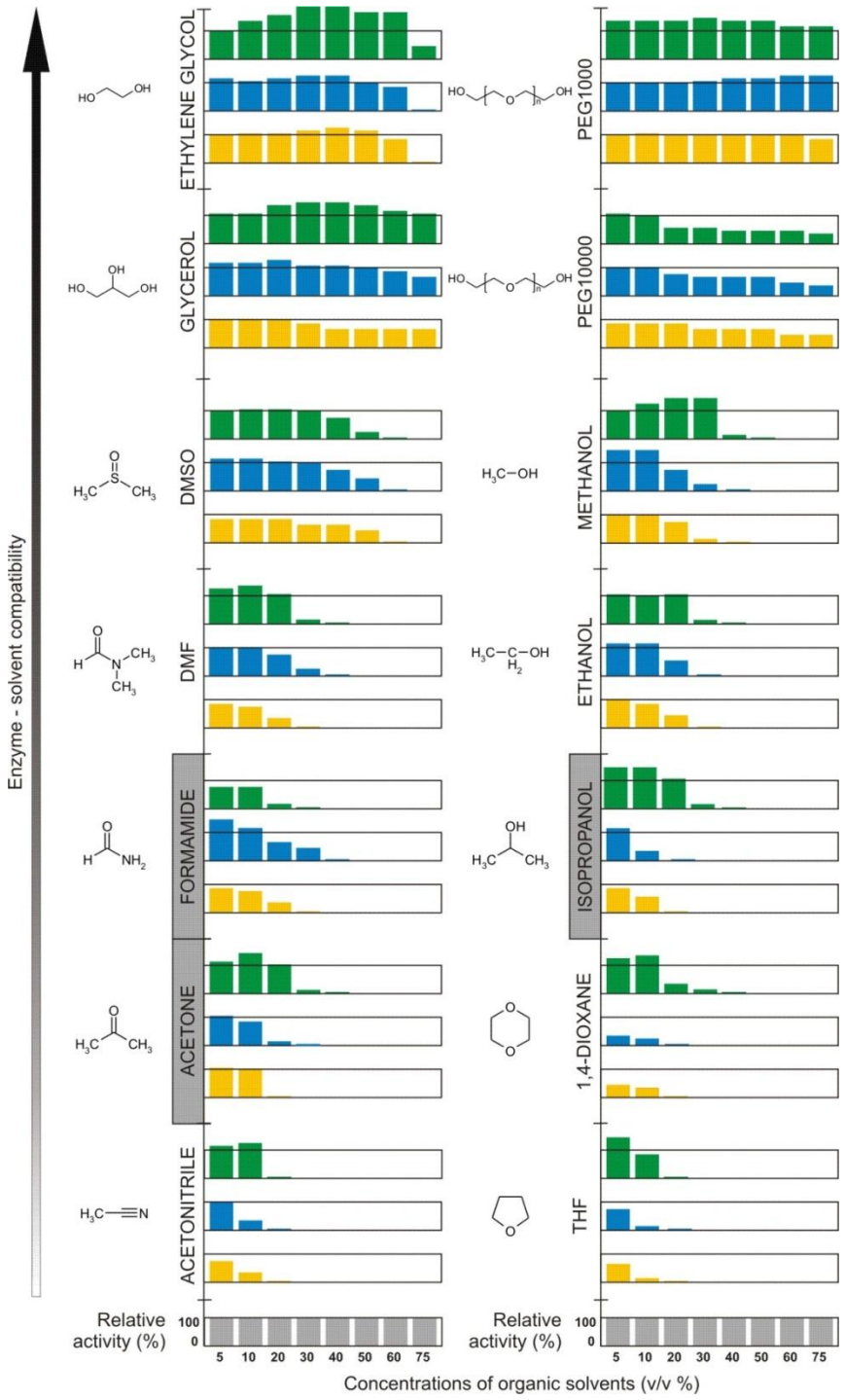

Figure 2.1.5. The relative activities of DbjA (green), DhaA (blue) and LinB (yellow) in the presence of 14 different organic solvents. The activities are expressed as the percentage of specific activity in glycine buffer (Stepankova et al., 2011).

Chapter 2.2

Material and method

2.2.1 Preparation of solutions

To prepare the solution first we need to build formamide, acetone, isopropanol and DMSO molecules. These molecules were built in Molden 4.8 software. The optimized structure and the partial charges of the organic molecules were calculated by Gaussian 03 package employing the Hartree-Fock method and 6-31G* basis set (Frisch et al., 2004). The geometries of organic molecules were optimized at the mp2/6-31G level. MKTOP Program (Ribeiro et al., 2008) was used to make the topology parameters for all organic molecules from the OPLSAA force field (Kalju et al., 2002; William et al., 1996; Yurii et al., 1995) (Figure2.2.1). The box of solvent with size x = 30, y = 30 and z = 30 Å was constructed by repeating the molecules in xyz dimensions. After 10 ns equilibration, the original box size was increased in xyz dimensions. Following that the box of the organic liquids were filled by SPC/E water molecules. After filling the box the number of water and organic molecules were balanced (Table 2.2.1) until reaching formamide 5%(v/v), acetone 20 %(v/v), isopropanol (ISPN) 10%(v/v) and DMSO 40%. These baths of organic solvent solutions were run for 20 ns until reaching proper density.

	Water	**Formamide 5%**	**Isopropanol 10%**	**Acetone 20%**	**NA^+**
DhaA	*12333*	*9834:241*	*9100:256*	*13645:823*	*18*
LinB	*12417*	*10982:274*	*10129:270*	*10492:632*	*11*
DbjA	*24447*	*27896:698*	*19210:512*	*18143:1092*	*14*

Table 2.2.1. The number of water molecule in pure water bath solution and the ratio of organic solvent to water molecules that were used to build solutions of formamide 5%, isopropanol 10%, and acetone 20%.

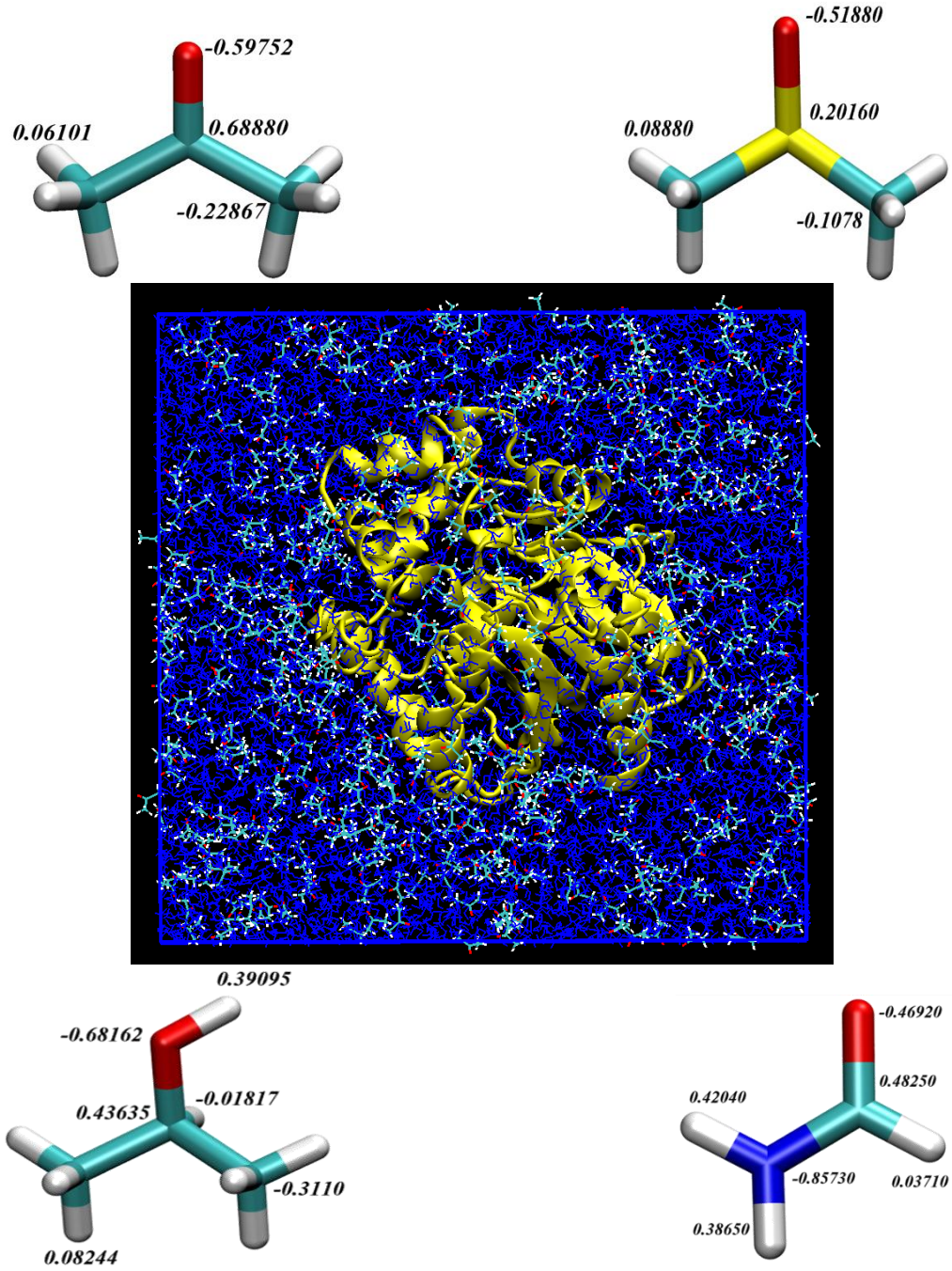

Figure 2.2.1. The geometry of formamide, isopropanol, DMSO, and acetone. The partial charges of each atom were calculated by ab initio methods. The middle figure shows DhaA solvation in acetone as an example of haloalkane dehalogenase solvations in organic solvent.

2.2.2 Preparation of protein structures

2.2.2.1 Wild type

The protein crystal structures DhaA (1CQW) (Newman et al., 1999), DbjA (3A2M) (Prokop et al., 2010) and LinB (1MJ5) (Oakley et al., 2004) were used in molecular dynamics simulations. In order to have the same structure as used in the experiments (DhaA from Rhodococcus rhodochrous NCIMB13064), three substitutions were made in the crystal structure of 1CQW: V172A, I209L and G292A. In the simulations the crystallographic water molecules were kept. Based on the pH memory phenomenon (Klibanov et al., 2001) the ionization state of the protonatable residues of all three enzymes was taken to be the same as that observed in water. Before starting the simulation, the crystal structures were energy-minimized in vacuum using the steepest-descent algorithm for at least 1000 steps.

2.2.2.2 Mutants

The wild-type structure DhaA with the PDB-ID 1CQW (Newman et al., 1999) was used as the starting structure for the simulations. DhaA57 (Leu95Val+Ala172Val) and DhaA80 (Thr148Leu+Gly171Gln+Ala172Val+Cys176Phe) models were prepared by Yasara molecular modeling software (Krieger et al., 2002 and 2004).

2.2.3 Molecular dynamics simulation

The minimized crystal structures were immersed in preequilibrated, extended simple point-charge (SPCE) water (Berendsen et al., 1981) with formamide 5%, ISPN 10%, acetone 20% or DMSO 40% in a rectangular box with a minimum distance of 1.5 nm between the protein and box edges. Sodium counterions were added by replacing water molecules to provide a neutral simulation box. All atoms were given an initial velocity obtained from a Maxwellian distribution at the desired initial temperature. In all the simulations, the proteins were restrained for 2ns equilibration with a force constant of 1000 kJ/mol/nm^2. During a 2 ns MD run the water and organic solvents were allowed to relax until the solvents get optimized around the protein. After the equilibration, the position restraints on the protein were removed and the system was gradually heated from 290 K to 300 K during 50 ps of simulation. All simulations were performed for 35ns. All MD runs and analysis of the trajectories were performed by using the GROMACS 3.3.3 software package (Berendsen et al., 1995; Lindahl et al., 2001), with an extended All Atom Optimized Potentials for Liquid Simulation (OPLSAA) force field

(Jorgensen et al., 1996). The simulations were made in the isothermal isobaric ensemble (NPT). For all calculations, temperature was maintained by coupling temperature and pressure baths using the Berendsen method (Berendsen et al., 1984) at 300 K and pressure at 1 bar by weak coupling to a bath using relaxation times of 0.1 ps. The pressure was maintained with a compressibility of 4.6×10^{-5}/bar. Lennard-Jones interactions are cut off at 10.0 A. Long-range electrostatic contributions are calculated using the particle-mesh Ewald (PME) method (Essman et al., 1995) with a direct interaction cutoff of 10.0 Å. A time step of 0.002ps was employed. The length of all covalent bonds was constrained by the linear constraint solver (LINCS) algorithm (Hess et al., 1997). The simulations were run with periodic boundary conditions. Molecular graphics images were produced by using VMD (Humphary et al., 1996) and PyMOL (Delano et al., 2002). The graphs were prepared with xmgrace software. (http://plasma-gate.weizmann.ac.il/Grace/).

Chapter 2.3

Results and Discussion

2.3.1 Structural stability of haloalkane dehalogenases in organic solvents

Enzyme structure and flexibility are important determinants of catalytic activity. Therefore, the effect of different solvent media (formamide, isopropanol, acetone) on the structure and flexibility of DhaA, LinB and DBjA were studied. Simulations were initiated using the crystal structure of these enzymes, which relaxed during the simulations. All simulations were run for 35 ns and the last 5 ns were chosen as an equilibrium part of the trajectory for analysis. Differences in the average structures in different media are quantified by calculating root mean square displacement (RMSD) between them (Table 2.3.3). The RMSD values show that the deviations from their initial structure in all cases are relatively small, less than 1.7 Å, indicating that the structures are stable along the simulation over a timescale of several nanoseconds. The 2D-RMSD plot, showing the root mean square deviation of every conformation in last 5ns to all other conformations in this time, demonstrates that each enzyme has a different reaction to each organic solvent. Figure 2.3.1 shows the 2D-RMSD calculated for DhaA in water (A), formamide (B), acetone (C) and isopropanol (D). The conformational space sampled by DhaA in the simulations in formamide is less than water and two other organic solvents. There are very few red points that show different structural changes at 30ns from the initial structure. By comparison, the 2D-RMSD map of LinB in different organic solvents with water shows that the enzyme structure is more stable in formamide and isopropanol, with larger effect in isopropanol. The enzyme structural change in most areas of the map is less than 0.7nm (Figure 2.3.2). In the case of DbjA, the 2D-RMSD map reveals that the enzyme structure is very stable in all solvents. In all of them, the deviation is less than 0.7nm. Among all these organic solvents, isopropanol has the strongest effect on DbjA structure. There are no red points in the 2D-RMSD map. Green points cover most of the area, which indicates that deviation of enzyme in this organic solvent is less than 0.4 nm. (Figure 2.3.3).

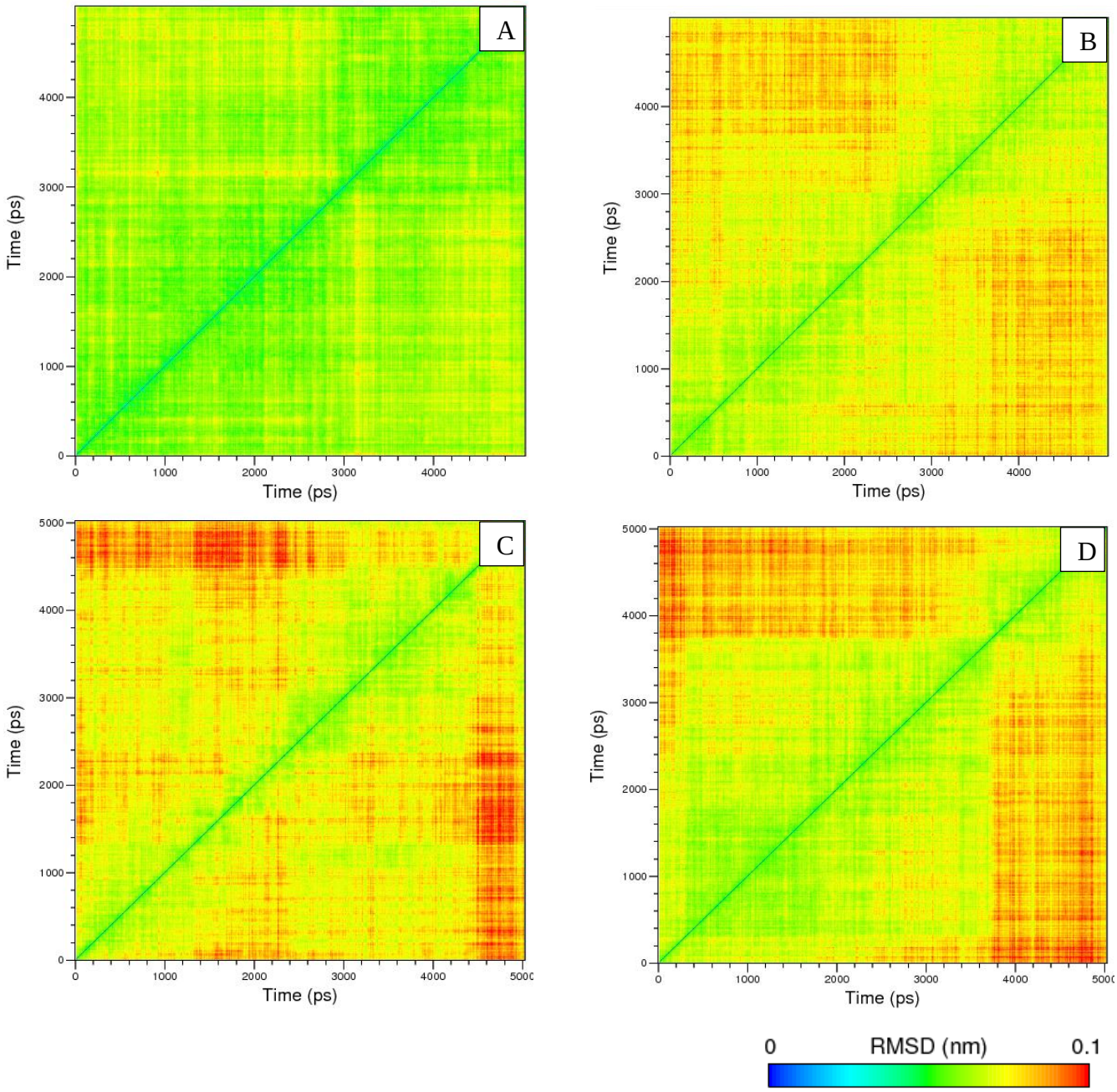

Figure 2.3.1. 2D-RMSD (Cα) plot for DhaA in water (A), formamide (B), acetone (C) and isopropanol (D) calculated from the last 5ns of the equilibrated part of the 35ns MD trajectory.

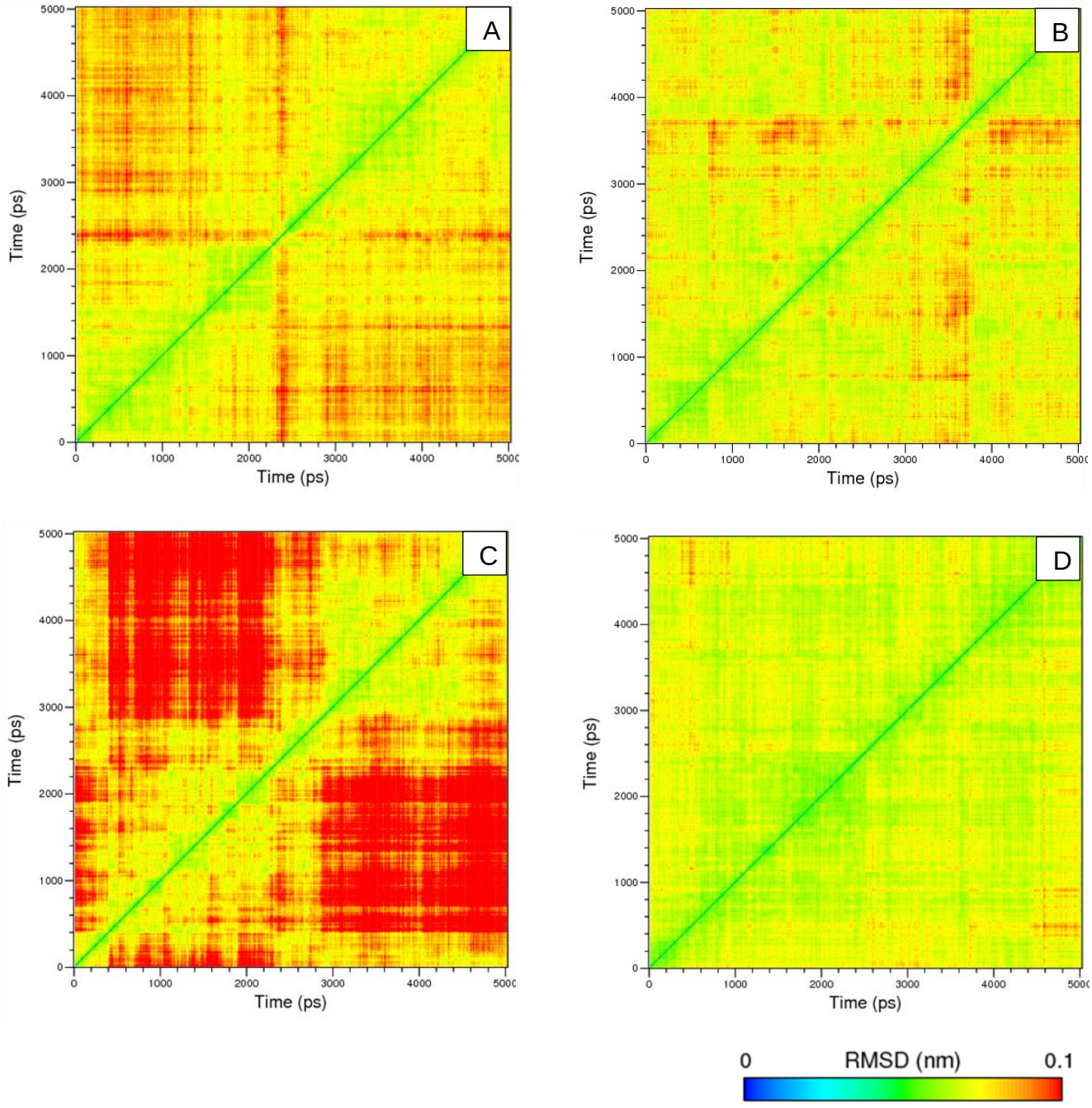

Figure 2.3.2. 2D-RMSD plot of LinB structure (Cα) in water (A), formamide (B), acetone (C) and isopropanol (D) calculated from the last 5ns of the equilibrated part of the 35ns MD trajectory.

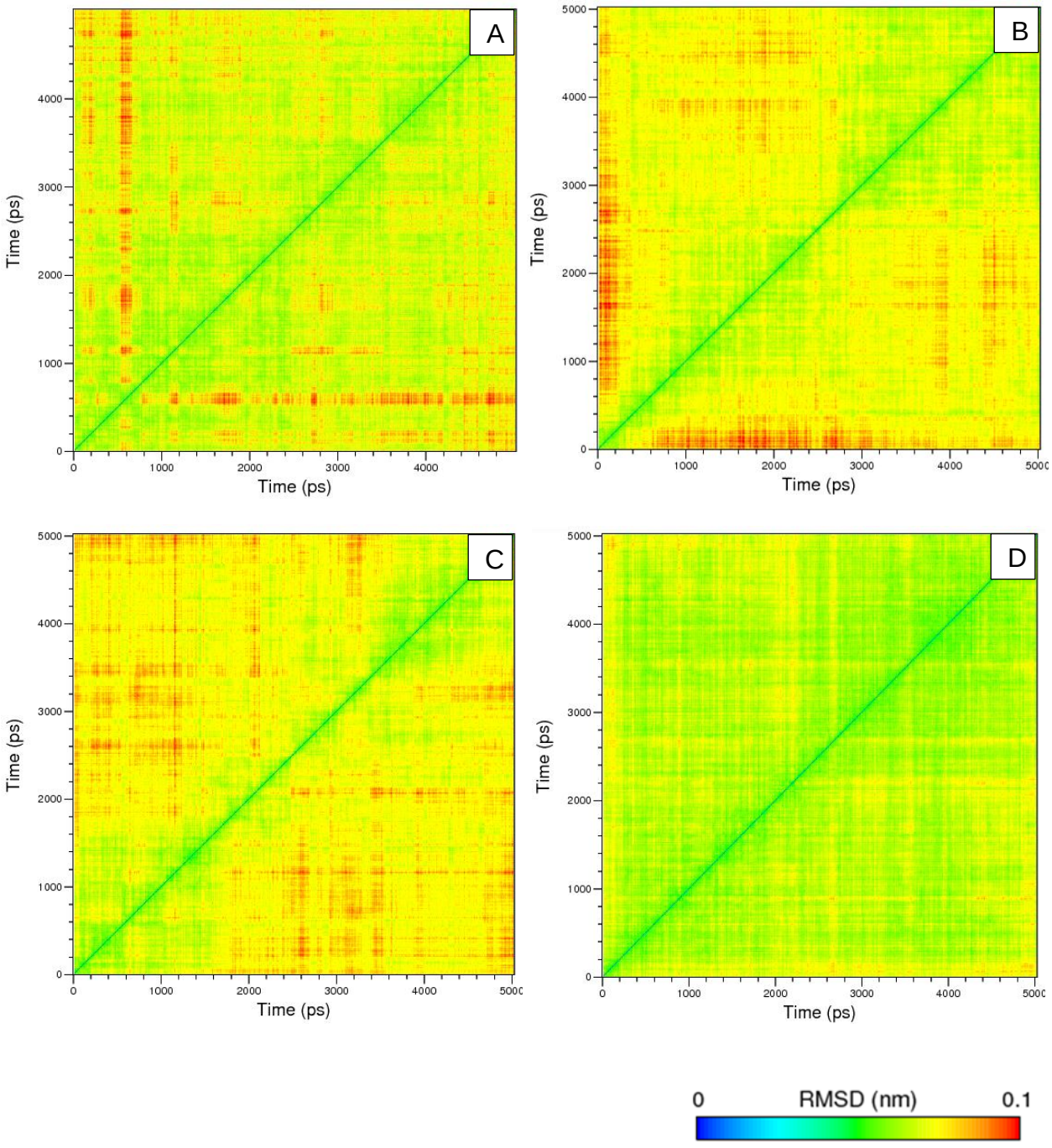

Figure 2.3.3. 2D-RMSD plot of DbjA structure (Cα) in water (A), formamide (B), acetone (C) and isopropanol (D) calculated from the last 5ns of the equilibrated part of the 35ns MD trajectory.

2.3.2 Structural properties of haloalkane dehalogenases in different organic solvents

2.3.2.1 General effect on structure

To evaluate the flexibility of the three enzymes in different solvents, the average B-factor per residue was calculated from the last 5ns of the simulation trajectories. The values show that in almost all enzymes CAP domain residues are more influenced by organic solvents. In all solvents, enzymes display lower flexibility in the core and the active site regions. The average structure of each enzyme obtained from last 5ns of the simulations trajectories in each solvent was superimposed onto each average structure in water. Figure 2.3.4 shows DhaA B-factors and its representative structure in formamide, acetone and isopropanol, in order, showing that the DhaA structure is either less flexible or is not influenced by the presence of organic solvents. The average 3D structure of DhaA in each solvent was aligned to the average structure in water to evaluate where solvent effects are located. Formamide influences part of α5, α8 and α11 helices, and α11 contains the His283 catalytic residue. Acetone mainly affects the CAP domain. All of α4, α5 and part of α8 are more stable. Like B-factor values in formamide, the B-factor in acetone also shows more rigidity. Similar to formamide and acetone, isopropanol also influenced DhaA CAP domain. Interestingly, the main domain did not show any changes in the isopropanol solution. It seems DhaA keeps its structural flexibility or rigidity similar to water solution. Part of the α4, α4-β6 linker (this linker connects CAP domain to the main domain) and very small part of the α5 are affected by isopropanol. By putting all these results together, it is possible to conclude that the DhaA structure is more stable or less flexible in the presence of these organic solvents.

B-factors were also measured for LinB dehalogenase (Figure 2.3.5). Except in acetone, LinB structure is more stable in the organic solvents. In the case of formamide, β6-α4 linker between CAP domain and main domain and α6-α7 linkers in CAP domain, close to the tunnel head, are more stable. In acetone β8 and α8-α9 CAP and main domain linker are more stable while the B-factors show high deviations in α3, α4-β6 CAP and main domain linker, α5,α6, α6-α7 linker. It seems the CAP domain in acetone is more flexible. In isopropanol, mainly cap and main domain linkers are involved with organic solvents. α3, α4- α5 linker and α8- α9 linkers are more rigid while α4 and α4-β6 linker are more flexible. In general, organic solvents do not have only rigidity effect on LinB structure. Some parts of enzyme are more flexible while other parts are either more stable or not changing. In contrast with two other haloalkane dehalogenases, both CAP and organic solvents influence the core domains of DbjA (Figure

2.3.6). The comparison of B-factor graphs in formamide and water shows that except for one small part in cap domain the whole DbjA structure has less deviation than in formamide solution. The part of α2, β6-α4 linker plus part of α4 helix, α9-β7 linker, β7-linker-α10, β8-α11 linker are less flexibility whereas α6-α7 linker plus part of α7 are more flexible. In acetone, β2-β3 linker, α4, part of α6 and α9 and α10-β7 linker are more rigid. In isopropanol mostly main domain is more stable. Except β4-α2 linker, the rest parts of DbjA structure including part of α5, β7-α10 linker, β8-α11 linker and α11 are more stable.

In general, by comparing all dehalogenase structures in both water and organic solvent solutions it is possible to conclude that organic molecules make the structures of these enzymes more stable (except LinB in acetone). In the case of DhaA and LinB, the main effect is on the CAP domain whereas in DbjA the organic molecules influence more the main domain.

In addition to root mean square deviation of structures and B-factors, other structural properties were analysed (Table 2.3.1). RMSD of catalytic pentad residues, the radii of gyration of the three enzymes in organic solvents, and their total solvent accessible surface areas did not significantly vary from simulations in water. In all three enzymes hydrophobic and hydrophilic patches are equally distributed over the surface (Table 2.3.2). Moreover, the solvent accessible surface area of hydrophilic and hydrophobic surface residues is similar for each enzyme in each organic solvent. Total B-factor was decreased in almost all solvents with the exception of only LinB in acetone where a 1.3-fold increase was observed (Table 2.3.1).

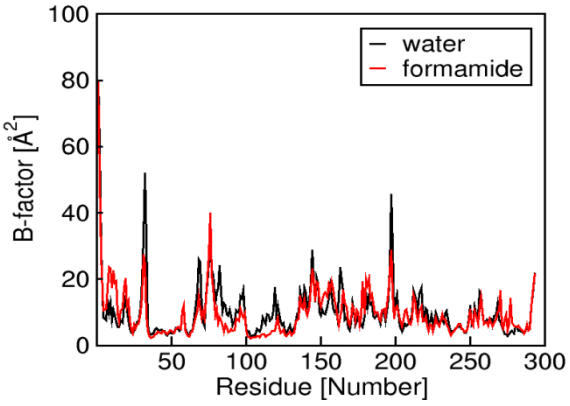

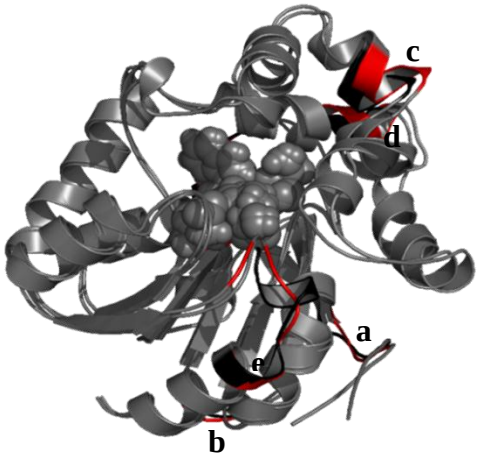

Fluctuated residues are:
a(7-14), b(30-33), c(161-164), d(195-198), e(270-280)

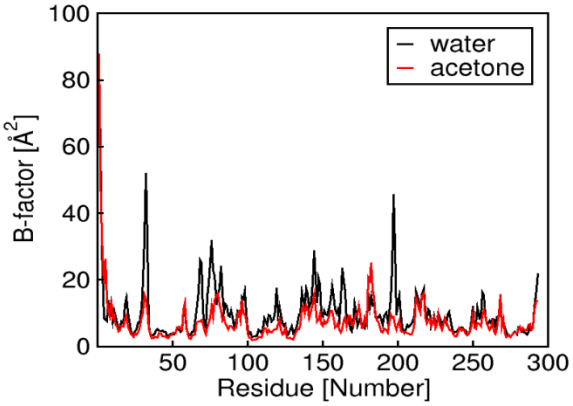

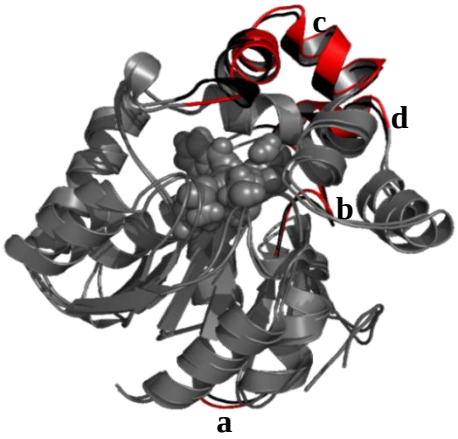

Fluctuated residues are:
a(29-32), b(65-78), c(142-165), d(194-201)

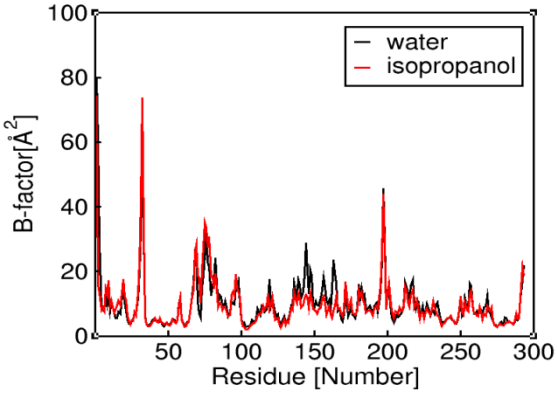

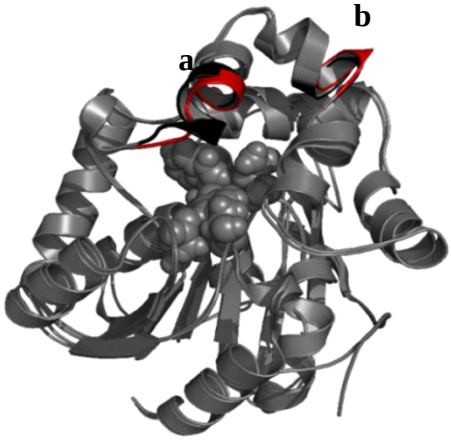

Fluctuated residues are:
a(142-149), b(162-165)

Figure 2.3.4. The average B-factor per residue, calculated from the last 5ns of the simulations trajectories for DhaA in pure water (left) and in organic solvents. Parts of the structure with different B-factors in organic solvent are shown in red and in water are shown in black.

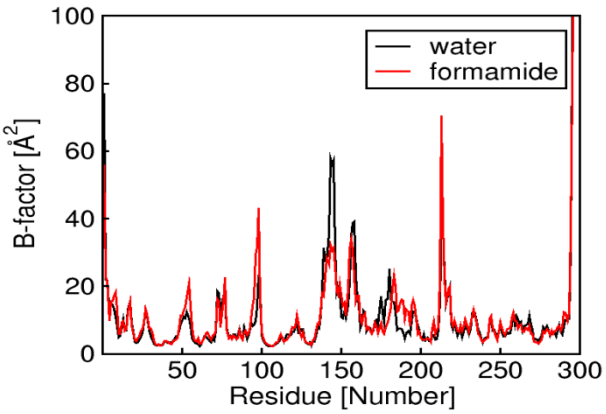

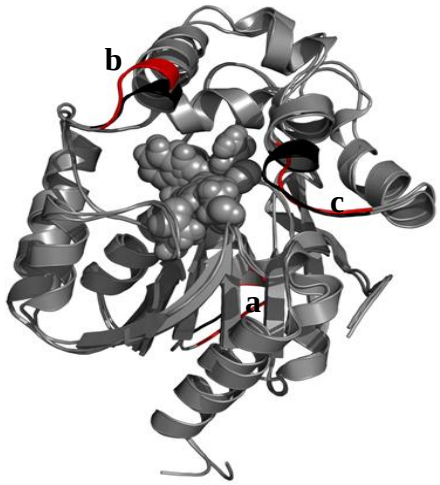

Fluctuated residues are:
a(94-98), b(142-145), c(173-180)

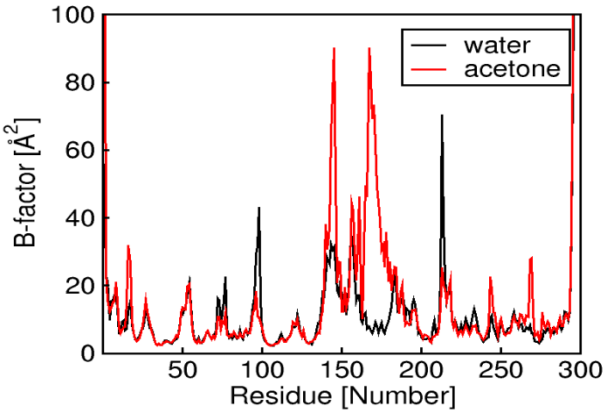

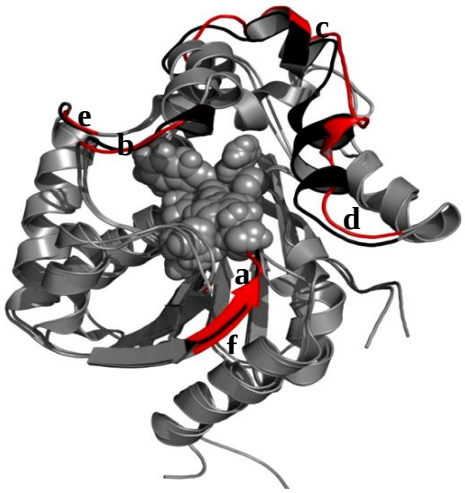

Fluctuated residues are:
a(95-99), b(140-146), c(154-161), d(163-180), e(212-215), f(266-270)

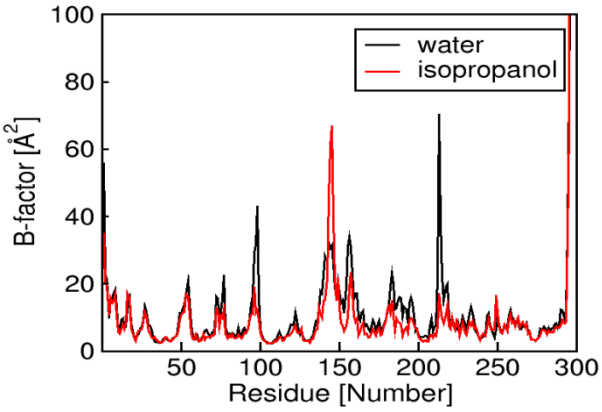

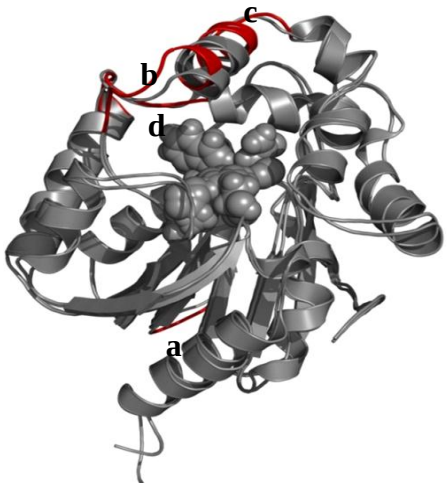

Fluctuated residues are:
a(95-99), b(137-146), c(150-158), d(207-218)

Figure 2.3.5. The average B-factor per residue, calculated from the last 5ns of the simulations trajectories for LinB, as in Figure 9.

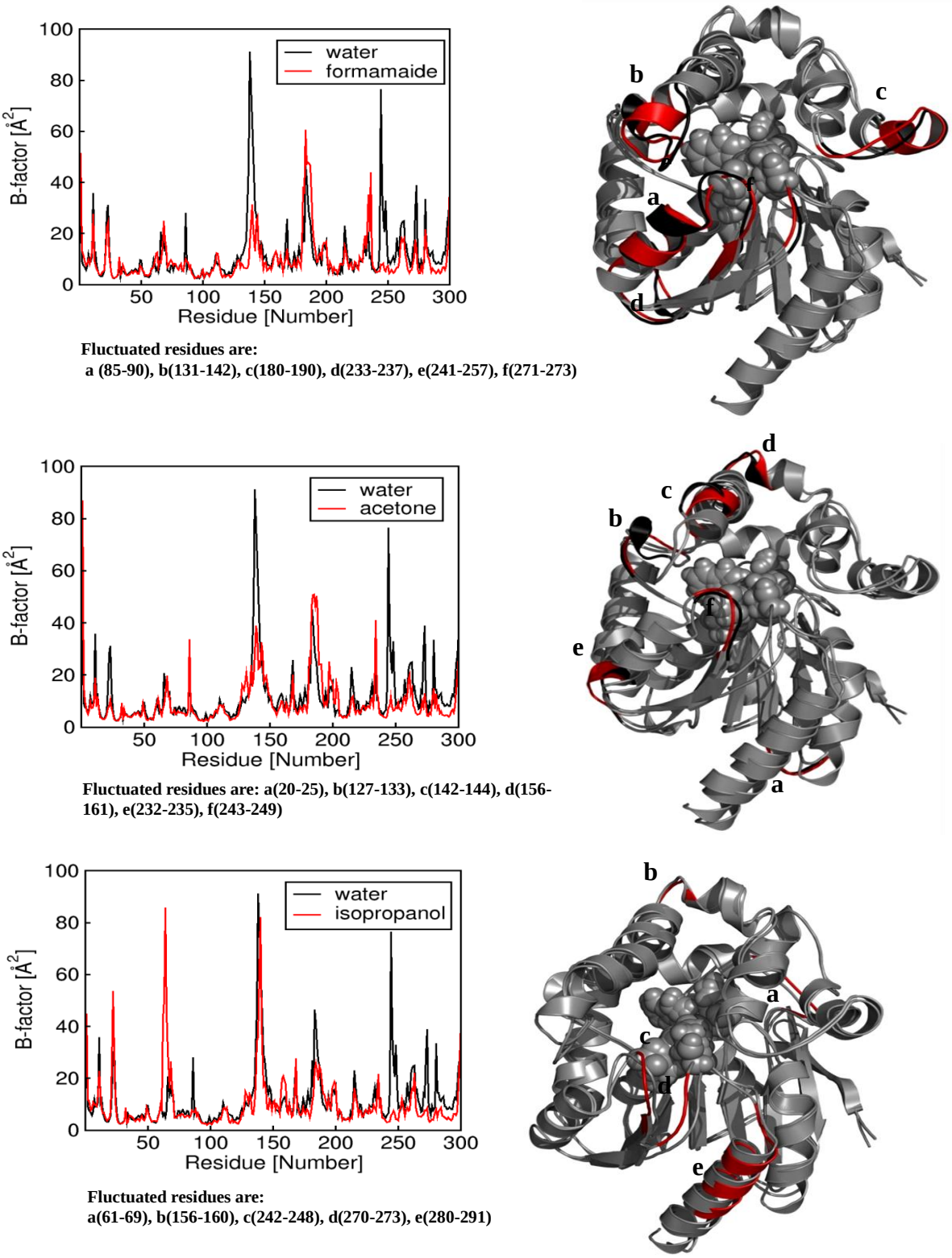

Figure 2.3.6. The average B-factor per residue, calculated from the last 5ns of the simulations trajectories for DbjA, as in Figure 9.

Enzyme	Solvent	RMSD, Å	RMSD of Active site, Å	Radius of gyration, Å	Total B-factors, Å^2	Solvent accessible surface area, Å^2
DbjA	Water	1.30±0.04	0.38 ± 0.008	17.90±0.04	3619±13	13,700±200
	Formamide	1.20±0.05	0.43 ± 0.008	18.00±0.04	2925±8	13,800±200
	Acetone	1.50±0.06	0.46 ± 0.01	18.10±0.04	2925±10	14,000±300
	Isopropanol	1.70±0.04	0.27 ± 0.006	17.90±0.04	2898±10	14,000±200
DhaA	Water	1.10±0.05	0.22 ± 0.005	17.80±0.03	3072±27	13,700±100
	Formamide	1.10±0.05	0.34 ± 0.006	17.90±0.03	2924±19	13,900±200
	Acetone	1.20±0.06	0.26 ± 0.006	17.80±0.04	2699±36	13,700±200
	Isopropanol	1.20±0.06	0.22 ± 0.005	17.80±0.04	2613±17	13,700±400
LinB	Water	1.40±0.06	0.4 ± 0.08	18.00±0.04	2987±9	13,800±200
	Formamide	1.40±0.06	0.36 ± 0.007	18.00±0.05	2873±10	13,900±250
	Acetone	1.40±0.05	0.4 ± 0.008	18.10±0.08	3908±16	14,400±300
	Isopropanol	1.10±0.05	0.4 ± 0.008	18.00±0.06	2399±8	14,000±200

Table 2.3.1. General structural properties of DbjA, DhaA and LinB in water and organic solvents.

Enzyme	Solvent	Hydrophobic area Å^2	Hydrophilic area Å^2
DhaA	Acetone	6800 ± 10	6900 ± 10
	Formamide	6900 ± 10	7000 ± 10
	Isopropanol	6900 ± 10	6800 ± 10
	Water	6800 ± 5	7000 ± 10
LinB	Acetone	6750 ± 20	7600 ± 10
	Formamide	6550 ± 20	7300 ± 10
	Isopropanol	6600 ± 10	7500 ± 10
	Water	65000 ± 10	7300 ± 10
DbjA	Acetone	6900 ± 10	7100 ± 20
	Formamide	6800 ± 10	7000 ± 10
	Isopropanol	6900 ± 10	7100 ± 15
	Water	6800 ± 10	6090 ± 10

Table 2.3.2. Hydrophobic and hydrophilic surface area of DbjA, DhaA, and LinB in water and organic solvents.

2.3.3 The behavior of solvent near the enzyme surface

The main significant effect of organic solvents is on the structure and dynamics of the water solvation shell around the enzyme. The population maps of formamide, acetone and isopropanol on the surface of the three enzymes shows all organic solvent molecules are mainly populated on the hydrophobic surface of DhaA, LinB and DbjA. Figure 2.3.7 shows the distribution of water and organic solvent molecules around the DbjA surface in formamide, acetone and isopropanol. As shown in Table 2.3.2, the hydrophobic and hydrophilic area in the three enzymes is the same and because the results were the same for all organic solvents, the results related to LinB and DhaA are not shown. The radial distribution function (RDF) of the acetone and water molecules at hydrophobic surface shows that in all enzymes the number of organic molecules is larger than the number of water molecules (Figure 2.3.8). To understand how many organic solvent molecules occupy the hydrophobic and/or hydrophilic surface, the percentage of the hydrophobic and hydrophilic surface covered by organic molecules was measured. Table 2.3.3 shows the percentage of occupied hydrophobic and hydrophilic surface of DhaA, LinB and DbjA enzymes with water and different organic solvents. In the presence of organic solvents, water molecules are repelled from the enzyme surfaces and replaced by organic solvents. Since the protein, specially hydrophobic surface, has a lower dielectric constant relative to the selected organic solvent solution (simonson et al., 1996) it is expected that the behavoiur of the solvents in the vicinity of the protein looks like the behavior of the solvents at air-water interface. For this reason the orientation and the behavior of the different organic solvents and water in the hydrophobic zone of the enzyme surface was investigated. Figure 2.3.9 shows the orientation of the formamide, acetone and ISPN close to the hydrophobic surface. The formamide points to the hydrophobic surface by its oxygen and CH group while acetone and ISPN point to the hydrophobic surface by their methyl groups.

In order to determine quantitative parameters describing the topography near the enzyme surface the radial distribution function for all of the organic molecules was determined. Figure 2.3.10 shows rdf of the formamide at the surface of all three dehalogenases. As it shows, formamide prefers to stay close to hydrophobic surfaces with its HCO group while its amide group stays far from the surface. VS-SFG studies of formamide molecules at air water interface show formamide with preference of the HCO group to point toward the vapor phase (Oberbrodhage et al., 1997; Anderson et al., 2005). In contrast, RDF of acetone molecules at the hydrophobic surface of all three enzymes shows there is no preference for acetone molecules to point their methyl (CH3) or carbonyl (C=O) groups toward the surface. Comparing the behavior of acetone molecules close to the hydrophobic surface and the acetone molecules at air water interface shows that the acetone is orienting to the surface by its carbonyl and one of its methyl groups at the same time (Figure 2.3.10). Since the two

methyl groups in acetone molecules are equivalent, the orientation frequency of both acetone methyl groups at the surface is the same. Therefore, it causes no difference in the RDF graph of carbonyl and methyl groups close to the hydrophobic surfaces (Chen et al., 2005). Like acetone and formamide RDF measurement of ISPN molecules in the vicinity of the hydrophobic surface shows similar behavior as its behavior at air water interface (Figure 2.3.10) (Kataoka et al., 2006). This result indicates the ISPN molecules point to the enzyme hydrophobic surfaces with their methyl groups whereas ISPN OH group points to the solution and makes hydrophilic interactions with water and/or ISPN molecules.

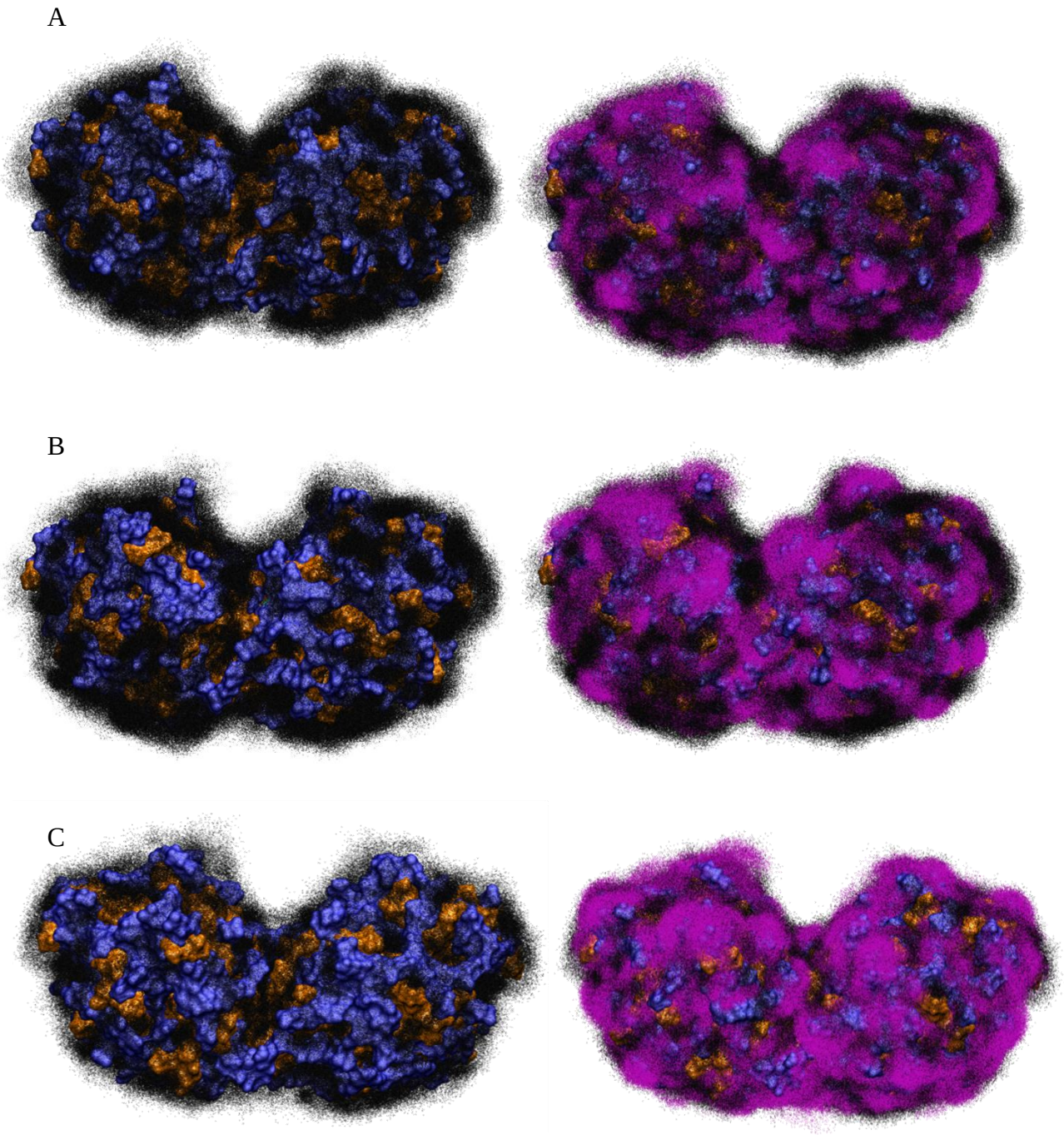

Figure 2.3.7. The position of water molecules (left, black points) and organic solvent molecules (pink) together with water molecules (right) during the whole trajectory (35ns)

Enzyme	Solvents	% Hydrophobic Area Covered by organic molecules	% Hydrophilic Area Covered by organic molecules	% Hydrophobic Area Covered by Water	% Hydrophilic Area Covered by Water
DhaA	ACETON	34,33	13,31	38,03	73,36
	FORMAMID	21,67	7,33	41,37	80,93
	ISPN	32,13	8,96	39,54	71,64
	WATER	–	–	47,31	83,35
LinB	ACETON	36,58	18,63	32,23	74,70
	FORMAMID	25,62	11,82	36,56	80,14
	ISPN	29,16	12,83	36,32	77,80
	WATER	–	–	43,91	87,70
DbjA	ACETON	37,44	15,83	26,89	66,67
	FORMAMID	29,43	10,62	30,84	74,33
	ISPN	33,34	11,41	29,82	72,45
	WATER	–	–	38,38	83,42

Table 2.3.3. The percentage of hydrophobic and hydrophilic area covered by water and organic molecules. The numbers are normalized relative to the number of each solvent molecule in every system.

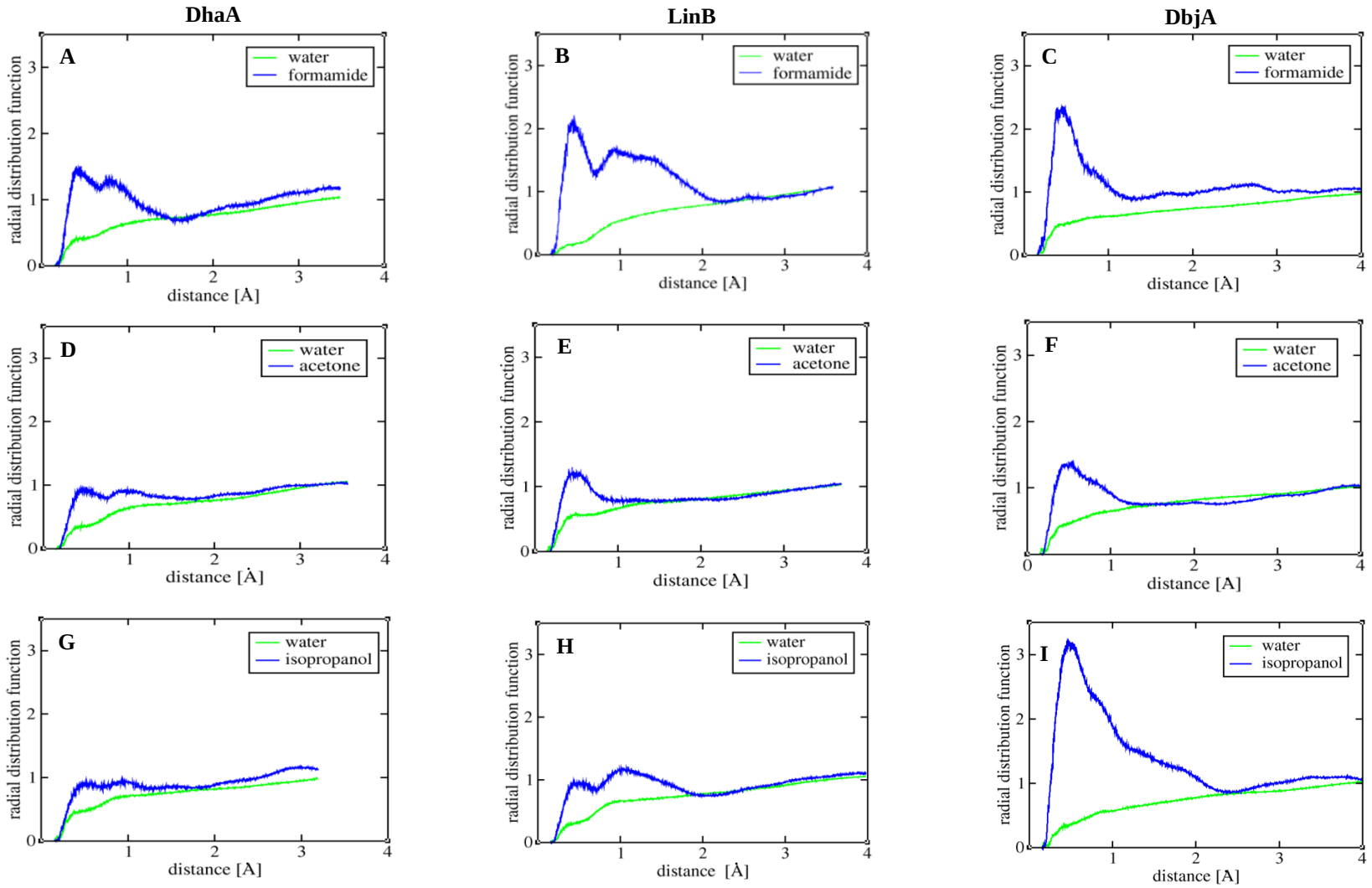

Figure 2.3.8. Radial distribution functions of organic molecules around selected hydrophobic surfaces in DhaA, LinB, and DbjA.

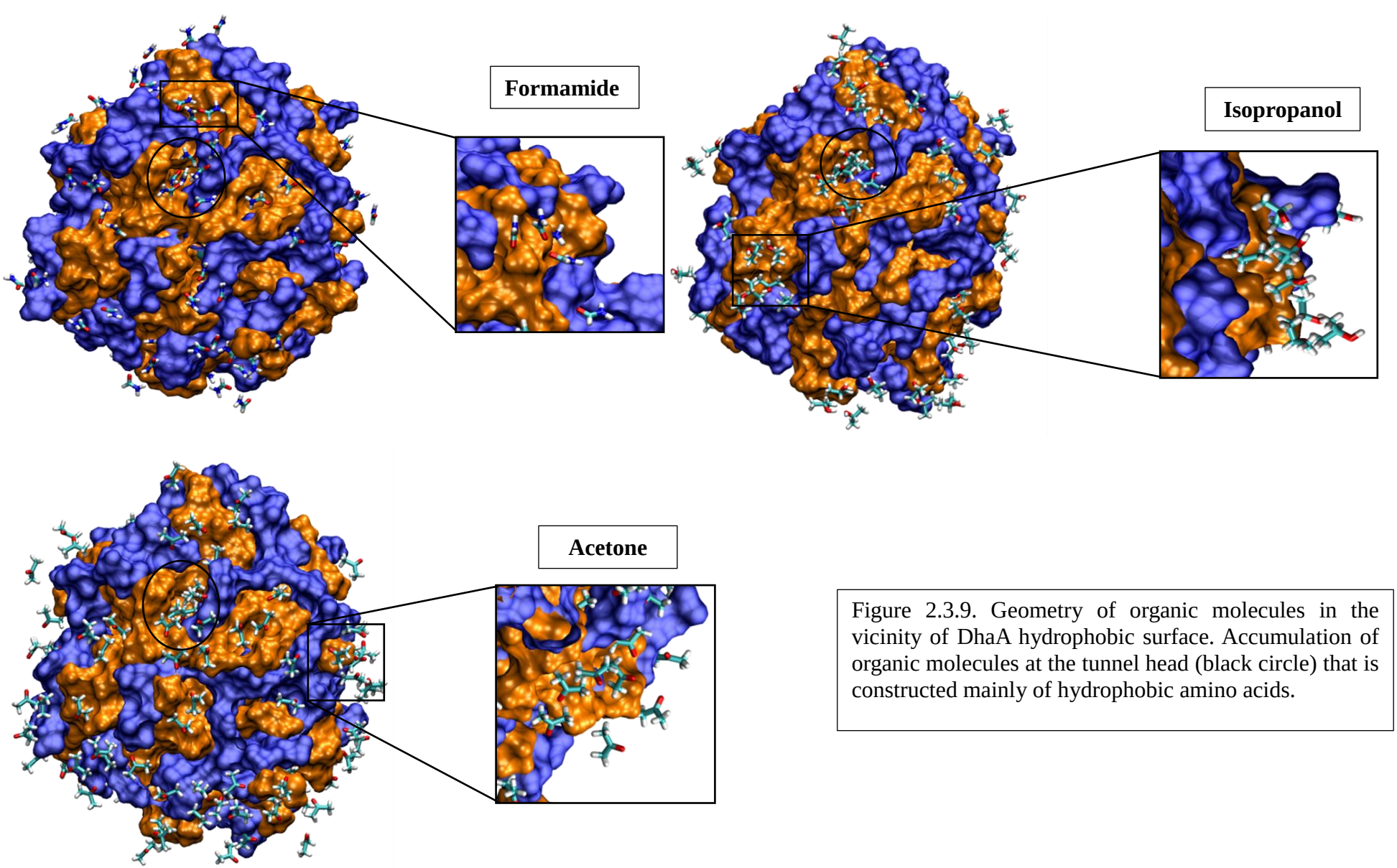

Figure 2.3.9. Geometry of organic molecules in the vicinity of DhaA hydrophobic surface. Accumulation of organic molecules at the tunnel head (black circle) that is constructed mainly of hydrophobic amino acids.

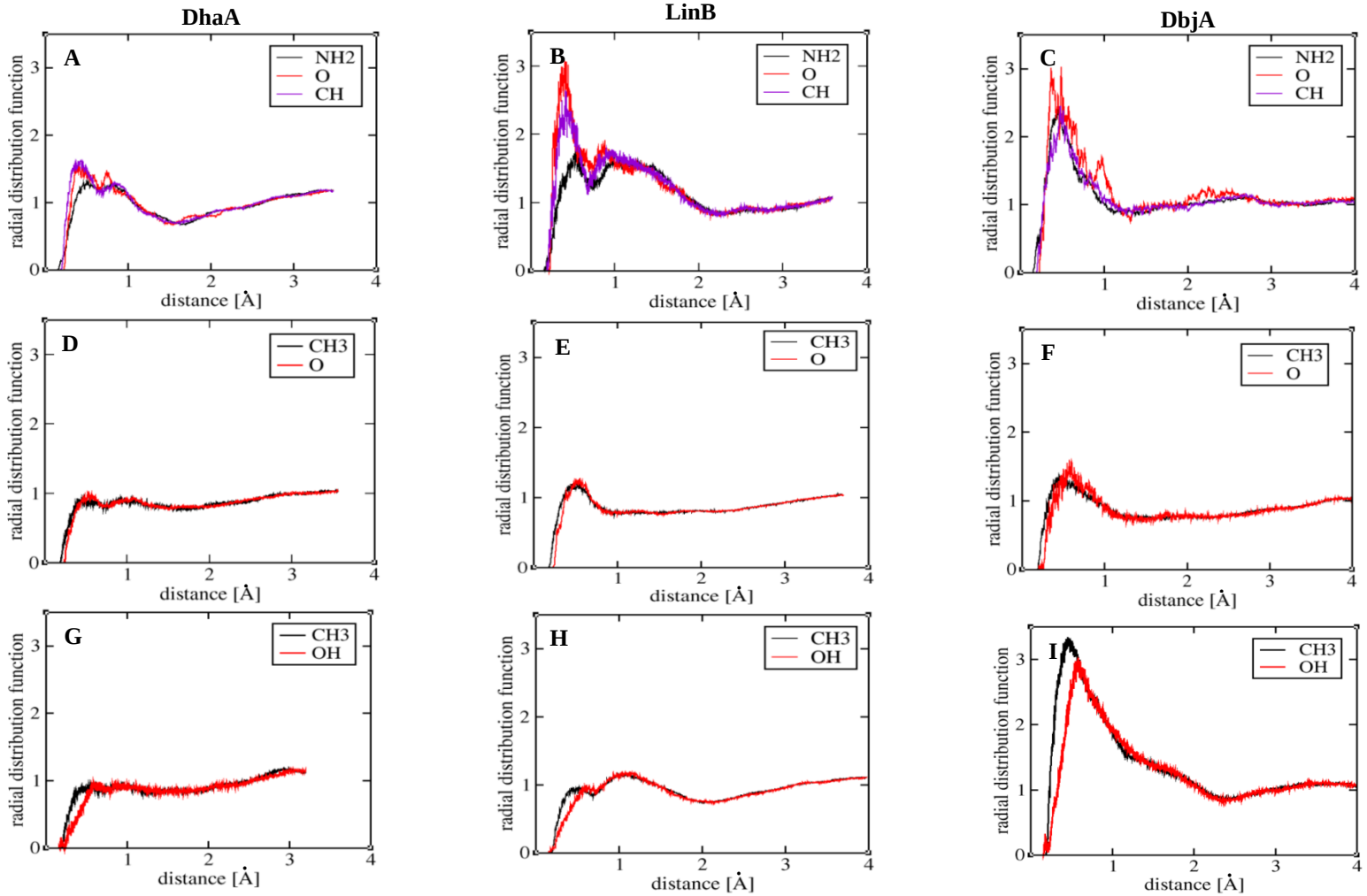

Figure 2.3.10. Radial distribution functions for different parts of organic molecules around selected hydrophobic surfaces in DhaA, LinB, and DbjA: Amide group (NH_2), Oxygen (O), and $C_\alpha H$ groups of formamide, methyl group (CH_3) and Oxygen (O) atom of acetone, and methyl group (CH_3) and hydroxyl group (OH) of isopropanol.

2.3.4 Special effect of organic solvents on DbjA

Among the three selected enzymes DbjA is the only one that can be made of two monomers(Figure 2.1.4). Hence, the structural change of this enzyme may be more dependent on solution properties. Two monomers are in contact together by two long helices. These two helices are constituted mainly by hydrophobic residues. Therefore it is expected that organic solvents may affect the contact of two monomers. Figure 2.3.7 shows the population of the different solvents around and between two monomers. It shows that the organic solvents could penetrate deep between two monomers and since both acetone and ISPN have tendency to make hydrophilic and hydrophobic interactions at the same time, they can be trapped in the network of amino acids (Figure 2.3.11, A,B). This network is made of six amino acids L51, P54, V55, L275, I273 and R292. Among these amino acids four of them belong to monomer A and two of them belong to monomer B. DbjA simulations in acetone solution show acetone molecules could penetrate to the network from both sides and stay there for the rest of the simulation (Figure 2.3.11, C). In the case of the DbjA in ISPN solution ISPN molecules from one side penetrate to the network and stay there but on the other side ISPN molecules exchange with bulk during the simulation (Figure 2.3.11, C). To find out the effect of trapped organic molecules on DbjA behaviour we measure α angle between the long helices to the z axis (Figure 2.1.4). Figure 2.3.12 shows the angle histogram of monomers A and B during the simulations. It shows that α is almost the same in water and formamide. The width of the histogram indicates the fluctuation of monomers in the range of 1-7 degrees. In the case of acetone and isopropanol the distribution is concentrated on the extreme range of angle fluctuations. The main reason for this effect is ISPN and acetone penetration. The persistence of actone and ISPN between the monomers locks their oscillation. This situation can be compared to a lock and key in which the amino acid network is the lock and acetone or ISPN is the key. To test the motion of the monomers from their initial situation (i.e movement of 2 monomers toward each other) we measure the covariance of the monomers (Figure 2.3.13). The graphs show that the motion of the monomers in acetone and ispn are more stable in comparison to the motion of the monomers in water or formamide. Since DbjA motion in acetone solution is locked by two acetone molecules from both sides the motion is less than the motion of DbjA monomers in ISPN solution.

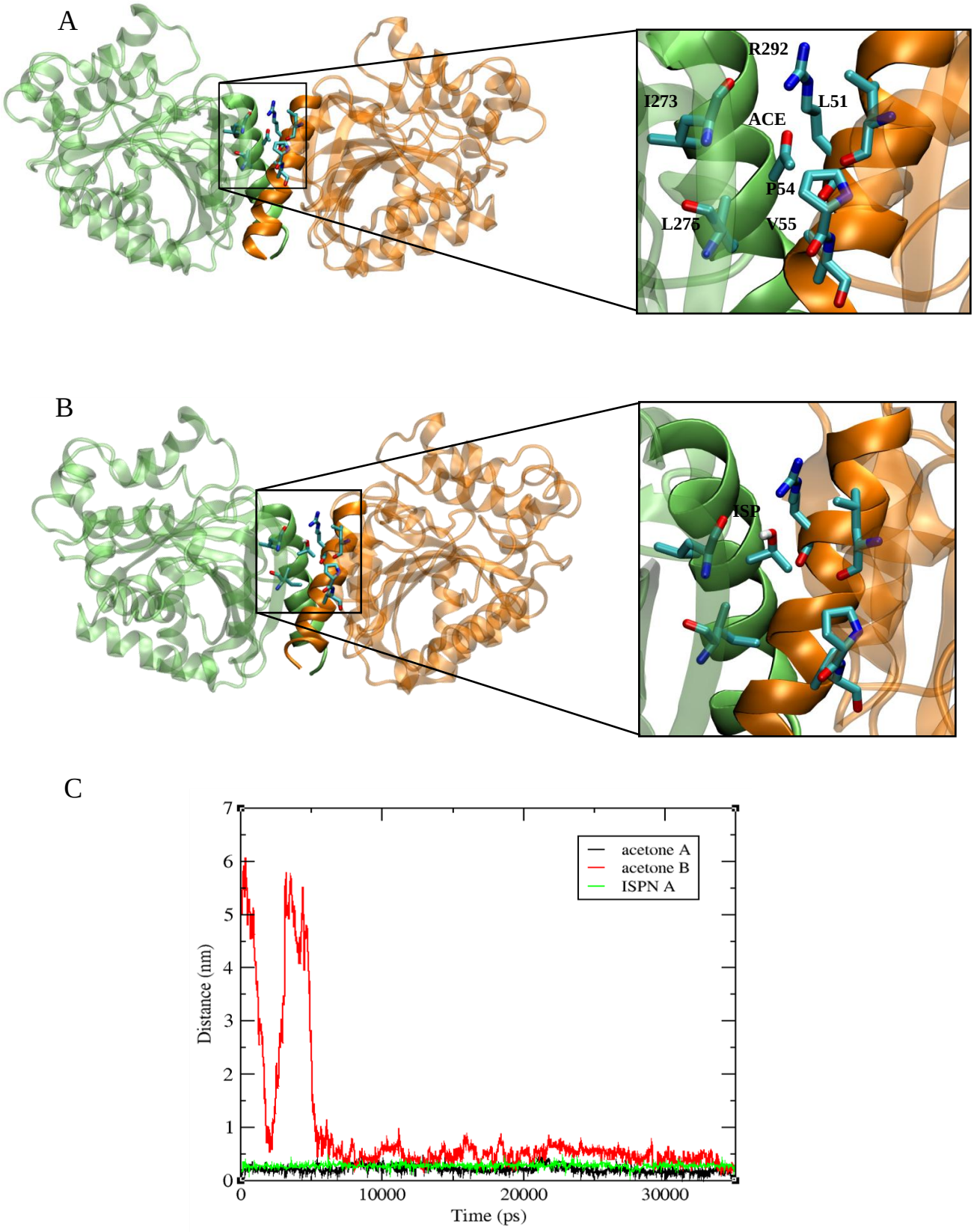

Figure 2.3.11. The network of amino acids in DbjA that trap acetone (A) and isopropanol (B) between two monomers. The hydrophobic parts of acetone and isopropanol contact I273, L275, V55, P54, L51 and the hydrophilic parts contact R292. One molecule of isopropanol is trapped on each side of the dimer and one molecule of acetone is trapped on only one side of the dimer. Graph C shows the residence time of each trapped molecule during the MD simulation.

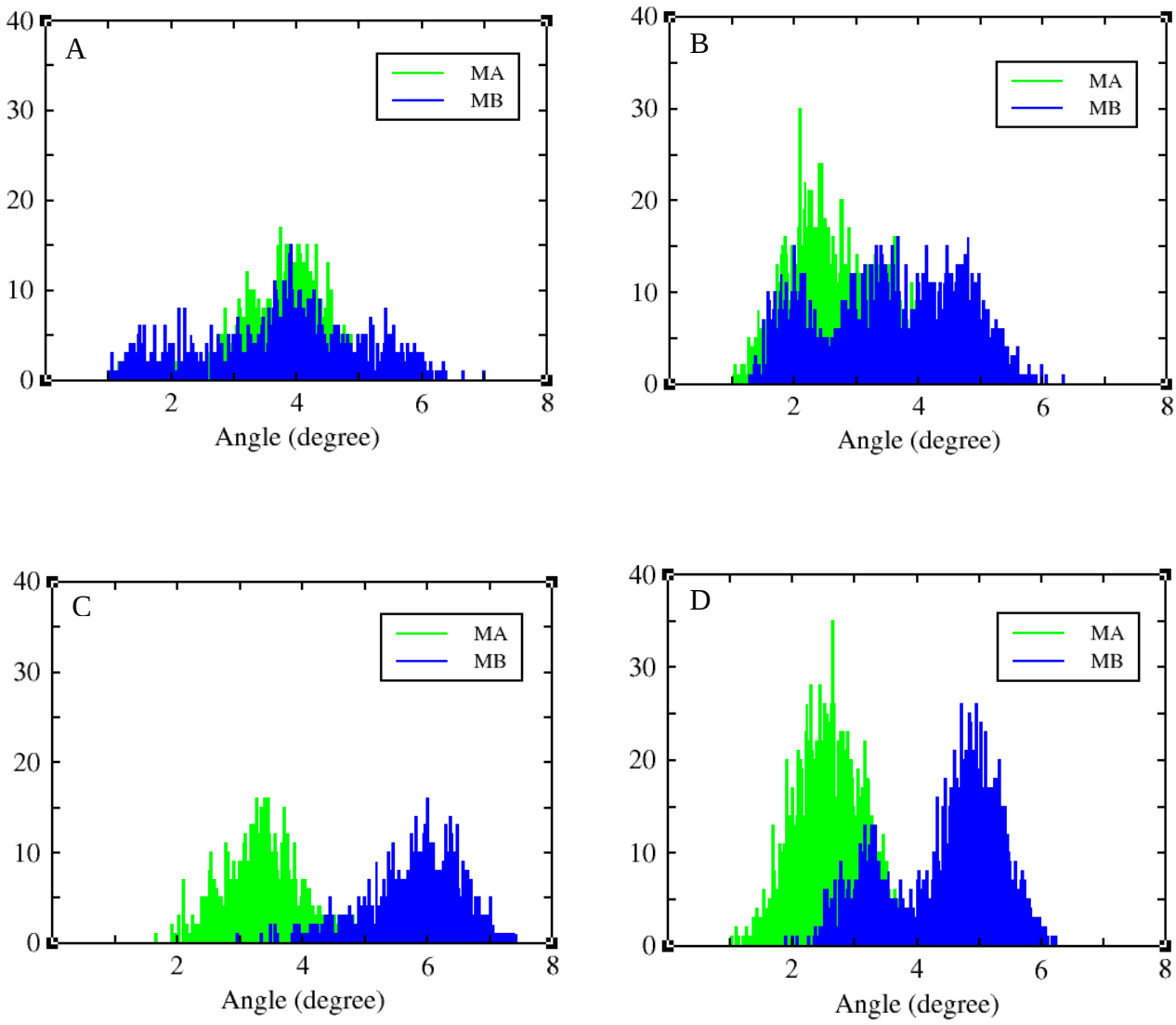

Figure 2.3.12. The distribution of α angles of monomer A (green) and monomer B (blue) in water (A), formamide (B), acetone (C), and isopropanol (D).

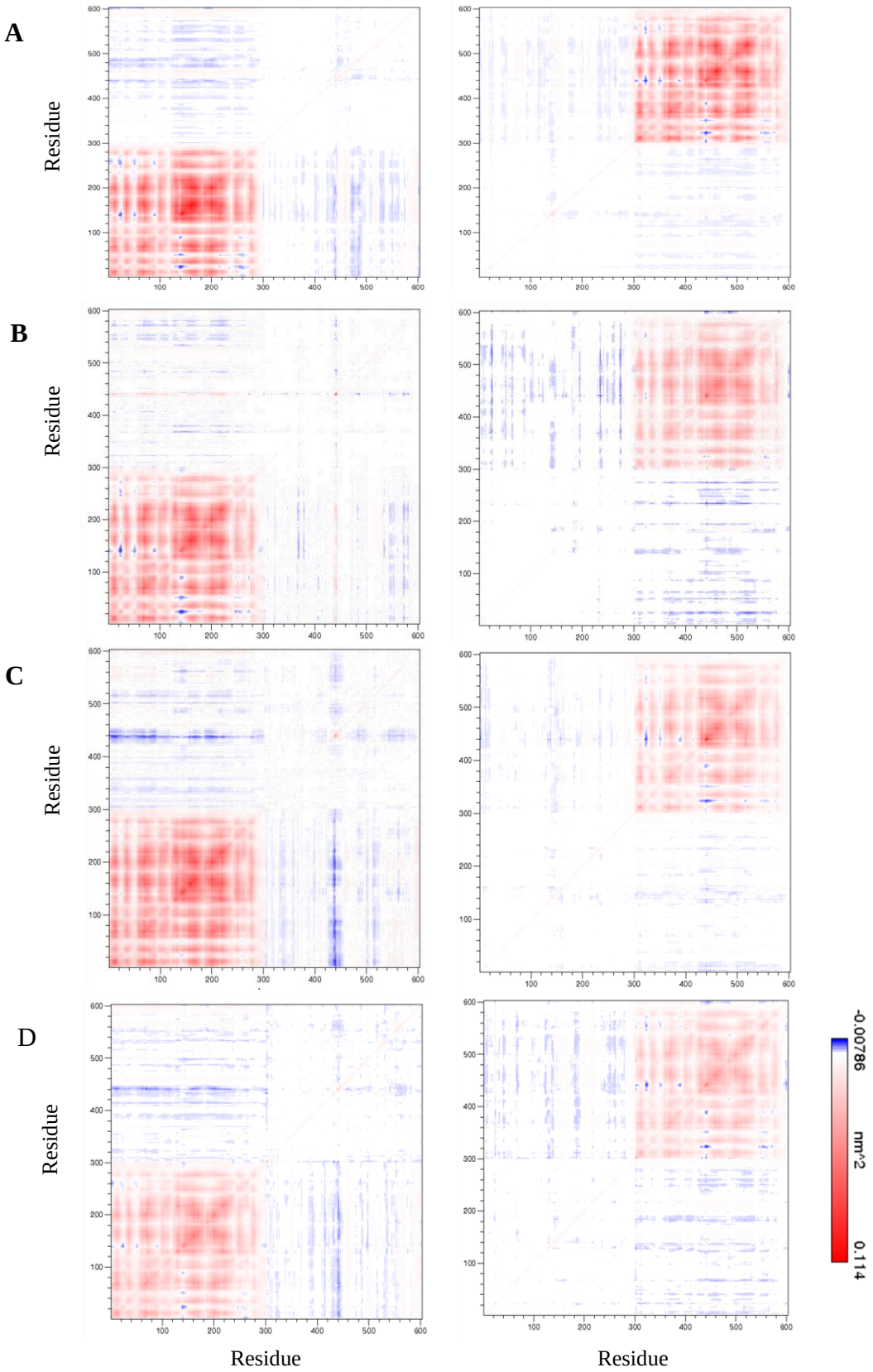

Figure 2.3.13. The covariance of monomer A and monomer B calculated from the last 2ns of MD trajectory shows monomer movement in water (A), formamide (B), acetone (C), and isopropanol (D).

2.3.5 Penetration of solvents to the active site

Although the organic solvents affect the enzyme surfaces and structures, the molecular dynamics simulations show that all 3 organic solvents are able to penetrate to the active site. However, the number of water and organic molecules filling the active site in individual enzymes were different. Figure 2.3.14 indicates the solvation of organic molecules relative to the total volume of the tunnel and active site. The newly developed CAVER software was used to determine the volume of the active site and entrance tunnel occupied by solvent molecules. It is obvious that the occupation of organic molecules is different in the different haloalkane dehalogenases. In the case of DbjA formamide has higher occupancy in the tunnel and active site relative to other organic molecules. In DhaA almost all organic molecules have the same occupancy in the active site, but acetone shows high occupancy inside the tunnel. Similar behavior is observed in LinB. Acetone is highly occupied in the tunnel while two other have the same value. Almost all solvents penetrate the active site with the same value. Solvation of the tunnel and active site with water in these three enzymes in all solutions correspond to the solvation of organic molecules (Figure 2.3.15). As it shown, in the case of the DbjA the solvation of the active site and tunnel by water molecules in formamide solution in both places is less than formamide. A similar trend is observed for DhaA and LinB (Figure 2.3.15). In addition to measuring the occupancy of solvent molecules in the tunnel and active site, the situation of organic molecules was studied in the tunnel and active site. It is observed that in all three enzymes the organic molecules form a chain in the tunnel. The residence of the organic molecules inside the active site was determined based on the distance of organic molecules from Histidine and Aspartate amino acids of the pentad catalytic residues (Table 2.3.4). In DbjA, DhaA and LinB in isopropanol, the organic molecules stay closer to Histidine than Aspartate. It seems organic molecules do not get deeper to the active site. However, in LinB formamide is closer to the Aspartate and isopropanol stays between Aspartate and Histidine catalytic residues. Recently determined structures of DhaA mutants (3FWH, 3G9X) in isopropanol have confirmed the binding of solvent in the active site.

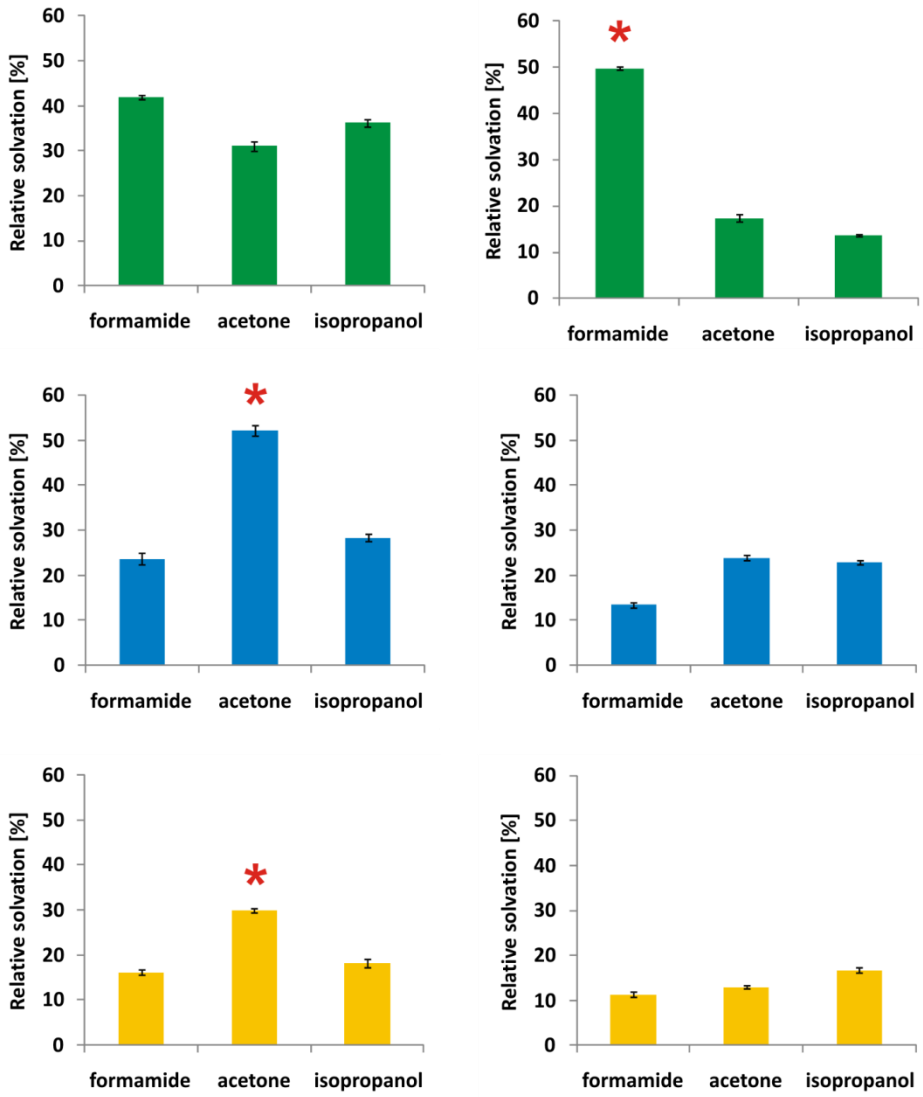

Figure 2.3.14. Solvation of the main tunnel (left) and the active site (right) of DbjA (green), DhaA (blue), and LinB (yellow) by organic solvent. Relative solvation describes the ratio of the volume of the main tunnel or active site occupied by solvent molecules to the total volume of the main tunnel or the active site. Red stars indicate conditions corresponding to the experimentally observed fall in enzyme activity.

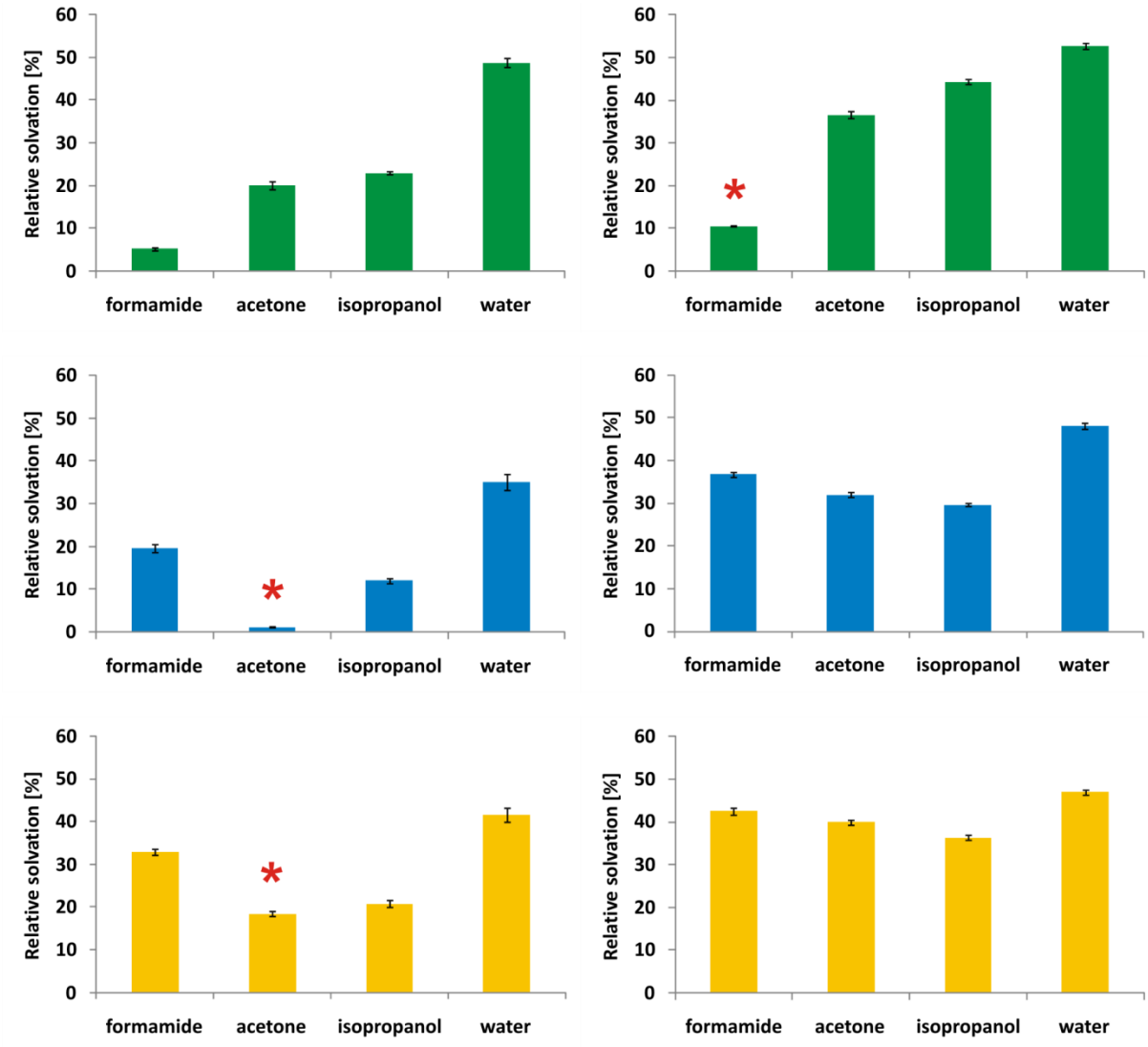

Figure 2.3.15. Solvation of the main tunnel (left) and active site (right) of DbjA (green), DhaA (blue) and LinB (yellow) by water, as in Figure 19.

	Solvents	Distance from aspartate (Å)	Distance from Histidine (Å)
DBJA	**Formamide**	6.0 ± 0.4	5.0 ± 0.3
	Acetone	7.7 ± 0.5	5.0 ± 0.6
	Isopropanol	8.0 ± 0.3	5.0 ± 0.2
DHAA	**Formamide**	6.3 ± 2.1	4.2 ± 0.6
	Acetone	7.7 ± 0.5	5.0 ± 0.6
	Isopropanol	6.0 ± 0.5	4.4 ± 0.4
LINB	**Formamide**	4.0 ± 0.02	5.8 ± 0.3
	Acetone	6.8 ± 0.05	6.9 ± 0.6
	Isopropanol	6.8 ± 0.09	4.5 ± 0.5

Table 2.3.4. The distance from organic molecules in the active site to catalytic residues aspartic acid and histidine.

2.3.6 Discussion

Based on the growing knowledge of the influence of organic solvents on enzyme structure, function and dynamics, and medium engineering to improve enzyme function in non-aqueous media, there has been significant interest in the molecular behavior of enzyme structure in solvents. The catalytic properties and the structure of three haloalkane dehalogenases DbjA, DhaA and LinB were studied in the presence of formamide 5% (v/v), acetone 20% (v/v) and isopropanol 10% (v/v). Although they all belong to the same family of enzymes, share identical topology of catalytic residues and have the same catalytic function, they exhibited different resistance toward the tested solvents. DbjA was activated in the presence of most tested organic solvents, while the activities of DhaA and LinB sharply decreased with increasing solvent concentrations. The variability in enzyme efficiency in organic solvents can be generally attributed to changes in enzyme conformation and flexibility, solvation/desolvation of the active site, energetics of substrate desolvation, steric hindrance that restricts the accessibility of the substrate and the possibility of competitive inhibition by the solvent molecules. To better understand the solvent enzyme interaction on a molecular level, the MD simulations were employed. Investigating the effect of the organic solvents and protein focused on the structural stability, topology of the organic solvents around the enzyme surface and the situation of organic molecules in the main tunnel and active site. The overall structures of all investigated enzymes were stable after 2 ns equilibration phase of molecular dynamics (MD) simulations with average RMSD of Cα atoms below 1.7 Å (Table 2.3.1). The radii of gyration of HLDs in organic solvents as well as their total solvent accessible surface areas did not significantly vary from simulations in water (Table 2.3.2). The flexibility of all studied enzymes expressed by their total B-factors decreased in almost all solvents with the exception of only LinB in acetone where a 1.3-fold increase observed (Table 2.3.1). Since the protein has low dielectric constant in solution the behavior of the organic solvents near the enzyme surface is similar to the behavior of organic solvents at the interface of water with air (with dielectric constant ~ 1). Formamide stays flat between the polar and non-polar parts of the enzyme surface. Meanwhile acetone and isopropanol mainly stay at nonpolar areas of the surface while their methyl groups face these regions. Because DbjA is a dimer the organic solvents have an additional effect on each monomer. From physico-chemical properties viewpoint, water and formamide are very similar. Thus, it is reasonable that the angle between monomer A and monomer B in formamide and water is only slightly different while the nature of acetone and isopropanol cause an increasing angle between the two monomers. In addition, covariance shows that the penetration of acetone and isopropanol between monomers make the motion of the two monomers more stable. Comparing these properties with the function and the activity of these three enzymes with the structural effect of organic solvents on the enzyme

surfaces may give a useful approximation of the general effect of organic solvents relative to their physico-chemical properties with considering the properties of protein surfaces.

Another effect of organic solvents studied in these simulations was their penetration into the enzyme active site. All three solvents entered the access tunnels and the enzyme active sites and stayed inside during 35 ns simulations. Penetration of polar organic solvent molecules inside the enzyme active sites or the tunnels has been reported for Candida Antarctica Lipase B (Graber et al., 2007; Trodler et al., 2008), subtilisin BPN' (Graber et al., 2007), subtilisin E (Janssen et al., 2004), subtilisin Carlsberg (Schmitke et al., 1998) and cytochrome P450 BM-3 (Roccatano et al., 2006; Kuper et al., 2007) based on MD simulations and co-crystallization experiments. The occupancy of active site by co-solvents was different in the individual enzymes. High occupancy of co-solvent is in agreement with the experimentally observed effects on activities. Despite different physicochemical properties of solvent molecules and different composition of enzyme active sites, all studied solvents were able to penetrate into the main tunnel and the active site causing dehydration of these regions in all studied haloalkane dehalogenases. The occupancy of LinB and DhaA main tunnels by acetone was significantly higher in comparison to formamide and isopropanol while in case of DbjA all solvents occupied its main tunnel to similar extent. On the other hand, only the active site of DbjA was massively filled by formamide molecules nearly replacing water molecules, whereas in all other cases the occupancy of active site by molecules of organic solvents was moderate. Except LinB in formamide, the rest of the organic molecules stay closer to the catalytic histidine than the aspartate residue.

In summary, water-organic solvent mixtures affect a number of physicochemical properties of all components of the enzymatic reaction mixture. Therefore, the effects of organic solvent on enzyme activity are rather complex and specific to each case. This extensive study led to the conclusion that variability in enzyme efficiency is not only a consequence of conformational changes but also due to the penetration of organic solvent molecules into the enzyme active site and/or the tunnel and different occupancy of these regions by the solvent. In broad context, this study opens the possibility to predict enzyme behaviour in water-solvent mixtures based on the correlation of enzyme performance with the extent of tunnel/active site occupancy by the solvent. For this purpose, accurate tuning of selection criteria that distinguish between harmless and deleterious impacts of solvent penetration into the tunnels or/and active sites of different groups of enzymes is required.

Chapter 2.4

Effect of mutation on DhaA stability

2.4.1 Introduction

Parallel to engineering of the reaction medium, an alternative method to higher enzyme efficiency is protein engineering. It has been shown that selectivity and catalytic properties of enzymes can be modified and tuned for a specific purpose. The combination of these two methods could improve enzymes activity more efficient. Haloalkane dehalogenase DhaA, from Gram-positive bacterium Rhodococcus rhodochrous NCIMB 13064 (Kulakova et al., 1997), exhibits activity with a broad range of halogenated substrates including 1, 2, 3-trichloropropane (TCP) (Bosma et al., 2003) and sulphur mustard (Prokop et al., 2006). Solubility of such hydrophobic substrates can be improved by addition of organic co-solvent to the reaction mixture. Therefore, stabilization of these enzymes in solutions with organic co-solvents, e.g. dimethyl sulfoxide (DMSO), was investigated. Experimental results reveal that the double mutant DhaA57 (L95V+A172V, Figure 2.3.16), DhaA80 (Thr148Leu+Gly171Gln+Ala172Val+ Cys176Phe) showed increased residual activity in the presence of 40% DMSO. The objective of the experimental study was to make individual single-point mutants and to characterize them by quantitative activity measurements in buffers with and without DMSO. The results identify structural features of DhaA determining its resistance towards organic co-solvents. The half-life in the target concentration 40% (v/v) of DMSO has been extended from minutes to weeks, while simultaneously increasing resistance towards elevated temperatures, with retaining the catalytic efficiency of the wild-type in DMSO. Consequently, To have more detailed explanation of these results at a molecular level, the molecular dynamic simulation of all three enzymes in DMSO 40% were run.

2.4.2 Result and Discussion

2.4.2.1 General effect on structure

DhaA mutants were analysed by MD in DMSO 40% solution. The results show that although DMSO molecules are present in both hydrophilic and hydrophobic areas, they accumulate more on the hydrophobic surfaces of the enzyme (Figure 2.3.17). Table 2.3.5 shows the percentage of hydrophobic and hydrophilic area of the DhaA covered by water and DMSO molecules. In the presence of DMSO the water molecules on the enzyme surface are stripped off. Table 2.3.6 points out the effect of DMSO on general properties of DhaA structure. Except for DhaA57 in pure water solution, in all situations, RMSD of the enzyme is less than 1.3 Å. The small rmsd of the active site

shows its stability during the simulation. The 2D-RMSD of the last 5 ns of MD simulation trajectories shows that introducing mutations, especially DhaA57, makes the structure more flexible. However, when the enzyme is in dmso solution, the structure is very stable. As it can be seen in all cases, the 2D-RMSD map is mainly covered by green points which means that the structural deviation is less than 1 Å (Figure 2.3.18). Total B-factors and the radius of gyration are the other parameters which are in aggrement with the effect of DMSO on enzyme stability.

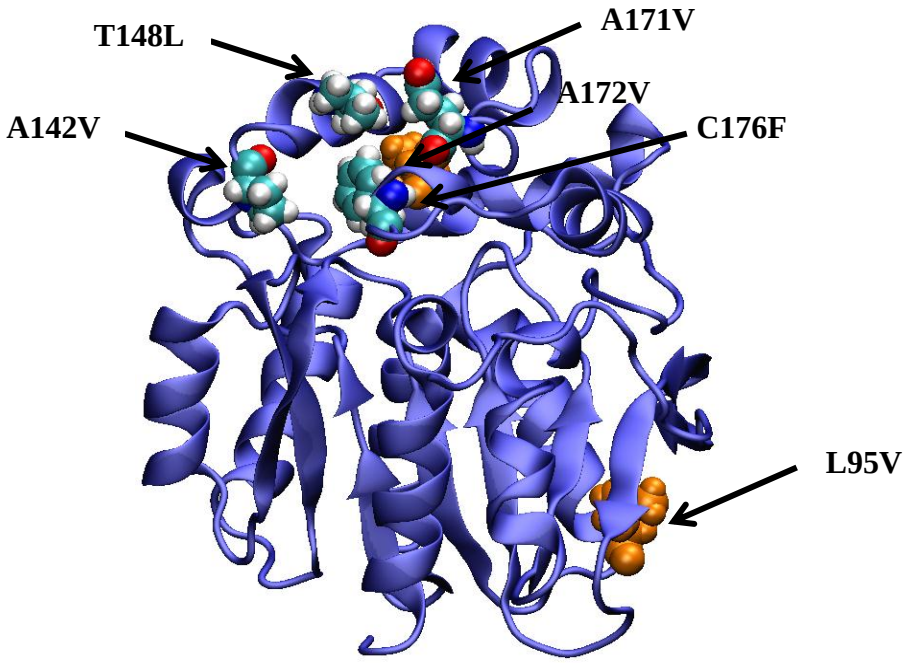

Figure 2.3.16. DhaA point mutations; DhaA57 (L95V+A172V) and DhaA80 (Thr148Leu+Gly171Gln+Ala172Val+Cys176Phe)

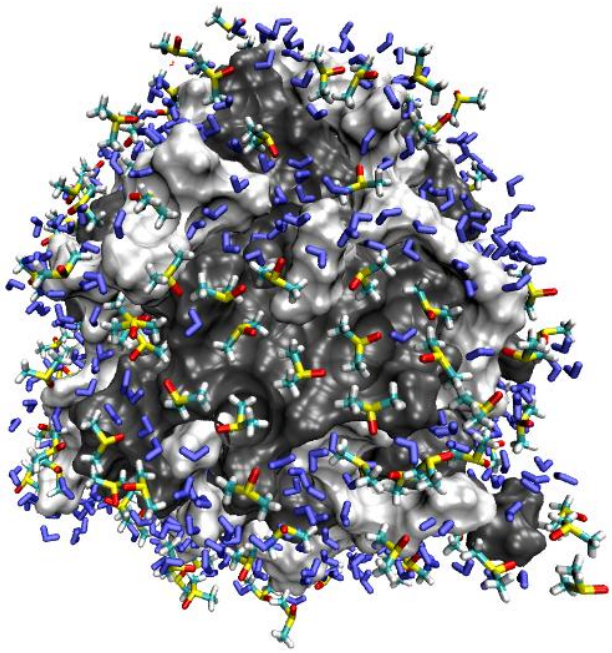

Figure 2.3.17. Distribution of water and DMSO molecules at hydrophobic (grey) and hydrophilic (white) surfaces of DhaA wild type.

Enzyme	solvent	Hydrophobic area percentage occupied by water molecules %	Hydrophilic area percentage occupied by water molecules %	Hydrophobic area percentage occupied by organic molecules %	Hydrophilic area percentage occupied by organic molecules %
DhaA	**water**	30.93	75.77	-	-
	DMSO	18.80	51.04	49.19	14.78
DhaA57	**water**	30.93	76.82	-	-
	DMSO	18.96	50.79	53.67	21.98
DhaA80	**water**	30.04	75.41	-	-
	DMSO	18.61	51.15	51.40	23.78

Table 2.3.5. Percentage of hydrophobic and hydrophilic surface areas covered by DMSO and water.

Enzyme	Organic Solvents	RMSD of Protein Cα, Å	RMSD of Active site Cα, Å	Total B-factor, Å2	Radius of Gyration, Å
DhaA	**water**	1.1 ± 0.05	0.27 ± 0.006	3072 ± 27	17.8 ± 0.003
	DMSO	1.1 ± 0.04	0.35 ± 0.08	1852 ± 4	17.7 ± 0.003
DhaA57	**water**	1.5 ± 0.06	0.6 ± 0.01	2888 ± 9	17.9 ± 0.05
	DMSO	1 ± 0.04	0.4 ± 0.11	1445 ± 3	17.8 ± 0.03
DhaA80	**water**	1.3 ± 0.05	0.6 ± 0.1	2201 ± 5	17.8 ± 0.03
	DMSO	1.2 ± 0.05	0.5 ± 0.08	1645 ± 3	17.7 ± 0.03

Table 2.3.6. General properties of DhaA structure in pure water and in DMSO solution.

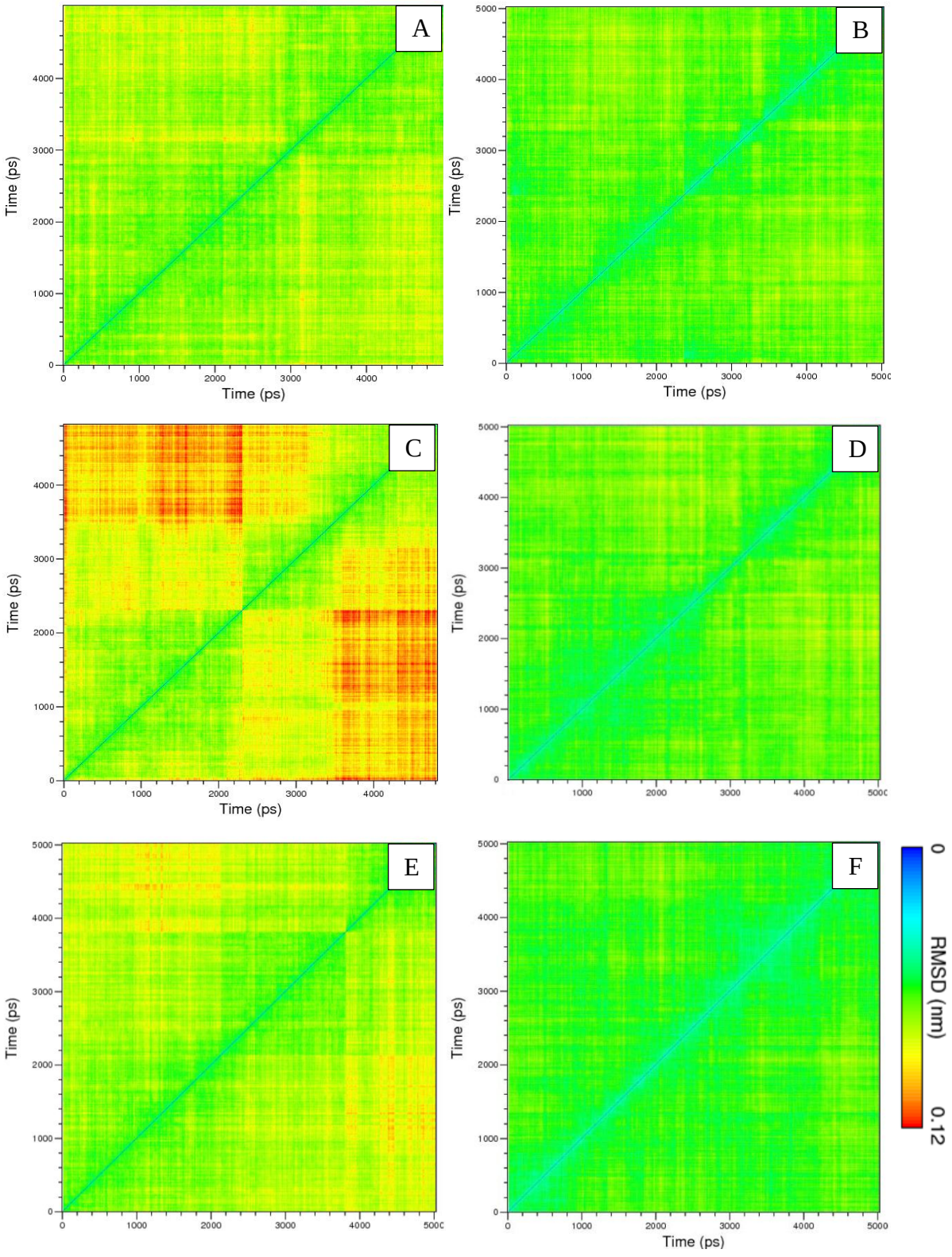

Figure 2.3.18. 2D-RMSD plot of DhaA wild type (A), DhaA57 (C), and DhaA80 (E) in pure water and in DMSO (B, D, and F).

2.4.2.2 Effects of mutations on structural stability

To show the effect of DMSO on the enzymes, the structures of DhaA wild type, DhaA57 and DhaA80 in the absence and presence of DMSO were overlaid. B-factor per residue graphs reveal that α2 and α6-α7 linker of DhaA wild type is more stable in DMSO solution (Figure 2.3.19). It seems that introducing the mutations in DhaA wild type (DhaA57) makes the CAP domain very flexible (Figure 2.3.20), and this flexibility becomes very stable in the presence of DMSO. β1, β3-α1linker , β6-α4 linker, α5 and α7 of DhaA57 reduce their flexibility in DMSO solution. In contrast with DhaA57, the DhaA80 mutant structure is more stable, specifically the CAP domain (Figure 2.3.20). DMSO does not have so much effect on DhaA80 stability. β3-α1 linker, α6-α7 linker, α8 and β7 secondary structures are more stable in DMSO solution (Figure 2.3.20).

In addition to the structural effects of DMSO, the number of solvent molecules in the active site, were measured in the absence and presence of DMSO. It already observed that, in the case of DhaA wild type and DhaA57 one DMSO molecule is able to penetrate to the active site during the simulation. However, no DMSO molecule entered the active site in DhaA80 mutant. In addition, the number of water molecules was also considered. All three enzymes show almost the same number of water molecules in their active sites. In the presence of DMSO, the number of water molecules shows the same reduction in all three enzyme variants.

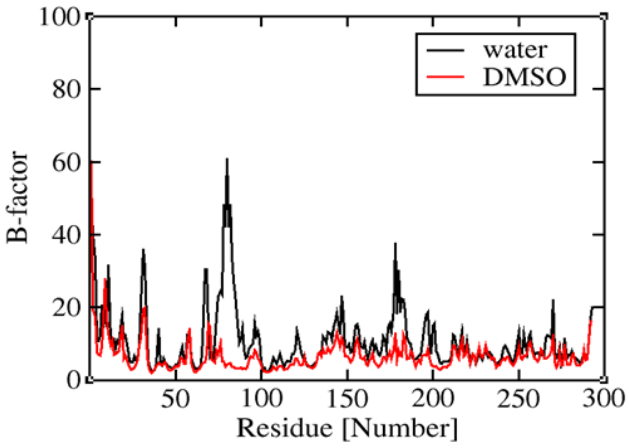

Fluctuated sequences are:
a (64-99), b(176-184)

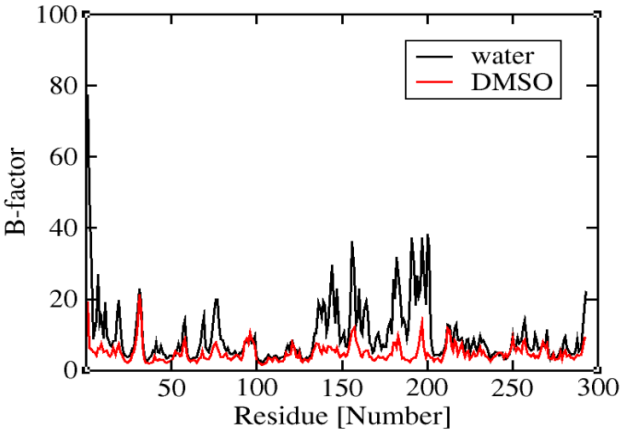

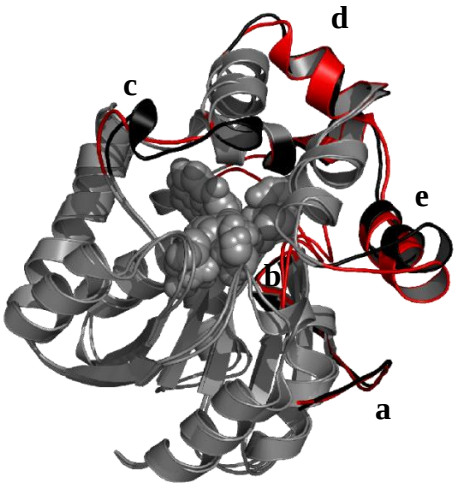

Fluctuated sequences are:
a (1-20), b(65-79), c(135-145), d(154-164), e(179-202)

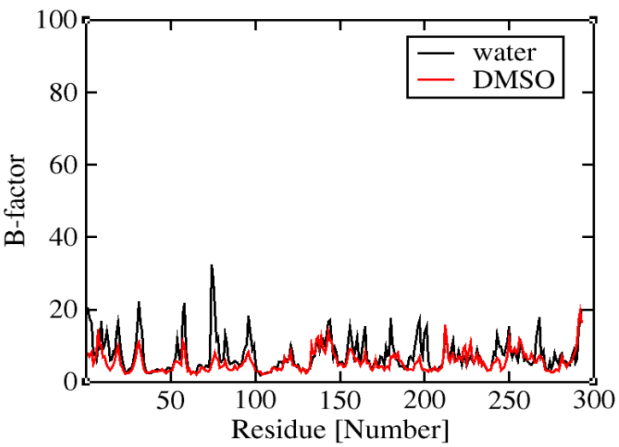

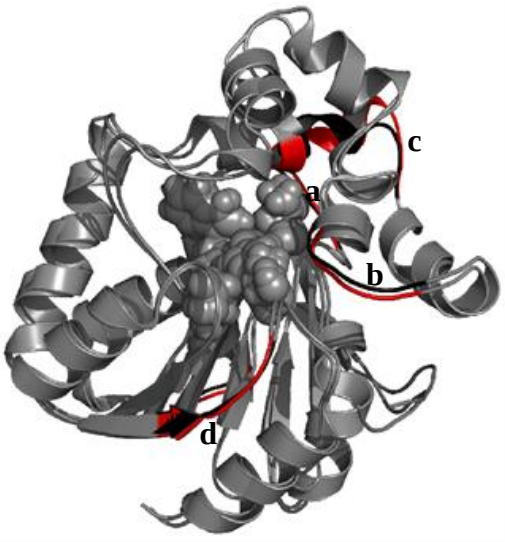

Fluctuated sequences are:
a (73-78), b (176-180), c (193-202), d (265-268)

Figure 2.3.19. The average B-factor per residue calculated from the last 5ns of the simulation trajectories.

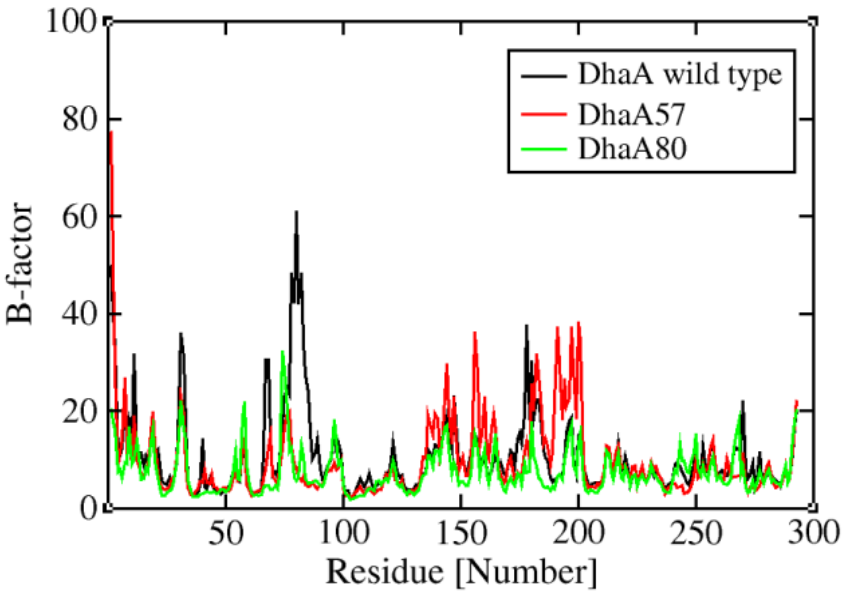

Figure 2.3.20. The effect of mutations on DhaA B-factors.

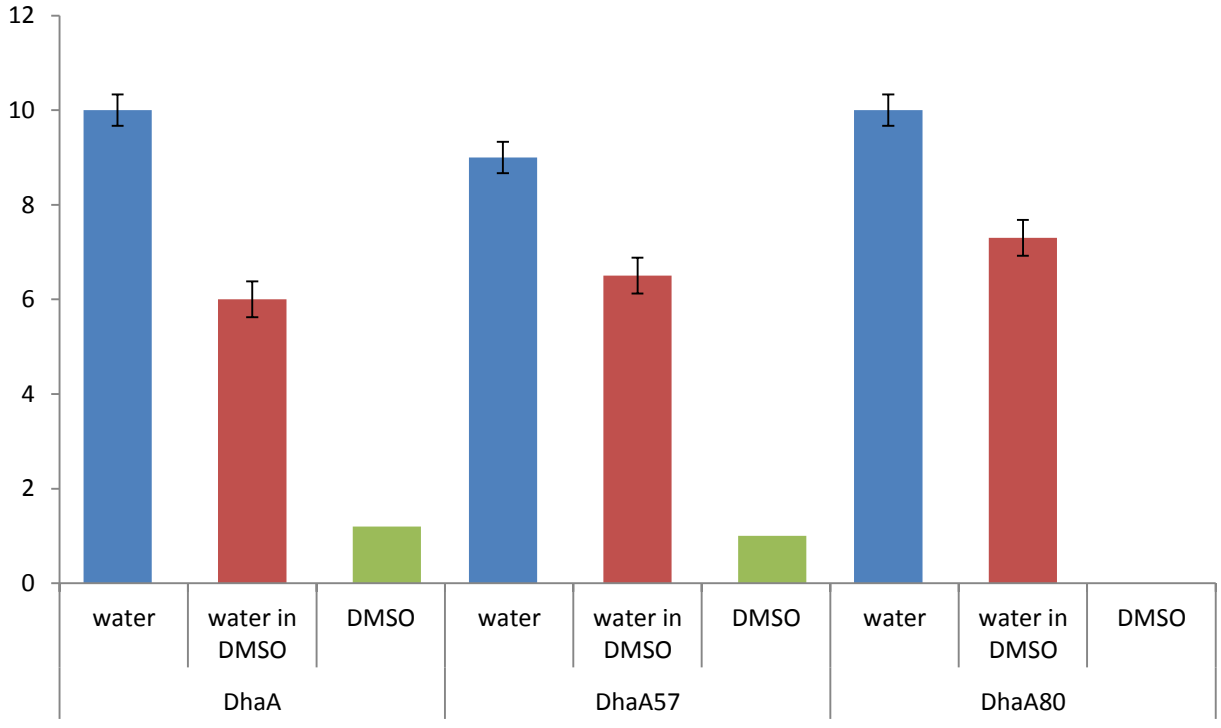

Figure 2.3.21. The number of solvent molecules in the active sites of wild type and mutant DhaA.

2.4.2.3 Discussion

The molecular basis of stabilization at higher temperatures can be explained by improved packing of the residues lining the access tunnel. Visual inspection of the structures of modeled variants shown that the side-chains of introduced substitutions make better intramolecular interactions with the other residues of the access tunnel. Explanation the improved resistance towards organic co-solvent is less straightforward and required use of computer simulations. Molecular dynamics (MD) simulations were therefore conducted with the wild-type DhaA and the variants DhaA57 and DhaA80 in the presence of 40% DMSO. Simulation of wild-type DhaA in a water environment was carried out for comparative purposes. Analysis of MD trajectories revealed that the introduction of mutations in the tunnel influences access of co-solvent molecules into the active-site cavity. Whereas the substitution A172V restricted the access of co-solvent molecules to the active-site cavity of DhaA57, four mutations Thr148Leu, Gly171Gln, Ala172Val and Cys176Phe in DhaA80 sealed the tunnel and completely prevented the access of the co-solvent to the active site during the entire simulation. The active-site accessibility for co-solvent molecules seems to be an essential determinant of enzyme resistance towards DMSO. Moreover, comparison of the wild-type simulation in water and DMSO revealed that the part of the CAP domain involved in the tunnel structure is less flexible. The number of water molecules in the active site before and after mutation of DhaA wild type to DhaA80 is the same, and on the other hand, no DMSO molecules could enter the active site. These results suggest that by mutation the access tunnel changes its diameter in response to a solvent environment containing DMSO. This result also explains the observed different effects of mutations on enzyme stability in water and in DMSO. The MD simulations provide insight to the molecular basis of protein stabilization by mutations in the access tunnel, and demonstrated the potential of MD for predictive purposes.

2.4.3. References

- Andersson G, (2007) Angle resolved ion scattering spectroscopy at surfaces of pure liquids: topography and orientation of molecules. Phys. Chem. Chem. Phys. 7:2942-2947.
- Bell G., Halling PJ, Moore BD, Partridge J, and Rees DG. (1995) Biocatalyst behaviour in low-water systems. TIBTECH. 13:468–473.
- Ben-Naim A. Hydrophobic Interactions, Plenum Press, New York and London, 1980.
- Bosma T, Pikkemaat MG, Kingma J, Dijk J, Janssen DB. (2003) Steady-state and pre-steady-state kinetic analysis of halopropane conversion by a rhodococcus haloalkane dehalogenase. Biochemistry. 42(26):8047-53.
- Berendsen HJC, Postma JPM, van Gunsteren and Hermans WFJ. (1981) Interaction models for water in relation to protein hydration. In: Intermolecular Forces. Reidel Publishing Company Dordrecht, 331–342.
- Berendsen HJC, van der Spoel D, and van Drunen R. (1995) GROMACS: A message-passing parallel molecular dynamics implementation. Comp Phys Comm. 91: 43–56.
- Berendsen HJC, Postma JPM, van Gunsteren WF, Di Nola A, Haak, JRJ. (1984) Molecular dynamics with coupling to an external bath. Chem Phys. 81:3684-3690.
- Butler LG. (1979) Enzymes in non-aqueous solvents. Enzyme Microb. Technol. 1:253-259.
- Chen H, Gan W, Wu BH, Wu D, Guo Y, Wang HF (2005) Determination of structure and energetics for gibbs surface adsorption layers of binary liquid mixture 1. Acetone + water. J Phys Chem B. 109:8053-63.
- Carrea G, Riva S. (2000) Properties and synthetic applications of enzymes in organic solvents. Angewandte Chemie (International Edition). 39:2226-2254.
- Chovancova E, Kosinski J, Bujnicki JM, Damborsky J. (2007) Phylogenetic analysis of haloalkane dehalogenases. Proteins, 67:305-316.
- Chatterjee S, Russell AJ. (1993) Kinetic analysis of the mechanism for subtilisin in essentially anhydrous organic solvents. Enzyme Microb. Technol. 15:1022-1029.
- Campbell D, Müller C, Reardon K. (2006) Development of a fiber optic enzymatic biosensor for 1,2-dichlorethane. Biotechnology Letters. 28:883-887.
- Damborsky J, Rorije E, Jesenska A, Nagata Y, Klopman G, Peijnenburg WJ. (2001) Structure-specificity relationships for haloalkane dehalogenases. Environmental Toxicology and Chemistry. 20:2681-2689.
- Damborský J, Koca J. (1999) Analysis of the reaction mechanism and substrate specificity of haloalkane dehalogenases by sequential and structural comparisons. Protein Engineering. 12:989-998.
- Delano W.L. (2002) The PyMOL Molecular Graphics System DeLano Scientific, San Carlos, CA, USA, http://www.pymol.org
- Essmann U, Perera L, and Berkowitz ML. (1995) A smooth particle mesh Ewald method. J Chem Phys.103: 8577-8592.
- Frisch MJTGW, Schlegel HB, Scuseria GE, Robb MA, Cheeseman, et al. (2004) Gaussian 03, Gaussian, Inc., Wallingford CT.

- Freeman A, Lilly MD. (1987) The effect of water-miscible solvents on the A'-dehydrogenase activity of free and PAAH-entrapped Arthrobacter simplex. Appl. Microbiol. Biotechnol. 25:495-501.
- Graber M, Iraque R, Rosenfeld E, Lamare S, Franson L, Hult K (2007) Solvent as a competitive inhibitor for Candida antarctica lipase B. Biochimica et Biophysica Acta (BBA) - Proteins & Proteomics 1774:1052-1057.
- Guagliardi A, Manco G, Rossi M, Bartolucci S. (1989) Stability and activity of a thermostable malic enzyme in denaturants and water-miscible solvents. Eur. J. Biochem. 183:25-30.
- Granot I, Aharonowitz Y, Freeman A. (1988) Cosolvent effect on A'-steroid-reductase activity of free and PAAH-entrapped Mycobacterium Sp. NRRL B-3805 cells. Appl. Microbiol. Biotechnol. 27:457-463.
- Halling PJ. (2000) Biocatalysis in low-water media: understanding effects of reaction conditions. Curr. Opin. Chem. Biol. 4:74–80.
- Hess B, Bekker H, Berendsen HJC, Fraaije JG. (1997) LINCS: A Linear Constraint Solver for Molecular Simulations J Comput Chem. 18:1463-1742.
- Humphrey W, Dalke A, Schulten K. (1996) VMD: visual molecular dynamics. J Mol Graph.14(1):33-8, 27-8
- Broos J, Visser JAJWG, Engbersen JFJ, Verboom W, Hoek AV, D N Reinhoudt (1995) Flexibility of enzymes suspended in organic solvents probed by time-resolved fluorescence anisotropy. Evidence that enzyme activity and enantioselectivity are directly related to enzyme flexibility, Journal of the American Chemical Society, Volume: 117, Issue: 51,Pages: 12657-12663
- Janssen DB. (2004) Evolving haloalkane dehalogenases. Current Opinion in Chemical Biology. 8:150-159.
- Klibanov AM. (2001) Improving enzymes by using them in organic solvents. Nature. 409:241–246.
- Kaur J, Sharma R. (2006) Directed evolution: an approach to engineer enzymes. Crit Rev Biotechnol. 26(3):165-99.
- Kalju k, Thomas C.B. (2002) Parameterization of OPLS–AA Force Field for the Conformational Analysis of Macrocyclic Polyketides J Comput Chem 23:977–996.
- Krieger E, Koraimann G, Vriend G. (2002) Increasing the precision of comparative models with YASARA NOVA--a self-parameterizing force field. Proteins. 47:3:393-402.
- Krieger E, Darden T, Nabuurs SB, Finkelstein A and Vriend G. (2004) Making optimal use of empiral energy functions: force field parameterization in crystal space. PROTEINS: Structure, Function, and Bioinformatics. 57(4):678-683.
- Kataoka S, Cremer PS. (2006) Probing molecular structure at interfaces for comparison with bulk solution behavior: water/2-propanol mixtures monitored by vibrational sum frequency spectroscopy. J Am Chem Soc. 128(16):5516-22.
- Kuper J, Wong TS, Roccatano D, Wilmanns M, Schwaneberg U. (2007) Understanding a Mechanism of Organic Cosolvent Inactivation in Heme Monooxygenase P450 BM-3. Journal of the American Chemical Society 129:5786-5787.

- Kulakova AN, Larkin MJ, Kulakov LA. (1997) The plasmid-located haloalkane dehalogenase gene from Rhodococcus rhodochrous NCIMB 13064. Microbiology. 143:109-15.
- Li C, Tan T, Zhang H, Feng W. (2010) Analysis of the Conformational Stability and Activity of Candida antarctica Lipase B in Organic Solvents. Journal of Biological Chemistry. 285:28434 -28441.
- Lindahl E, Hess B, van der Spoel D. (2001) GROMACS 3.0: A package for molecular simulation and trajectory analysis. J Mol Mod. 7:306–317.
- Goto M, Kamiya N, Miyata M, Nakashio F. (1994) Enzymic Esterification by Surfactant-Coated Lipase in Organic Media. Biotechnol. Prog. 10 (3):263–268.
- Maurel P. (1978) Relevance of dielectric constant and solvent hydrophobicity to the organic solvent effect in enzymology. J. Biol. Chem. 253:1677-1683.
- Marek J, Vevodova J, Smatanova IK, Nagata Y, Svensson LA, Newman J, Takagi M, Damborsky J. (2000) Crystal structure of the haloalkane dehalogenase from Sphingomonas paucimobilis UT26. Biochemistry. 39:14082-14086.
- Newman J, Peat TS, Richard R, Kan L, Swanson PE, Affholter JA, Holmes IA, Schindler JF, Unkefer CJ, Terwilliger TC. (1999) Haloalkane dehalogenases: structure of a Rhodococcus enzyme. Biochemistry, 38:16105-16114.
- Nagata Y, Hynkova K, Damborsky J, Takagi M. (1999) Construction and characterization of histidine-tagged haloalkane dehalogenase (LinB) of a new substrate class from a gamma-hexachlorocyclohexane-degrading bacterium, Sphingomonas paucimobilis UT26. Protein Expression and Purification. 17. 299-304.
- Oakley AJ, Klvana M, Otyepka M, Nagata Y, Wilce MC, Damborský J. (2004) Crystal structure of haloalkane dehalogenase LinB from Sphingomonas paucimobilis UT26 at 0.95 A resolution: dynamics of catalytic residues. Biochemistry. 2004 Feb 3;43(4):870-8.
- Oberbrodhage J, Morgner H, Tapia O, Siegbahn HOG (1997) Molecular dynamics simulation of the free surface of liquid formamide. Int. J. Quantum Chem. 63: 1123–1131.
- O'Daly JP, Crumbliss AL, Henkens RW. (1990) Activity of carbonic anhydrase immobilized on porous silica beads in organic media. Biotechnol. Appl. Biochem. 12: 11-19.
- Ollis DL, Cheah E, Cygler M, Dijkstra BW, Frolow F, Franken SM, Harel M, Remington SJ, Silman I, Schrag J, Sussman JL, Verscheuren KHG, Goldman A. (1992) The alfa/beta hydrolase fold. Protein Engineering. 5:197-211.
- Prokop Z, Oplustil F, DeFrank J, Damborsky J. (2006) Enzymes fight chemical weapons. Biotechnology Journal. 1.1370-1380.
- Pieters RJ, Spelberg JHL, Kellog RM, Janssen DB. (2001) The enantioselectivity of haloalkane dehalogenases. Tetrahedron Letters. 42:469-471.
- Prokop Z, Sato Y, Brezovsky J, Mozga T, Chaloupkova R, Koudelakova T, Jerabek P, Stepankova V, Natsume R, van Leeuwen JG, Janssen DB, Florian J, Nagata Y, Senda T, Damborsky J. (2010) Enantioselectivity of haloalkane dehalogenases and its modulation by surface loop engineering, Angew Chem Int Ed Engl. 49(35):6111-5.
- Poelarends GJ, Zandstra M, Bosma T, Kulakov LA, Larkin MJ, Marchesi JR, Weightman AJ, Janssen DB. (2000) Haloalkane-utilizing Rhodococcus strains isolated from geographically distinct locations possess a highly conserved gene cluster encoding haloalkane catabolism. Journal of Bacteriology. 182:2725-2731.

- Ruth M. Lynden-Bell, Simon Conway Morris, John D. Barrow, John L. Finney, Charles Harper, Water and Life: The Unique Properties of H2O. CRC press, New York, 2010
- Ribeiro AAST, Horta BAC, and Alencastro RB. (2008) MKTOP: A Program for Automatic Construction of Molecular Topologies. J. Braz. Chem. 19(7);1433-1435.
- Roccatano D, Wong TS, Schwaneberg U, Zacharias M (2006) Toward understanding the inactivation mechanism of monooxygenase P450 BM-3 by organic cosolvents: a molecular dynamics simulation study. Biopolymers. 83:467-476.
- Simonson T, Brooks LC (1996) Charge Screening and the Dielectric Constant of Proteins: Insights from Molecular Dynamics. J. Am. Chem. Soc. 118:8452-8458.
- Schmitke JL, Stern LJ, Klibanov AM (1998) Organic solvent binding to crystalline subtilisin1 in mostly aqueous media and in the neat solvents. Biochem. Biophys. Res. Commun. 248:273-277
- Sato Y, Monincova M, Chaloupkova R, Prokop Z, Ohtsubo Y, Minamisawa K, Tsuda M, Damborsky J. (2005) Two rhizobial strains, Mesorhizobium loti MAFF303099 and Bradyrhizobium japonicum USDA110, encode haloalkane dehalogenases with novel structures and substrate specificities. Applied and Environmental Microbiology. 71:4372-4379.
- Veronika Štěpánková, Morteza Khabiri, Jan Brezovský, Antonín Pavelka, Babak Minofar, Rudiger Ettrich, Radka Chaloupková, Jiří Damborský (2011) Molecular mechanisms of haloalkane dehalogenases activation and inhibition by water-miscible organic solvents Proc. Natl. Acad. Sci. U.S.A. submitted
- Tejo BA, Salleh AB, Pleiss J (2004) Structure and dynamics of Candida rugosa lipase: the role of organic solvent. J Mol Model. 10(5-6):358-66.
- Tanford, C. The Hydrophobic effect: Formation of Micelles and Biological Membranes, Wiley, New York, 1980.
- Trodler P, Pleiss J (2008) Modeling structure and flexibility of Candida antarctica lipase B in organic solvents. BMC Struct. Biol 8:9.
- Vermue M.H., Tramer J. (1995) biocatalysis in non-conventional media: Medium engineering aspects. Pure & Appl. Chem. 67(2):345-373,
- Vazquez-Duhalt R, Semple KM, Westlake DWS, Fedorak PM. (1993) Effect of water-miscible organic solvents on the catalytic activity of cytochrome c. Enzyme Microb. Technol. 15:936-943.
- William L, Jorgensen DS. Maxwell, and Julian Tirado-Rives. (1996) Development and Testing of the OPLS All-Atom Force Field on Conformational Energetics and Properties of Organic Liquids J. Am. Chem. Soc. 118:11225-11236.
- Yurii PP, Bernd M.R. (1995) Structure and dynamics of liquid formamide Chemical Physics. 190:61-82.

Part II

Kv1.3 CHANNEL

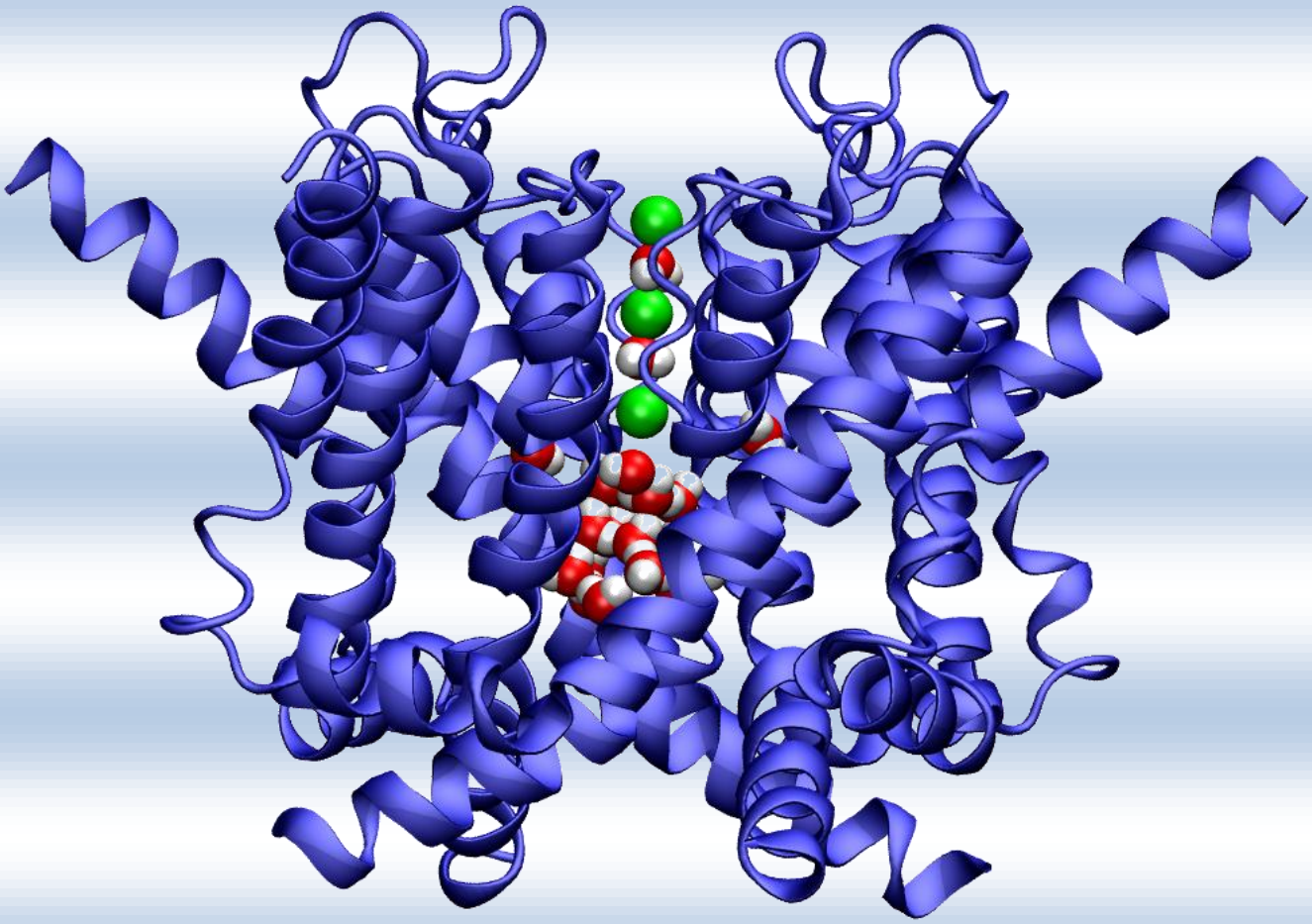

CHAPTER 3

The role of sterically constrained beta branched residues and charybdotoxin interaction in voltage gated potassium channels

3.1 Introduction

3.1.1 Membrane

A biological membrane is a biomolecular layer of lipids which protect cells from environment. It plays as a permeable barrier to exchange the essential molecules like water, ions, glucose, and lipids from environment with the wasted metabolism products inside the cell. Even though the cell membrane is penetrable to many molecules but still the high dielectric constant of lipid bilayers restrict the exchange of ions through it and thus makes it extremely slow (Parsegian., et al. 1969). Hence, existence of transporters and ion channels as a conductive pathway could dominate the lack of this property as rate limiting step. Therefore, selective permeability of the plasma membrane makes the cell to keep a constant pH ~7 and internal ionic composition (Lodish., chapter 5, 2003)

3.1.2 Ion channels

Ion channels are a class of integral membrane proteins which act as selective passage of specific ions through the cell membrane (Alberts et al., 1996). They are very sensitive to chemical and physical stimuli and once they receive such signal they can open to select the ions and close to prevent their passage. For this reason they are very important in different physiological processes like Cardiac contraction, neural transmission, temperature sensing, insulin release, regulation of apoptosis, cellular pH and oxidative stress, and etc (Hille., 1992). In addition to be selective to ions, they are able to distinguish the ions like K^+ vs Na^+ from each other. Different electrostatic potential between internal and external sides of the cell membrane makes the force to passage the ions through the membrane and as a result, ions channels became the fastest biological devices that able to pass up to 10^8 ions per second (Hille., 1992; Catterall et al., 1995; Jan and Jan., 1997). Ion permeation from extra cellular to intra cellular has several steps. First, ions diffuse from solution towards channel mouth.

Second, ions dehydration occurred after being trapped by amino acids in channel mouth. Third, the ions passed through the pore, and finally, after passage through the pore they will again solvated by the water molecules on the other side of the pore.

3.1.3 Voltage-gated potassium channels

Potassium channels are a species of ion channels which are found in both excitable and non-excitable cells (Shieh et al., 2000). They have a significant role in many cellular process such as controlling the electrical behavior of cell membrane, action potential, cell proliferation (Wonderlin and Strobl., 1996), apoptosis (Burg et al., 2006), hormone secretion and etc (Bauer and Schwartz., 2001). There are different types of K^+ channels which one of them is called Voltage-dependent potassium channels. These types of K^+ channels have a gating mechanism which put the channel 2 different state; opening as activation state and closing as deactivation state. These channels by having this specific king of property are able to control the K^+ ions current in respond to different stimuli including changes in membrane potential, intracellular biochemical ligands, temperature, and mechanical stretch. Channel opening or activation is caused by changes in membrane potential, concentration of specific ligands. When the stimuli removed, channel goes to closing or deactivation state. The rate of both opening and closing state is controlled by different voltage or concentration. Although the factors which affect these two states are known in detail but still the mechanisms that make the differences in the rate of activation and deactivation are not known. In addition to these two state K^+ channels have a process called inactivation. In this state channel stops conducting in the presence of activating stimulus. There are two type of inactivation including N-type (or fast) and C-type (or slow) inactivation (Choi et al., 1991; Hoshi et al., 1991) N-type inactivation which exist in few type of K^+ channels, happen in first several milliseconds of a strong depolarization. The reason that it called N-type inactivation is that the amino (N) terminus of the channel is involved in this process. The N-terminal ‘peptide ball’ occludes the pore from the internal side of the channel. Removal of the N-terminal particle uncovered a slower type of inactivation (Hoshi et al., 1990; Zagotta et al., 1990). On the other hand, C-type which occurs in almost all channels, is associated with the region closed to the selectivity filter and outer vestibule of the channel. C-type inactivation is sensitive to many factors such as the permeate ion species, several mutations in the selectivity filter, in the upper part of S6 and in the pore helix (López-Barneo et al., 1993; Cordero-Morales et al., 2006; Rauer and

Grissmer., 1999; Panyi et al., 1995; De Biasi et al., 1993). The reason that they called C-type inactivation is because the structural part involved in this process were located more toward the carboxyl (C) terminus of the channel than those involved in N-type inactivation (Choi et al., 1991) (Figure 3.1). KcsA was the first crystal structure of the potassium channels that was solved by Doyle et al in 1998. This potassium channel has a simplest structure among the rest of the K^+ channels.

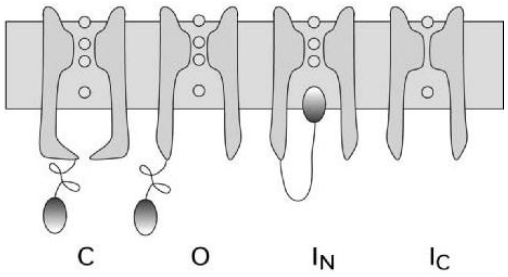

Figure 3.1. Schematic view of four channel states, closed state (C), open state (O), N-type inactivated (IN) and C-type inactivated (IC) (B) (from chung et al., 2006).

Thus it is a good candidate to representation of the conduction pathway of all K^+ channels. This channel consists of only two transmembrane domains. After that, Long et al in 2005 and follow that chen et al in 2010 solved the larger K^+ channel structures namely Voltage-dependent potassium ion channels (Kv1.2 channels). This event opens a new door in mechanistic investigations of the Kv channels. Almost all conduction pathways are now designed and interpreted in light the of the structure of these two channels. The crystal structure revealed that, the voltage-gated potassium channel (Kv) channel is a homotetrameric with four voltage sensors and one central pore domain (cavity). Figure 3.2A shows the secondary structure of Kv channels. Each subunit has four transmembrane helices labeled as S1, S2, S3, and S4. These four domains build a voltage-sensor domain and have main role in sensing the voltage. Among them, S4 domain contains a series of positively charged amino acid residues, mainly arginine, and is the first helix which responsible for sensing changes in voltage (Aggarwal et al., 1996; Seoh et al., 1996).

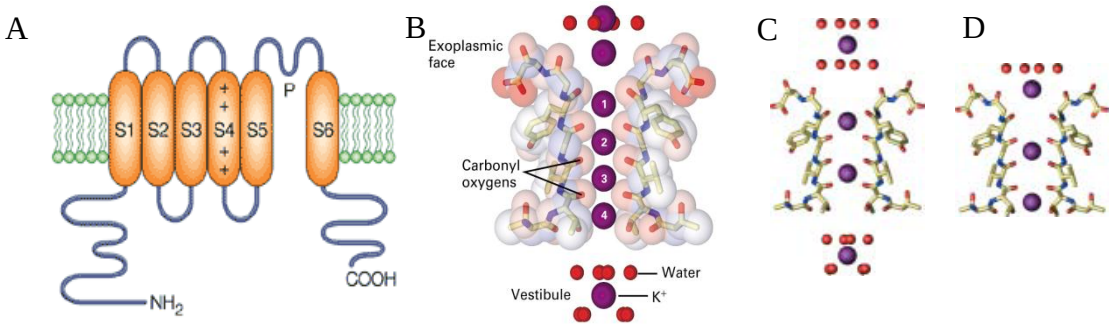

Figure 3.2. General secondary structure of K^+ channels, (A) (from Choe et al., 2005), The position K^+ ions inside the selectivity filter a K^+ channel, (B), two mechanisms for K^+ conduction through the selectivity filter, (C, D), (from Lodish et al, 6th edition, chapter 7).

The other two transmembrane helices S5 and S6 make the central pore domain. These two helices are connected by a P (pore) loop, form the selectivity filter, and outer vestibule of the channel. Selectivity filter forms the narrow region of the conduction pathway to passage and select the K^+ ions over the other dominant monovalent ions like Na^+. Amino acids in the selectivity filter region (TVGYG) are highly conserved among K^+ channels and it used as signature for the identification of K^+ channel coding genes (Heginbotham., et al 1994; Schlegel., et al 1982; Jiang et al., 2002; Kuo et al., 2003; Long et al., 2007; Zhou et al., 2001). These amino acids have a special arrangement in such a way that the backbone carbonyl groups point towards the center of selectivity filter. This property has been shown to allow the dehydration of small cations, which are strongly solvated by water molecules in the solution (Zhou et al., 2001).

There are four binding site inside the selectivity filter containing S0, S1, S2, S3 and S4. During the passage of K+ ions the selectivity filter is occupied by two or three K+ ions with one water molecule between them. Based on the crystal structure of KcsA (Figure 3.2B), (Zhou et al., 2001; Bernèche et al., 2003), there are two mechanisms for K^+ conduction through the selectivity filter. In the first mechanism K+ ions in the selectivity filter between two equally occupied sites 1 and 3, separated by a water molecule at site 2 and the second mechanism K+ occupied sites 2 and 4 with a water molecule at site 3. Inbetween higher resolution diffraction shows a new state which called intermediate state. In state include the third ion in S0 position [0, 2, 4] (Figure 3.2C), (Bezanilla et al., 2000; Sigworth et al., 1994; Jiang et al., 2003; Long et al., 2005; Long et al., 2005)

3.1.4 The Kv1.3 Voltage-Gated Potassium Channel

The Kv1.3 channel, a *Shaker*-related voltage-gated potassium channel is a member of a large family of mammalian potassium channels (Gutman et al., 2005; Yu et al., 2005). The channel may play a role in multiple sclerosis and autoimmune diseases due to its effect on T-lymphocytes (Beeton et al., 2005). This channel, like most voltage-gated potassium channels, is composed of four subunits, which are symmetrically arranged around the central pore. Each subunit is formed by connecting the voltage-sensing module (S1-S4) to the ion permeation

module (S5-P-S6) (Figure 3.2A). The fourth transmembrane segment (S4) with a conserved structural motif acts as a voltage sensor. Upon depolarization, positive charges in this motif move from “inside” to “outside”. As a consequence of this conformational change the intracellular bundle crossing can change to trigger pore opening or activation and the reverse process named deactivation or closing the channel (Yellen et al., 2002; Bezanilla et al., 2000; Lee et al., 2009). Some recent studies indicated a network of interactions behind the selectivity filter. It seems this network has supportive effects on stabilization of the open state in some potassium channels. Disruption or weakening of this network by mutations had destabilizing effects on the selectivity filter that were followed by the facilitation of slow inactivation (Cordero-Morale et al., 1997). This typical intrinsic C-type inactivation and the high efficiency block by scorpion peptide toxins make it easy to distinguished the Kv1.3 wild type channel from other voltage-gated potassium channels (Gutman et al., 2005). Thermodynamic mutant cycle analysis was used to identify the interacting pairs of residues between the toxin and the channel (Hidalgo 1995). Moreover, topological studies also provide the possible interaction points between toxins and potassium channels (Aiyar et al., 1995). All these data together show that, peptide blockers belonging to the α-KTX family have a triangular interacting surface with the potassium channels. Hereby, the conserved amino acid Lys (K27 in ChTX) in the center of this surface protrudes into the channel pore. Several positively charged and aromatic amino acids (Arg, Lys, and Tyr) around the central Lys can interact with channel residues stabilizing toxin-channel binding (Aiyar et al., 1995; hidalgo et al., 1995; Mackinnon et al., 1990).

3.1.5 Kv1.3 voltage-gated potassium channel blockers

It has been shown that Kv1.3 channels have crucial role in modulating immune system functions by specific blockers as therapeutic components in of stroke, epilepsy, and cardiac arrhythmias (Chandy et al., 1984; DeCoursey et al., 1984; Lewis and Cahalan, 1988). Scorpion toxin peptides are one kind of the blockers which are able to block the ion passage through Kv1.3 channel by physically occluding the pore. Two of scorpion toxins which strongly block Kv1.3 channels are ChTX (Charybdotoxin) and MgTX (margatoxin). The ChTX consists of 37-amino acid which is isolated from the venom of the scorpion Leiurus quiquestratus (Miller et al., 1985). It was the first toxin shown to block voltage-gated channel and Ca2+ activated K^+ channel (IKCa1) of lymphocyte cells with higher affinity in compare to other blockers (Grissmer et al., 1993; Sands et al., 1989). It blocked Kv1.3 currents and suppressed lymphocyte proliferation at nanomolar concentrations (Freedman., 1992; Price.,

1989). Since ChTX blocked both Kv1.3 and IKCa1 channels, it was not clear that which channel is involved in the activation process. For this reason other blocker function were compared to ChTX in order to find out its selective role. Among other toxins, MgTX, were discovered as selective for Kv1.3 over IKCa1 and it shows that it is able to depolarize resting T-cells and prevent their activation similarly to ChTX. This observation proved that in resting T-cells the membrane potential is fixed by Kv1.3 channels and the role of IKCa1 channels in this function is negligible (Leonard et al., 1992). MgTX is a 39-residue peptide with 44% sequence identity to ChTX (Bruce et al., 1994) (Figure 3.3). The specificity of ChTX and MgTX to Kv1.3 channels and 1:1 interaction between Kv1.3 and theses two toxins, make them very good candidate to use as probes to investigate and study the function and structural properties of this channel. The results could provide useful information for the design of more specific and potent drugs with potential therapeutic use. The ChTX was used in this study to explore the binding site of hKv1.3, a channel that plays an important role in T-cell activation and B-cell differentiation (Chandy et al., 1984; DeCoursey et al., 1984; Wulff et al., 2004)

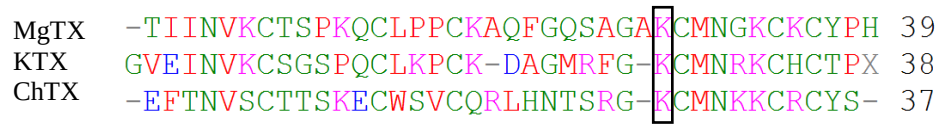

Figure 3.3. Sequence alignment of MgTX, KTX, and ChTX. K28 in MgTX, K27 in KTX and ChTX are the key residues to block the pore (black box).

3.1.6 Aim of the present work

In the present study a novel effect of scorpion toxins on the hKv1.3_V388C mutant channel was discovered. Recent work revealed that C-type inactivation depends on side-chain volume in the vicinity of the selectivity filter (Hamil et al., 1981), but the detailed structural mechanisms underlying this steric effect are not completely clear. The present work exploits the finding that the V388C mutation in the pore helix accelerates channel inactivation but can be partially reverted by the nearby mutation H399T. The first mutation alters the effect of toxins on blocking the pore changed. Instead, the toxins impede the inactivation of the mutant channel. Molecular dynamics simulations demonstrated that the structural features of this mutation enable some toxins to act as inactivation gating modifier. These findings suggested that structure-activity relationships in the regions flanking the pore may be complex.

This part of the thesis is focused on the details of Kv1.3 wild type and mutant channels, ChTX structures, and the interaction between these toxins with the channel. Mutations, homology modeling, docking, free energy calculations, and molecular dynamics (MD) simulations were applied to study the molecular mechanisms of the structural changes, ionic permeation, ion selectivity, and toxin binding. Using a molecular model of the channel embedded in a membrane-mimicking environment, the functional and dynamic properties of the channel were investigated, taking into account the full complexity of the protein, toxins, ions and water interactions.

Three main issues are addressed by the present study:

1. Molecular dynamics simulations and electrophysiology data are used to elucidate the role of these residues flanking the selectivity filter, suggesting a mechanism that relies on the steric constraints inherent to beta-branched side-chains.

2. The interactions of ChTX with the channel are described in detail, including binding, exposure mode and their differences between hKv1.3 wild type and mutants.

3. Fundamental aspects of ChTX-hKv1.3 interaction, and binding free energy during the unbinding process, are studied in detail, with particular focus on the effect of bath solutions to correlate the results with experimental electrophysiology data.

Chapter 3.2

Material and methods

3.2.1 Homology Modeling.

All available X-ray structures of K channels except for that of Kv1.2 are of bacterial homologues of mammalian channels. It is generally recognized that homology modeling of proteins is the most accurate method to predict 3D structure for molecular dynamic simulation and mechanism investigation (Li et al., 2007; Ginalski et al., 2006). Thus, in the absence of an experimentally determined crystal structure, homology modeling could provide a reasonable 3D structure. Both mouse and human Kv1.3 (mKv1.3 and hKv1.3) voltage gated potassium channels have high sequence identity with Kv1.2 potassium channel, which supports the suitability of generating a three-dimensional model of the voltage gated hKv1.3 potassium channel for structural analysis, molecular dynamics and docking studies. Primary structures of human Kv1.3 (hKv1.3), mouse Kv1.2 (mKv1.2) were aligned using CLUSTAL W version 1.83 (Thompson et al., 1994) (Figure 3.4A). The sequence alignment shows 94% sequence identity and contains no gaps. All-atom homology models of the mKv1.3 S4/S5/S6 domains were generated using as a template the crystal structure of Kv1.2 (PDB: 2A79) with 2.9 Å resolution. Several three-dimensional models of the tetrameric S4/S5/S6 module of hKv1.3, including all non-hydrogen atoms, were then built and examined by the Modeller 9v2 package (Fiser et al., 2003). The tertiary structure models were checked with Procheck (Laskowski et al., 1993) and the most favored was selected as the final model. The Φ, Ψ torsion angles of 89.8% of the residues had values within the most favored areas and 8.9% of the residues had values within additionally allowed regions of the Ramachandran plot. No residues were found in disallowed regions. The overall g factor of the structures obtained showed a value of –0.37. The g factor should be smaller than –0.5 and values greater than –1.0 require further investigation. It has been shown that there is a strong correlation between the percentage sequence identity between two proteins and the similarity of their three-dimensional structures (Chothia et al., 1984). Previously, several homology models for Kv1.3 based on the crystal structure of KcsA were reported (Yu et al., 2004). However, the 30.93% sequence identity and 62.89% similarity between KcsA and Kv1.3 is expected to limit the accuracy of the sequence alignment and the resulting homology model. In general, it can be difficult to obtain a good homology model when the percentage sequence identity is <30%. Therefore the work presented in this thesis represents an improved homology model of the structures of

mammalian and human homologues than those extrapolated from bacterial K^+ channel structures.

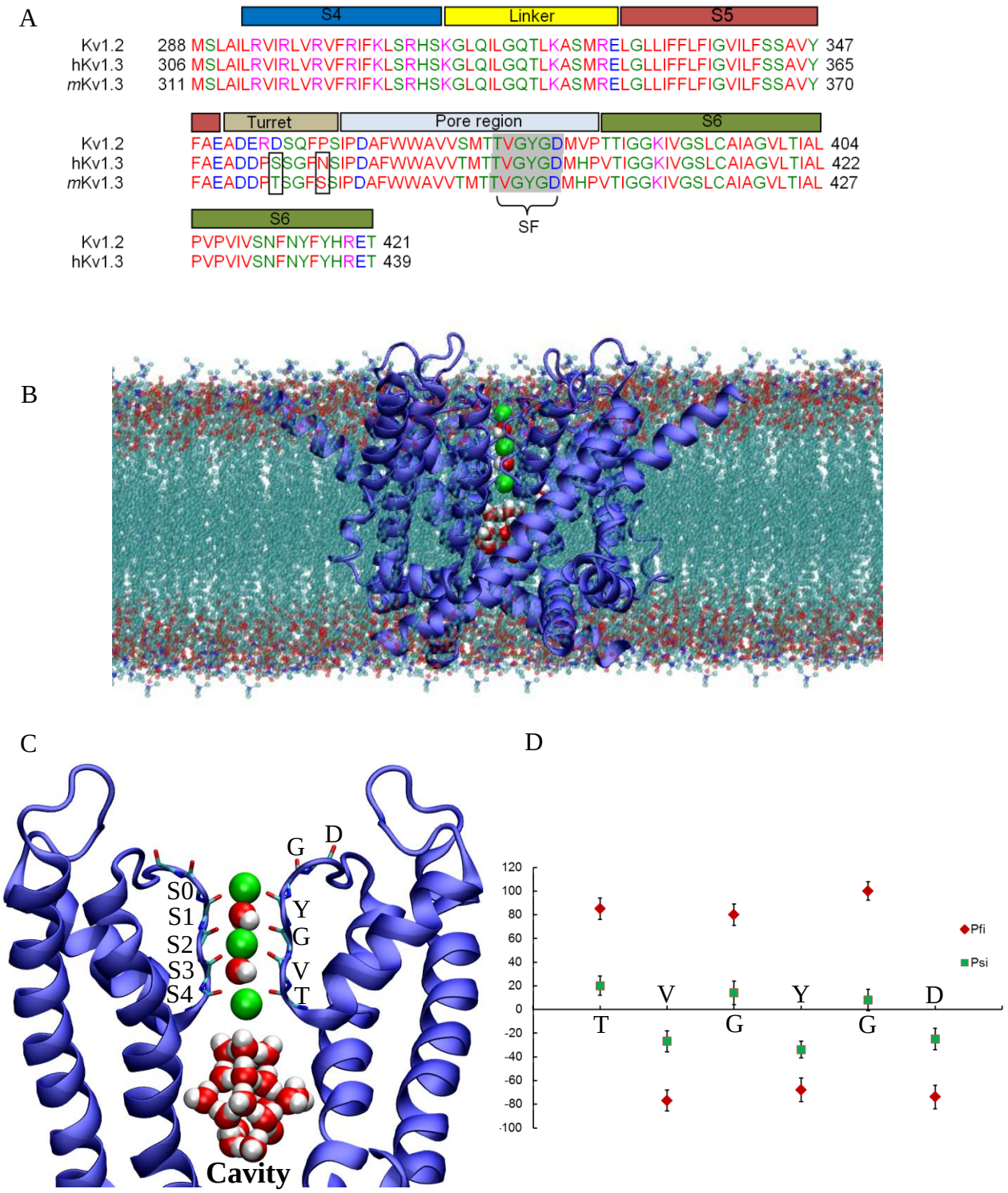

Figure 3.4. Sequence alignments of Kv1.2, hKv1.3, and mKv1.3 (A). The view of *h*Kv1.3 model embedded in POPC membrane (B). K^+ ions placed at S0, S2, and S4 position in selectivity filter with water molecules between them at position S1 and S3. The cavity filled with water molecules (C). Dihedral angles Phi and Psi of selectivity filter residues (D).

3.2.2 Constructing mutated channels

After making a reasonable homology model for hKv1.3 based on mKv1.2, mKv1.3 model structure was also constructed by introducing mutations at the few amino acids that differ between hKv1.3 and mKv1.3. In addition to mKv1.3 wild type three hKv1.3 mutant systems also were built by this method, including:

a. hKv1.3_V388C, point mutation at position 388 (valine to cysteine)

b. hKv1.3_H399N, point mutation at position 399 (histidine to asparagine)

c. hKv1.3_V3889_H399T, double mutation at positions 388 (valine to cysteine) and 399 (histidine to threonine)

All mutations were constructed in YASARA (Krieger et al., 2002, 2004).

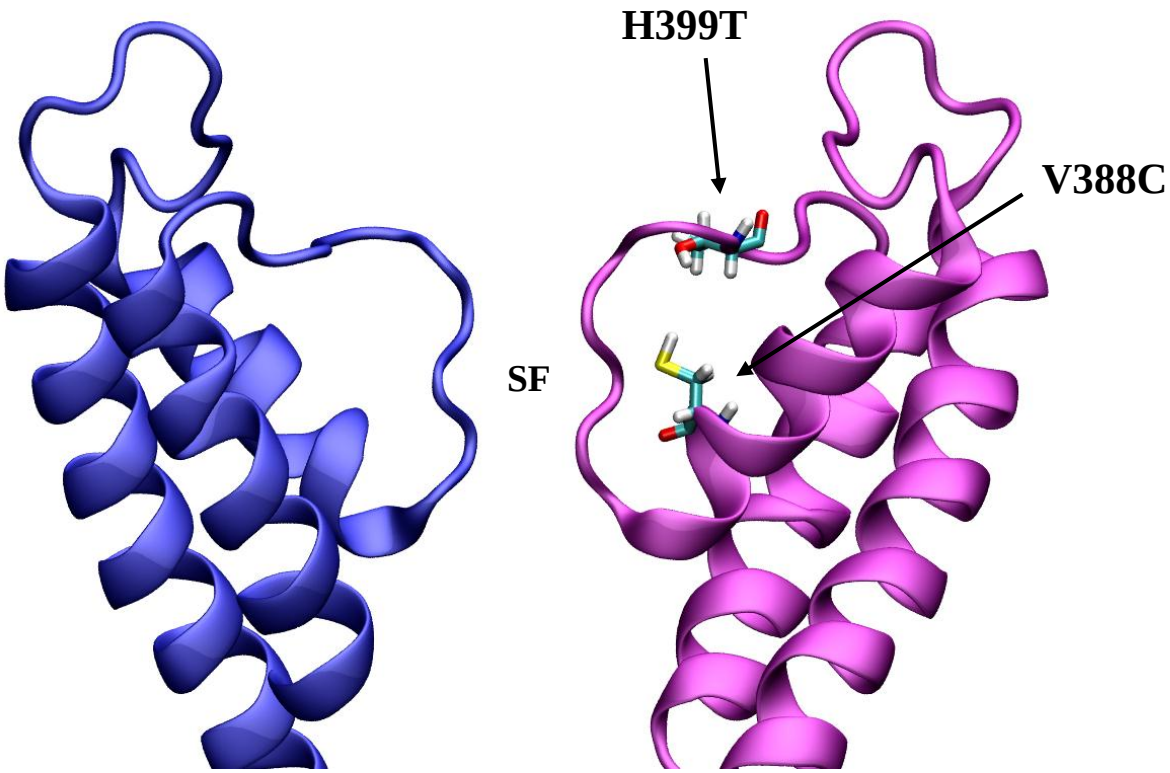

Figure 3.5. Point mutations in hKv1.3 structure; hKv1.3_V388C and hKv1.3_V388C_H399T.

3.2.3 Docking of ChTX scorpion toxins to mKv1.3 and hKv1.3 wild type and mutants

The NMR structures of ChTX (PDB ID: 2CRD) was used. The conformation of mKv1.3 and hKv1.3 wild type, single, and double mutants resulting from 30-40 ns molecular dynamics simulations was chosen as the initial structure for docking. Both toxins were docked into the equilibrated model structures using AutoDock 4.0 (Morris et al., 1998) as implemented in YASARA Structure (Krieger et al., 2004 and 2002) (Figure 3.6). Solvent and lipids were removed from the system. Docking of ChTX with the model structures of mKv1.3 and hKv1.3 was achieved by positioning two contacts in accordance with the data of Aiyar et al. (1995): the side chain of Lys27 in ChTX in its extended conformation was placed into the central axis of the pore, and the side chain of Arg25 was placed in close steric contact with the carboxyl group of Asp381 and Asp397 of one of the subunits. The final docked results were compared to previously report docking results of ChTX with Kv1.3 model (Yu et al., 2004) and found to be in good agreement. The final channel-toxin complexes were then embedded into the POPC bilayer as described in following section. All three systems were then solvated and 21 chloride counter ions were added to neutralize the system. Since the presence of K^+ ion inside the selectivity filter (SF) will affect the conformation of bound toxins, K^+ was removed from SF (Chen et al., 2009). However, it was shown that in the presence of ChTX a single potassium cation occupies the S4 position in the SF (Yu et al., 2005; chen et al., 2009).To mimic the effect of potassium on SF structure, a harmonic constraint with a force constant 2.5 Kcal/mol.$Å^2$, corresponding to the force of K^+ inside the SF (Furinia et al., 2009), was used to restrain C-alpha of TVG aminoacids, equivalent to S4 position, in the selectivity filter.

3.2.4 Inserting the channel and toxin-channel complex into POPC membrane

The tetrameric channel structure was embedded into a preequilibrated palmitoyloleoyl phosphatidycholine (POPC) bilayer containing 512 phosholipid molecules following a new method, INFLATEGRO (Kandta et al., 2004), that relies on placing the lipids and protein on a widely spaced grid and then 'shrinking' the grid until the desired density is reached (Figure 3.4B). The bilayer was based on the 128-lipid bilayer kindly provided by DP Tieleman

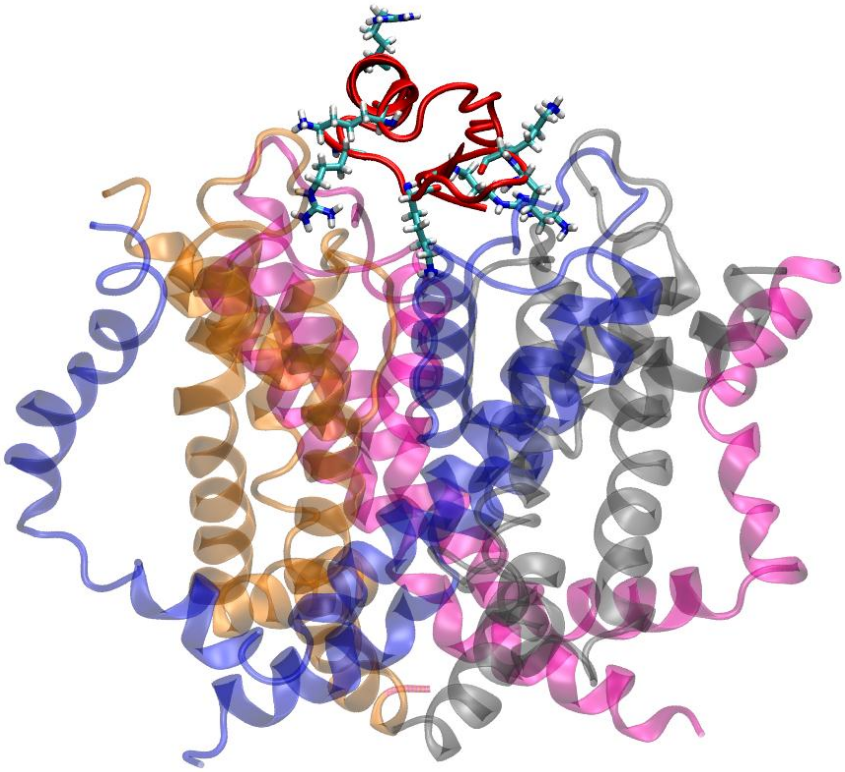

Figure 3.6. The last snapshot of docked ChTX with hKv1.3 channel after 35ns equilibration.

(Tieleman et al., 2006). The procedure used GROMACS 4.0.7 (Berendsen et al., 1995, Lindahl et al., 2001) with the all-atom force field OPLSAA (Jorgensen et al., 1996) adapted for POPC lipids using parameters based on those by Berger et al. (Berger, O et al 1997) and Marrink et al. (Marrink, S. J 1998). During the procedure most of the structure of the bilayer stays intact, reducing equilibration time and the resulting 498 lipids are neatly packed around the protein. In a second and third copy of the final embedded structure the two single mutants hKv1.3_V388C and hKv1.3_H399N and the double mutant hKv1.3_V3889_H399T were constructed in YASARA (Krieger et al 2002, 2004). Before solvating the final structures three potassium ions were placed inside the selectivity filter in exactly the positions found in the crystal structure at sites S0, S2, and S4. Water molecules were placed at site 1 and 3 as described (Morten Ø et al 2010, Hellgren et al 2006) (Figure 3.4C). All three systems were solvated in Simple Point Charge water molecules (Berendsen et al., 1981). For the central cavity the same water density as for the bulk is assumed (Capener et al., 2002). Potassium and chloride ions were added to reach a final salt concentration of 100-160 mM KCl and electric neutrality.

3.2.5 Molecular dynamics simulations

Simulations were performed by using GROMACS 4.0.7 software package (Berendsen 1995, Lindahl 2001) with an extended All Atom Optimized Potentials for Liquid Simulation (OPLSAA) (Jorgensen et al., 1996) force field. Molecular dynamics simulations were carried out in the NPT ensemble using a 2 fs time step and periodic boundary conditions. Initial velocities were assigned randomly applying a Maxwell distribution at 300 K. SETTLE (for water) and SHAKE (non-water) algorithms (Ryckaert et al., 1977) were used to constrain covalent bond lengths. Lennard-Jones and electrostatic interactions were cut off at 10.0 Å, and long-range electrostatic interactions were computed using the Particle-Mesh Ewald method (Essmann et al., 1995). The temperature was kept at 300 K by separately coupling the protein and solvent to an external temperature bath (ι= 0.1 ps). The pressure was kept constant at 1 bar by weak coupling (ι= 2.0 ps) to a pressure bath according to Parrinello-Rahman (Parrinello et al., 1981; Nos´e et al 1983) using semi-isotropic mode. The pressure was maintained with a compressibility of 4.6×10-5/bar.

3.2.6 Umbrella sampling and Potential of Mean Force (PMF) calculations

The free energy profile of ChTX unbinding was estimated employing the PMF method with umbrella sampling. The distance between the center of mass of ChTX and the membrane was sampled with roughly 0.05 nm spacing. A total of 26 windows, with an extra 10 windows to improve the sampling in selected regions, were collected. For each of these windows, the system was subjected to a 4 ns umbrella sampling MD simulation with the force constant of 50 kcal/mol/$Å^2$ applied to the center of mass of ChTX. Afterwards, the Weighted Histogram Analysis Method (WHAM) (Chodera et al 2007), which is included in the GROMACS suite, was employed to calculate the free energy profile of the unbinding of ChTX from the membrane protein

Chapter 3.3

Results and Discussion

3.3.1 Effect of point mutations on hKv1.3 wild type structure and ChTX-channel complex

Protein structure and flexibility are important determinants of function. Therefore, the effect of different mutation on the structure and flexibility of hKv1.3 channel protein was studied. Simulations were initiated using the model structure derived by homology with the Kv1.2 crystal structure. The protein structure relaxes during the simulation. Differences in the average structures of the channels in different media are quantified by calculating root mean square displacement (RMSD) between them. RMSD values between time-averaged structures for the structures of hkv1.3 and hkv1.3_V388C_H399N are relatively small, less than 2.3 Å (Figure 3.7A). In the case of hKv1.3_V388C the RMSD value is around 2.8 Å. Although the graph shows that the structure is stable after 17ns but still this value indicates the lack of significant structural differences in the protein backbones over a timescale of several nanoseconds. Thermal fluctuations lead to fluctuations in structure during the course of MD simulation. The extent of this structural flexibility is quantified by time-averaged RMSF values (Figure 3.7B). Individual residues from part of the trajectory in which the structure is already stable indicate the part of the enzyme which is influenced by mutation. Comparison of RMSFs of the backbone C_α atoms in wild type, single and double mutant channels implies changes flexibility of the selectivity filter in the single mutant. All three channels show a common single peak which associated with the turret region and N-terminus of the pore helix (Figure 3.7B, red circle). The large peak indicating that the positions of the residues in this area fluctuate highly. In addition, there is another peak in RMSF that corresponding to high fluctuations of the selectivity filter in the single mutant channel (Figure 3.7D, black circled area). While the single mutant has prominent fluctuations around the mutation 388 and selectivity filter area, these two areas shift back to the wild type pattern by introducing the second mutation at position 399. Therefore we focused our attention more to the highly fluctuate regions. As shown previously a multipoint network behind the selectivity filter has a critical role in the conformational stability of the filter and modulation of the C-type inactivation (Cuello et al., 2010). Thus, attention was focused on the interactions in the same region, between residues Val388, Trp384, Asp397 and residues His399 and Pro400 that lie in

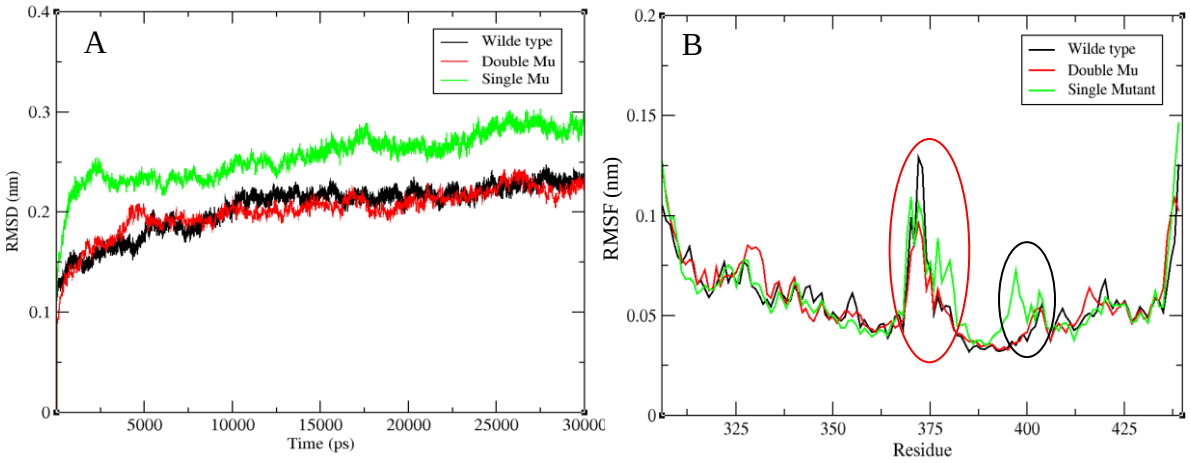

Figure 3.7. Root mean square deviation for Cα of the channel during the molecular dynamics before adding ChTX (A). Root mean square fluctuations in the equilibrated phase of the molecular dynamics simulation of *h*Kv1.3 in 100mM KCl. Wild type (black), double mutant (red) and single mutant (green). The black circle highlights the selectivity filter region and the red circle shows turret region. (B)

the P-loop and P-S6 linker in monomer D (Figure. 3.8). The first three residues make a triad network behind the selectivity filter. Valine has a hydrophobic contact with the indole ring of Trp384 in the pore helix, filling the space below the tryptophan by its methyl group which keeps the indole ring in a stacked position towards the valine. Moreover, because valine belongs to the beta-branched amino acids, it has limited rotameric possibilities that cause significant restrictions in the network behind the selectivity filter (Figure 3.8.A) (Carey et al., 2011; Dunbrack et al., 1993). This restriction orients the tryptophan ring to support a hydrogen bond between the indole nitrogen and the carboxyl group of Asp397. Asp397 is one of the key determinant residues in C-type inactivation, occupying a key position with its side chain located between the selectivity filter and pore helix (jager and grissmer 1998). Introducing the non β-branched amino acid cysteine instead of valine would permit flexibility and alter the network behind the selectivity filter (Figure 3.7B). In addition, the sulfhydryl group in the V388C mutation has a smaller volume and does not have any possibility for interacting with the Trp384 indole group. Therefore this free indole group can rotate and participate in a conformational change. As a result of this change its hydrogen bonding with Asp397 cannot be maintained and the side chain of Asp397 flips into the solvent and stays solvated (Figure 3.8B). The overall result of these changes is a more flexible selectivity filter (Figure 3.7B). In contrast, introducing the β-branched amino acid threonine at position 399 in

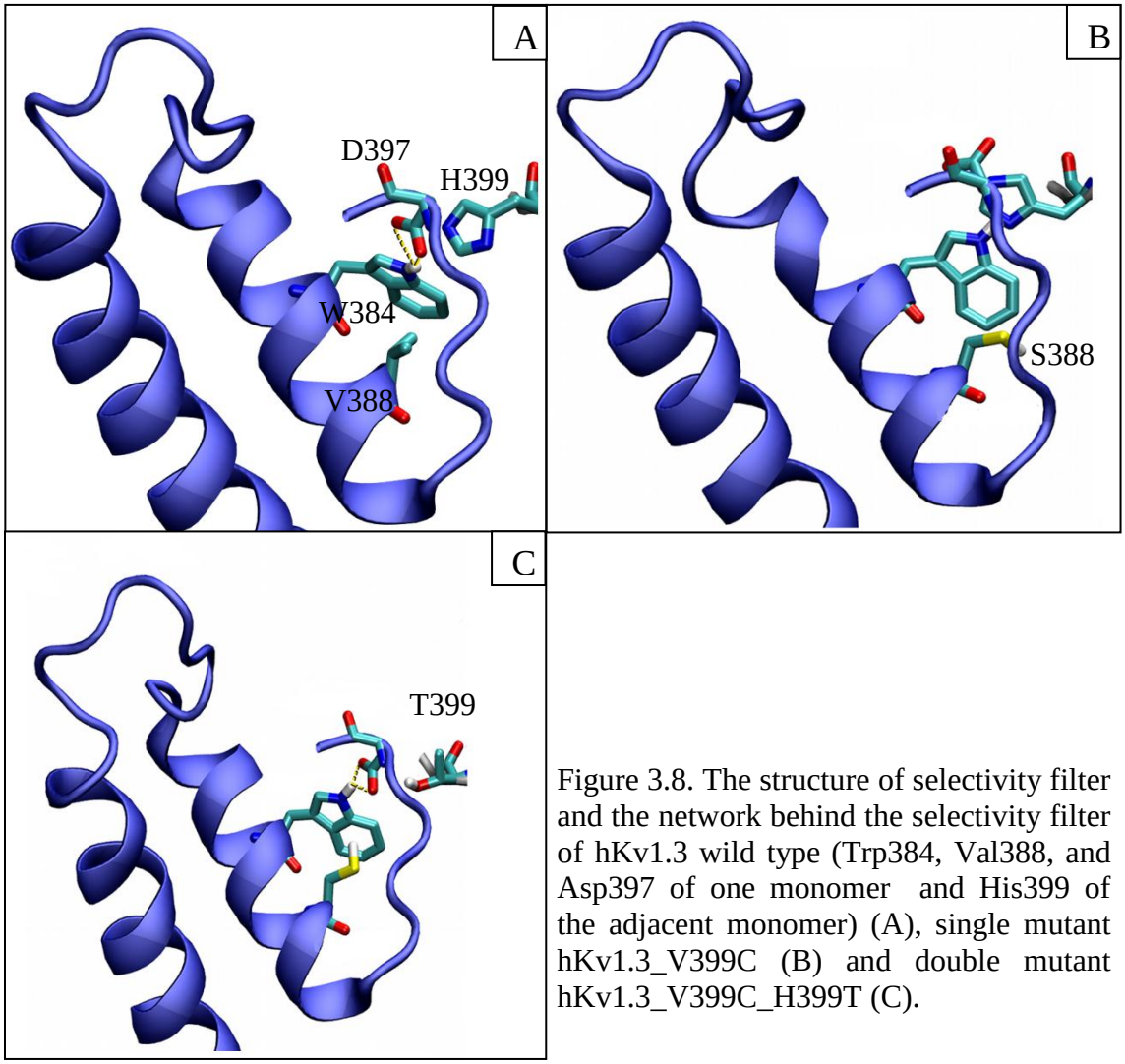

Figure 3.8. The structure of selectivity filter and the network behind the selectivity filter of hKv1.3 wild type (Trp384, Val388, and Asp397 of one monomer and His399 of the adjacent monomer) (A), single mutant hKv1.3_V399C (B) and double mutant hKv1.3_V399C_H399T (C).

The double mutant exhibited a completely different behavior, very similar to the wild type (Figure 3.8C). The simulation clearly showed that the methyl group of the Thr399 from the adjacent monomer has a strong hydrophobic contact with the $C_{\beta}H_2$ group of the Asp397. In addition, rotameric restriction of Thr399 as a β-branched amino acid acts as a steric hindrance preventing the conformational change of the Asp397 side chain toward the solution as observed in the single mutation. Consequently, the stabilized Asp397 carboxyl maintains its hydrogen bonding with Trp384 indole nitrogen as in wild type. This new interaction behind the selectivity filter restores the rigidity that was lost in the single mutant channel. Several lines of evidence have suggested that residues in the pore helix arrange a multipoint network behind the selectivity filter to modulate inactivation rate (Cordero-Morales et al 2011). Comparing inactivation rates of wild type, single and double mutant derived from experimental data shows a reasonable correlation with molecular dynamics information about network features behind the selectivity filter. Molecular dynamics results suggested that the

mutation at position 388 has an indirect effect on the outer part of the selectivity filter. As discussed above, this single mutation promotes to change the orientation of Asp397 side chain at outer pore while this phenomenon was not observed in wild type and double mutant.

3.3.2 Flexibility of the selectivity filter can affect toxin-channel interaction

Since the mutations change the network behind the selectivity filter, they may also affect hKv1.3 ChTX interactions. Thus, ChTX was docked to hKv1.3 wild type, hKv1.3_V388C, and hKv1.3_V388C_H399N mutants after 35 ns molecular dynamics simulation. ChTX completely occludes channels with its Lys27 residue. The RMSD of ChTX and channels are stable few nanoseconds after starting the simulation except for hKv1.3_V388C in which the RMSD of both channel and toxin is stable after 18 ns (figure 3.9A and B). The jump in the hKV1.3_V388C RMSD suggests a possible structural change. The molecular dynamics trajectory reveals that ChTX is stable until 18 ns and blocking the channel but after this time ChTX starts to tilt to one side of the channel and subsequently K27 does not block the selectivity filter. After tilting, water molecules can pass through the selectivity filer. In wild type and the double mutant, ChTX completely blocks the channel and no conformational change was observed (Figure 3.10A). The distance of ChTX K27 to residues Y395 and G394 of the selectivity filter was also measured, showing that ChTX-K27 is closer to the G394 carbonyl group than to T395 in the double mutant, whereas in hKv1.3 wild type it is very close to Y395 (Figure 3.9C). Measuring the distance between ChTX and the channel center of mass from the last 5ns of trajectories also shows that ChTX is sitting higher than on the hKv1.3 and to hKv1.3_V388C_H399T channels, which are almost the same (Figure 3.9D). To understand the reason for this difference the distances between the four monomers in the channels were measured (figure 3.10C). In the single mutant hKv1.3_V388C the selectivity filter loses its supporting network and becomes more flexible, allowing it to become wider and allowing ChTX-K27 to penetrate deeper. To visualize the differences for ChTX sitting in each channel, the ChTX-hKv1.3 complex structures were overlaid on each other (Figure 3.10A). ChTX sitting in wild type and double mutant is similar, while ChTX-hKv1.3_V388C shows a different configuration. Moreover, tilting of ChTX to one side of the channel allows three channel subunits to come closer to each other and to decrease their interaction to the fourth monomer. This phenomenon makes the fourth monomer more flexible, permitting deformation of the selectivity filter and causing the outer vestibule to lose its stability and

finally fold back (Figure 3.10 B). There is no interaction between ChTX and monomer A of the single mutant channel. Eventually, the tilt of ChTX, loss of the interactions with one monomer, and distortion of the SF. Detailed examination of the structure shows that the orientation of the outer vestibule is related to the deviation of the pore helix from its original conformation due to disruption of the amino acid network behind the selectivity filter (Figure 3.10C).

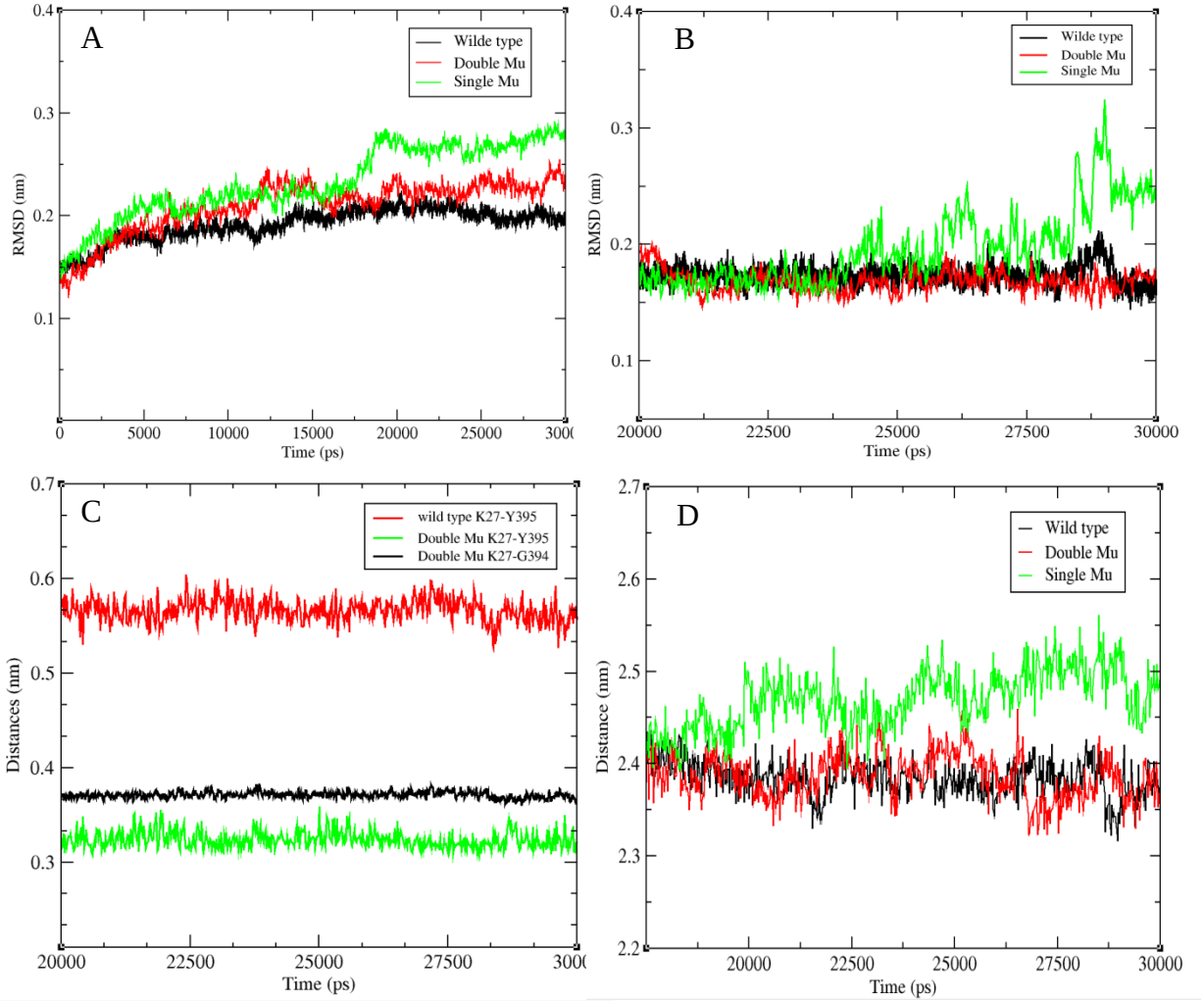

Figure 3.9. Root mean square fluctuations in the equilibrated phase of the molecular dynamics simulation of channel in complex with ChTX in 100 mM KCl. hKv1.3 wild type (black), single mutant hKv1.3_V388C (green), double mutant hKv1.3_V388C-H399T (red) (A). RMSD of ChTX Cα in complex with hKv1.3 wild type (black), single mutant hKv1.3_V388C (green), double mutant hKv1.3_V388C-H399T (red) (B). Distances of ChTX lysine 27 from tyrosine 395 in Kv1.3 wild type, black; tyrosine 395 in Kv1.3 double mutation, red; glycine 394 in Kv1.3 double mutation, green, over the last 10 ns of the simulations (C). Distances between ChTX toxin and the center of mass of the selectivity filter in hKv1.3 wild type, black; double mutation, red; single mutation, green, over the last 15 ns of the simulations (D).

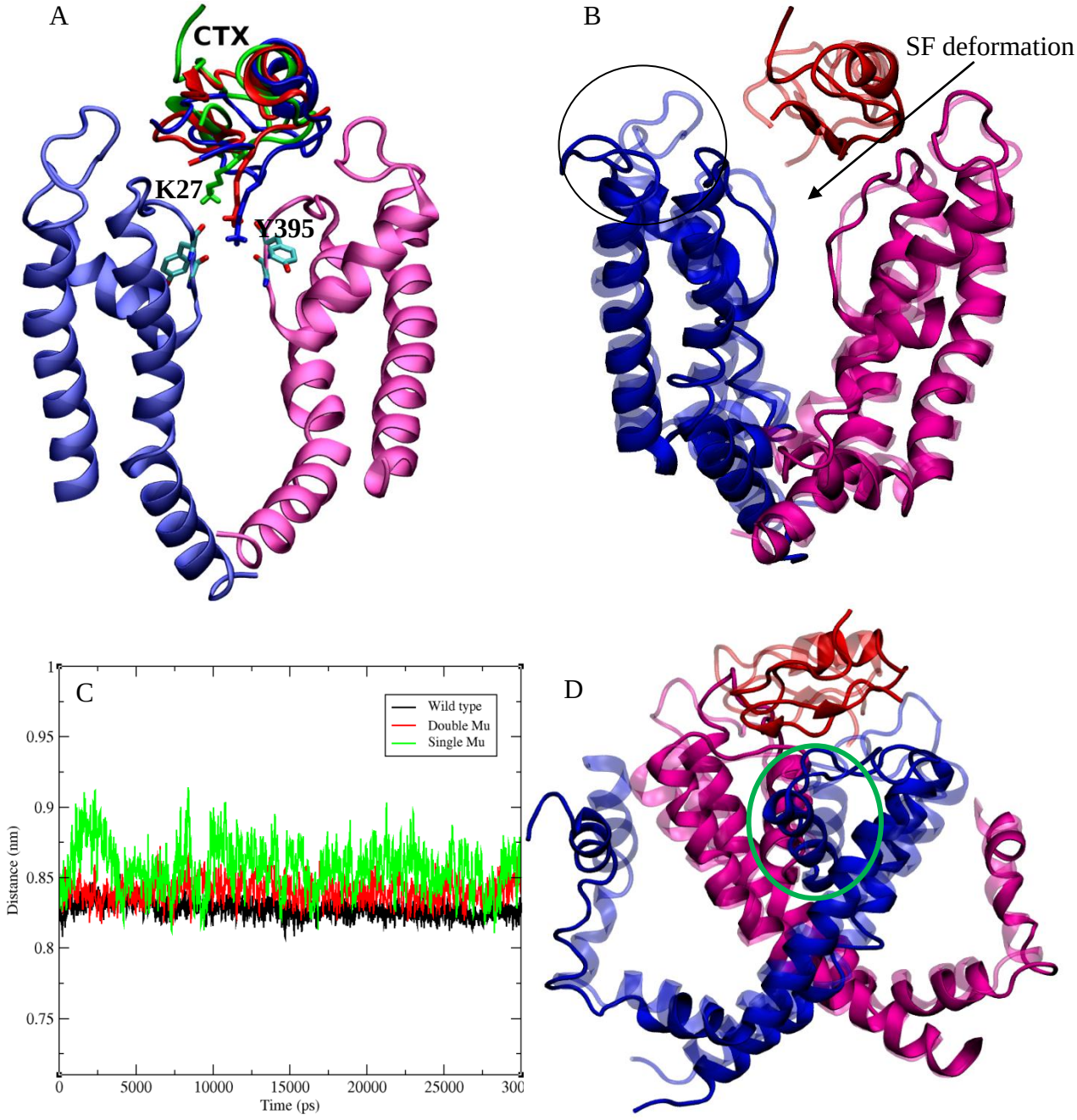

Figure 3.10. The position of the docked ChTX is shown for wild type in red, for the single mutant in green and for the double mutant in blue. Lys27 is shown in a skeletal representation. Only two monomers with omitted S4 helices and polar hydrogens are shown for clarity (A). Tilting of the docked ChTX toxin during the molecular dynamics simulation in the single-point mutant. Monomer A, blue, Monomer B, magenta, WT is shown transparent in the background for comparison. The change of toxin position observed in hKv1.3_V388C relative to its position in wild type. and deformation of SF and outer vestibule (black circle) in hKv1.3 single mutant (B). Average distances between the four monomers in Kv1.3 wild type (C). Shift of pore helix during the molecular dynamics simulation in the single-point mutant (green circle) (D).

3.3.3 ChTX-hKv1.3 dissociation process

The interaction of ChTX with mKv1.3 wild type was studied during umbrella sampling. Umbrella sampling is a method for the calculation of the free energy landscape. The aim of the umbrella sampling simulation is to predict the macroscopic properties of molecules like ligand-enzyme interactions from its microscopic state and energy barriers by determining the energy landscape. Thus, the ChTX unbinding free energy was also estimated by umbrella sampling following potential mean force (PMF). Keeping ChTX restrain in every 0.5 Å far from the channel surface along Z direction with the harmonic biasing potential in order to reach equilibration state in given distances provide the opportunity to study the behavior of ChTX regarding to channel surface in more detail. Docked ChTX-mKv1.3 channel was run for 4 ns in order to reach equilibrium state. The root mean squared deviation (RMSD) of less than 1 Å during the 4ns equilibration simulation that followed the docking shows that there is no significant conformational change or induced fit in the structure of mKv1.3 or ChTX (Figure 3.11).

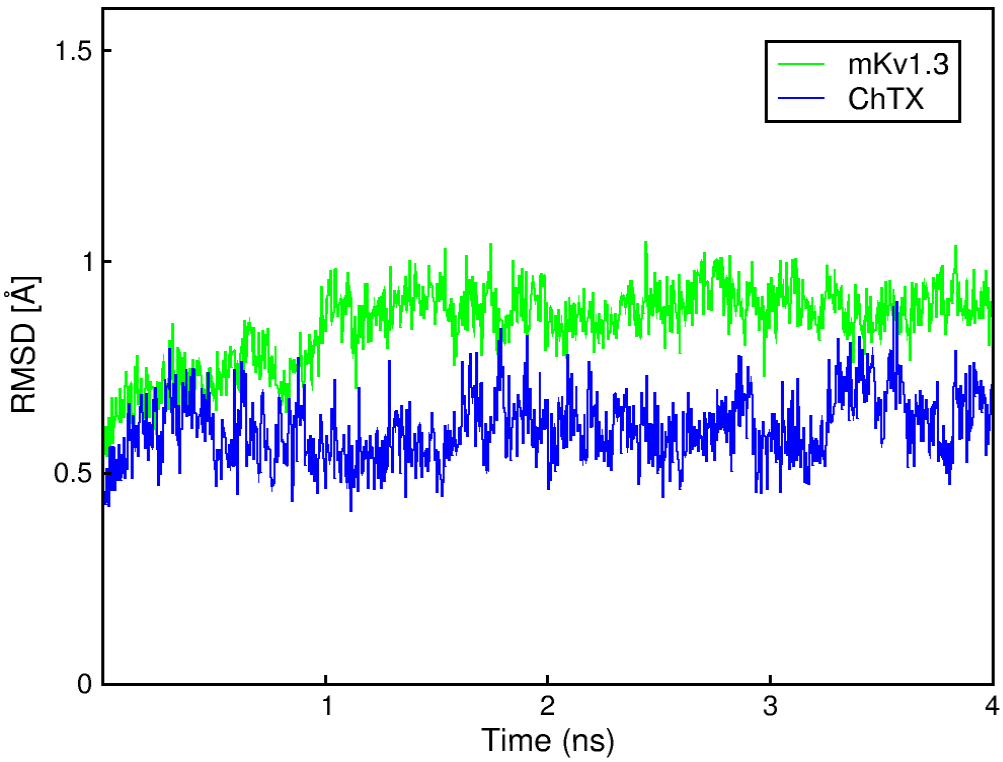

Figure 3.11. Root mean square deviation of ChTX and mKv1.3 channel in complex conformation.

The last snapshot from the equilibration simulation of docked ChTX-mKv1.3 was used as an initial conformation for the next simulation, which was run in order to investigate the unbinding process and to be able to perform free energy calculations. Two sets of directed molecular dynamics (MD) simulations was run using low molar and high molar KCl in the solvent to explore additionally the effect of KCl ions. The minimium distance of center of mass of each ChTX residue was measures to determine the contact amino acids between ChTX and mKv1.3. In general, 15 residues are located in a distance as close as 2 Å from the channel (Figure 3.12). Among them, residues Q18 and S24 don't have any particaularly strong interaction with the channel. The reason for them being close to the channel is their vicinity to the interaction residues nearby. Residues H21 and N22 were not reported as interaction residues in ChTX-Kv channels interaction, in previous studies. The other 13 residue are potentially interacting and are shown in table 3.1.

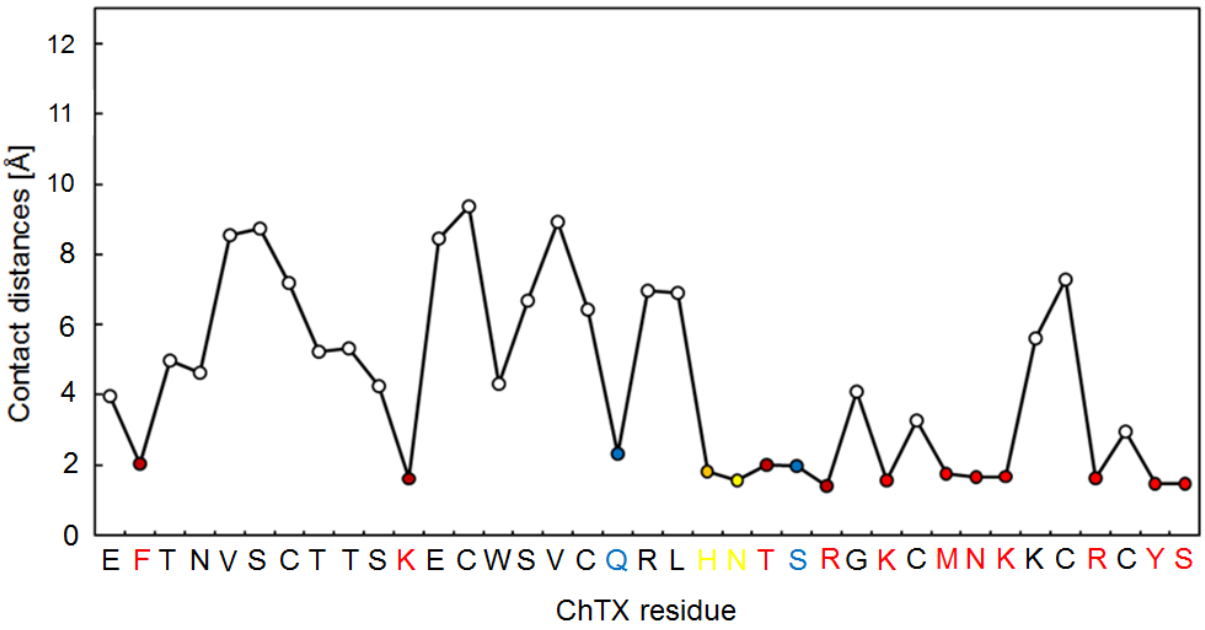

Figure 3.12. Average distances of ChTX residues to the channel in the ChTX-mKv1.3 complex. The measured distances are the average minimum distances between the center of mass of each individual toxin residue and the channel in the first window of umbrella sampling. Residues without a specific interaction but close to the channel surface are shown in blue, residues having specific interactions in our simulations (newly reported interaction points) are shown in yellow, and residues having specific interactions in our simulations and available experimental data are shown in red.

ChTX	F2	K11	H21	N22	T23	R25	K27	M29	N30	K31	R34	Y36	S37
mKv1.3	S378(A)	S379(D)	G380(D)	P377(B)	G380(C)	D402,D386 (A)	Y400 (A,B,C,D)	H404 (D)	S378(D)	D402 (D)	S378 (A)	D386(C)	K411(A)

Table 3.1: Major interactions between pairs of amino acid residues of ChTX and mKv1.3 while ChTX is blocking the channel

The MD simulation of ChTX unbinding process in the presence of K^+ ions show that the potassium ions, due to the negatively charged surface of the Kv1.3 channel, gradually start to take the place of ChTX on the channel during the unbinding process, eventually covering the channel surface (Figure 3.13). The figure shows that while ChTX is getting farther from the channel's surface, the number of potassium ions on the surface is increasing. Figure 3.14 shows the position of of K^+ and Cl^- ions on the surface of the channel after the completion during unbinding process. Since the channel surface close to the pore region consists mainly of negatively charged amino acids, potassium ions were strongly attracted to this part of the surface of the channel. Analysis of the distribution of K^+ around the selectivity filter indicated

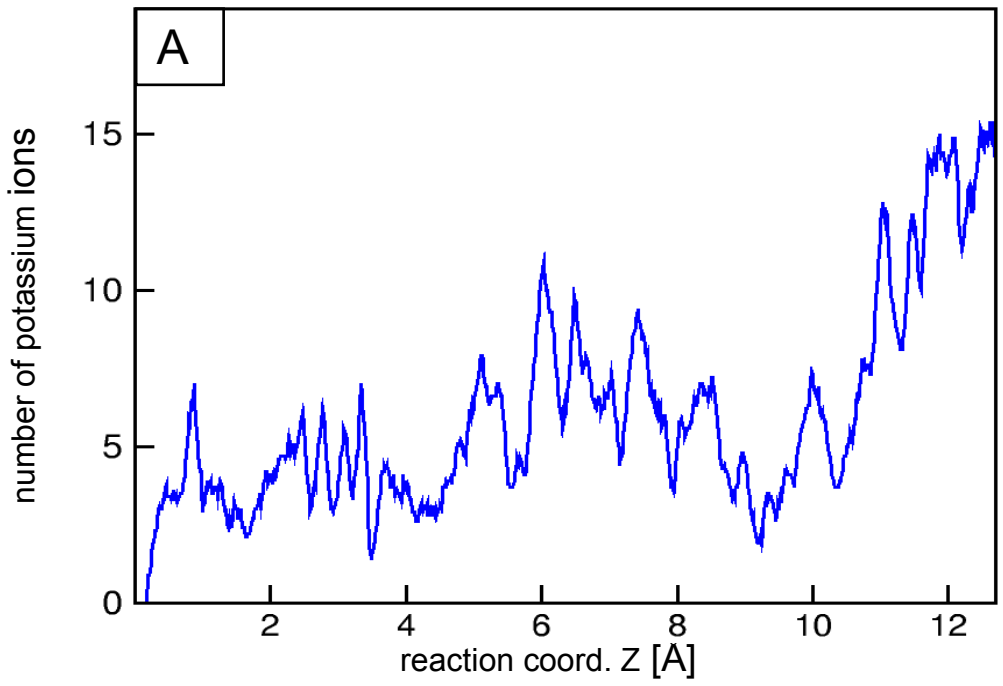

Figure 3.13. Number of potassium ions in a proximity of less than 10 Å from the channel during the unbinding process.

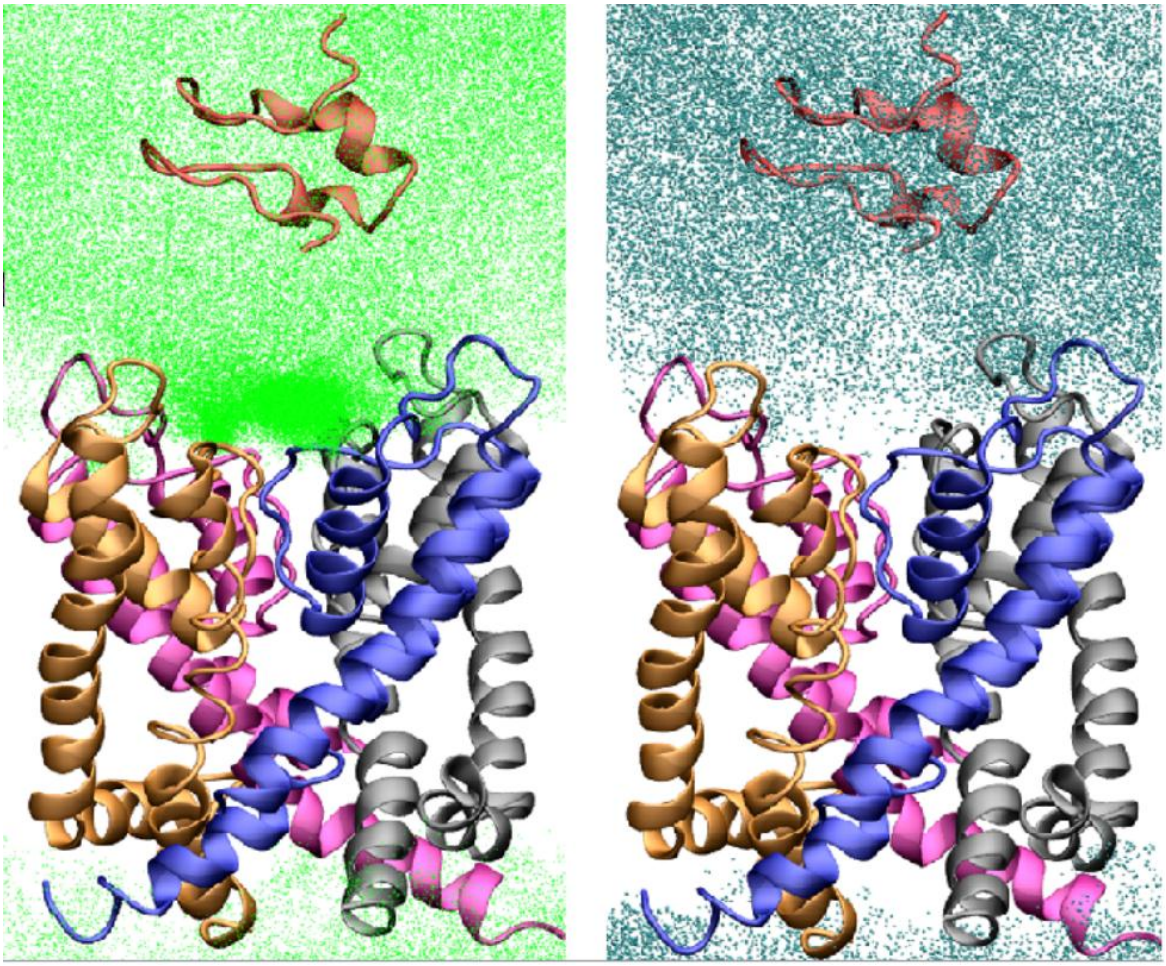

Figure 3.14. Positions of K^+ ions and Cl^- ions in the unbinding process for high K^+ concentration. All positions that either K^+ ions (left, green) and Cl^- ions (right, cyan) were in during the whole simulation from all umbrellas are shown. Both ChTX and channel geometries are taken from the last snapshot of the last umbrella sampling window. For clarity, S4 helices are not shown.

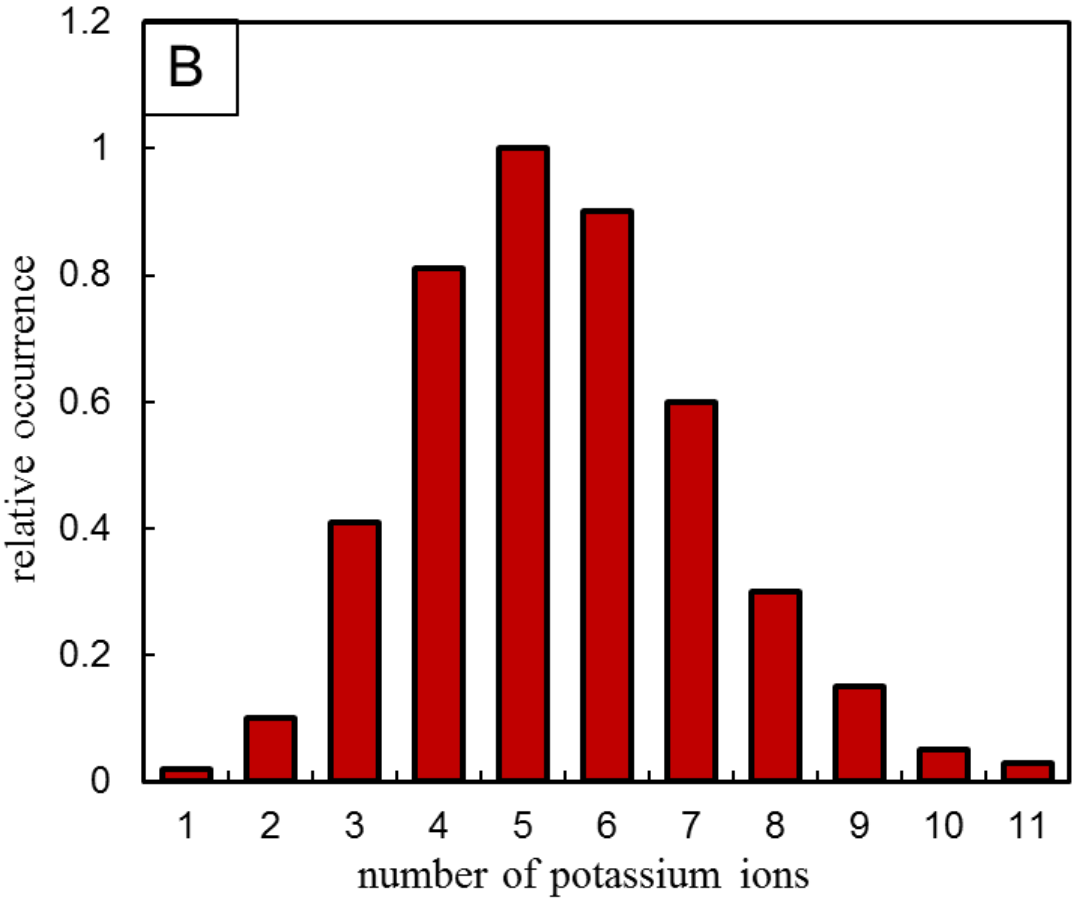

Figure 3.15. The relative occurrence of potassium ions after unbinding of ChTX in a distance of less than 3.5 Å from the the selectivity filter defined by Y400, G401, D402, M403, H404, and P405 pore region amino acids. In the histogram the relative numbers of K^+ within the 3.5 Å distance are shown. The relative occurrence values are normalized in order to get a unit value for the most probable number of K^+. The histogram shows, on average, five ions in surface contact with the selectivity filter (B).

that there are on average 5 potassium ions closer than 3.5Å to the surface of the selectivity filter (Figure 3.15). So far, the general aspects of the unbinding process of ChTX from mKv1.3 were considered. To identify the influence of potassium ions on the ChTX–mKv1.3 complex, we performed free energy calculations on the system using the potential mean force (PMF) method. Interestingly, the results showed no difference between the total unbinding energy of ChTX in water versus the unbinding energy in KCl solution (Figure 3.16). The total free energy curves calculated with the PMF method for both solutions are in good agreement at large distances; however, the PMF curves exhibit a slightly different behaviors when the toxin is still close to the channel surface at a distance of 1-5 Å with the toxin actually loosing

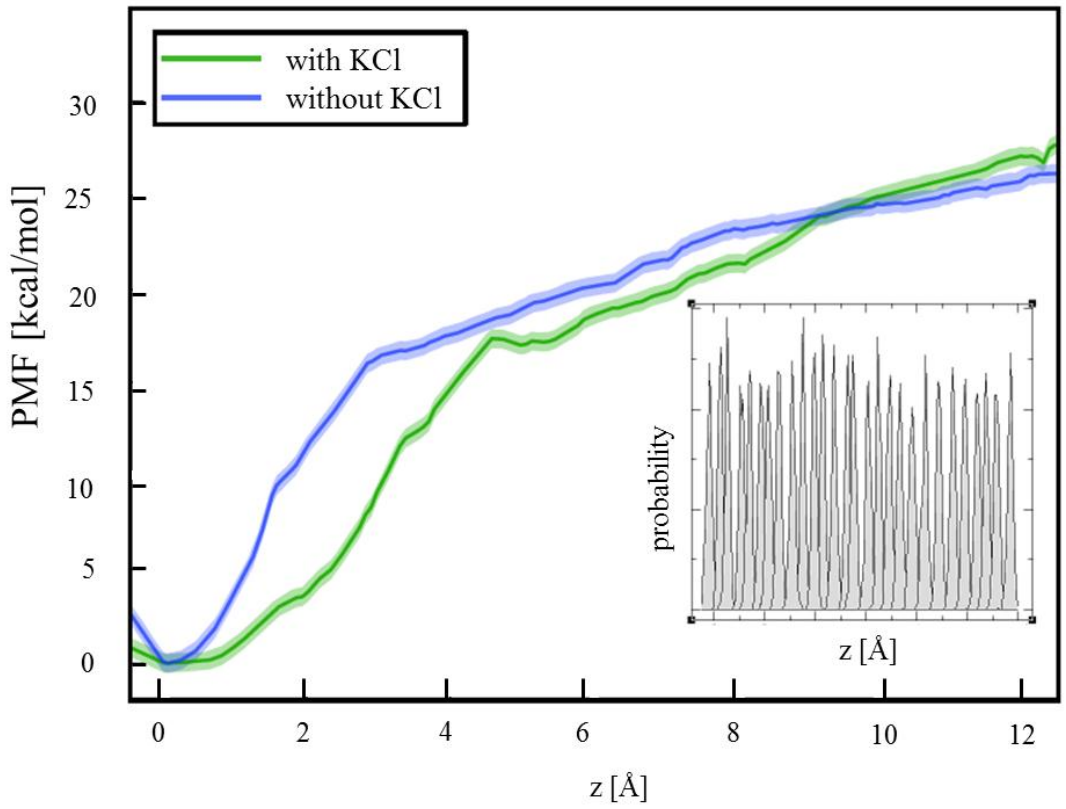

Figure 3.16. Comparison of the PMFs obtained from the umbrella sampling simulations of ChTX-mKv1.3 in high and low molar KCl using the force constants of 50 kcal/mol/Å^2. Overlapping between the individual umbrella sampling histograms is depicted in the inset for the high molar KCl system, and is qualitatively similar for low molar KCl). By considering the error bars, free energy values in both cases are the same.

the electrostatic interactions between K27-Y400 and R25-D386**.** At this short distances unbinding is influenced by the presence of ions, as the potassium ions compete with the toxin for the negative charge of the carboxyl group of the aspartic acid and the carbonyl group of the tyrosine backbone. Figure 3.16 shows the channel and toxin complex after 4 ns of equilibration in the first window of umbrella sampling. ChTX-K27 extends into the selectivity filter and has an electrostatic interaction with the cabonyl group of Y400 in all monomers. The guanidium group of ChTX-R25 bridges over D386 and D402. In addition, ChTX-K11 has an electrostatic contact with the carbonyl group of S379. Inbetween both sidechains, R25 and K11, there is kept the aromatic ring of ChTX-W14 like in a sandwich, constraining the ChTX to a particular structural conformation. MD simulations of ChTX unbinding during umbrella sampling show that CTX does not lose all of its interactions with Kv1.3

simultaneously. ChTX still keeps interactions with residues K11, N22, R25 while other contacts are becoming detached. These three amino acids act as a hinge during unbinding process, which makes ChTX unbinding resemble the opening of the lid of a pitcher. Figure 3.17 shows the conformation of ChTX when ChTX-R25 loses its interaction with both aspartic acid residues. The guanidium group of ChTX-R25 flips into a horizontal conformation with respect to the channel surface and makes a hydrophobic interaction with the methyl group of V369 and a new interaction with H404. Following these changes, the only direct contacts left are hydrophobic interactions of ChTX with the channel. Once all short-range electrostatic interactions have been disappeared, ChTX unbinding happens rapidly. This process is influenced by the presence of potassium ions. RDF of potassium ions around the carbonyl oxygen group of P379 and D402 and the carboxylic group of D386 (Figure 3.18) show that the potassium ions are attracted by S379, D402 and D386 in the channel, replacing residues R25 and K11 of ChTX, when the ChTX-channel interactions are already weakened by the larger distance (Figure 3.19).

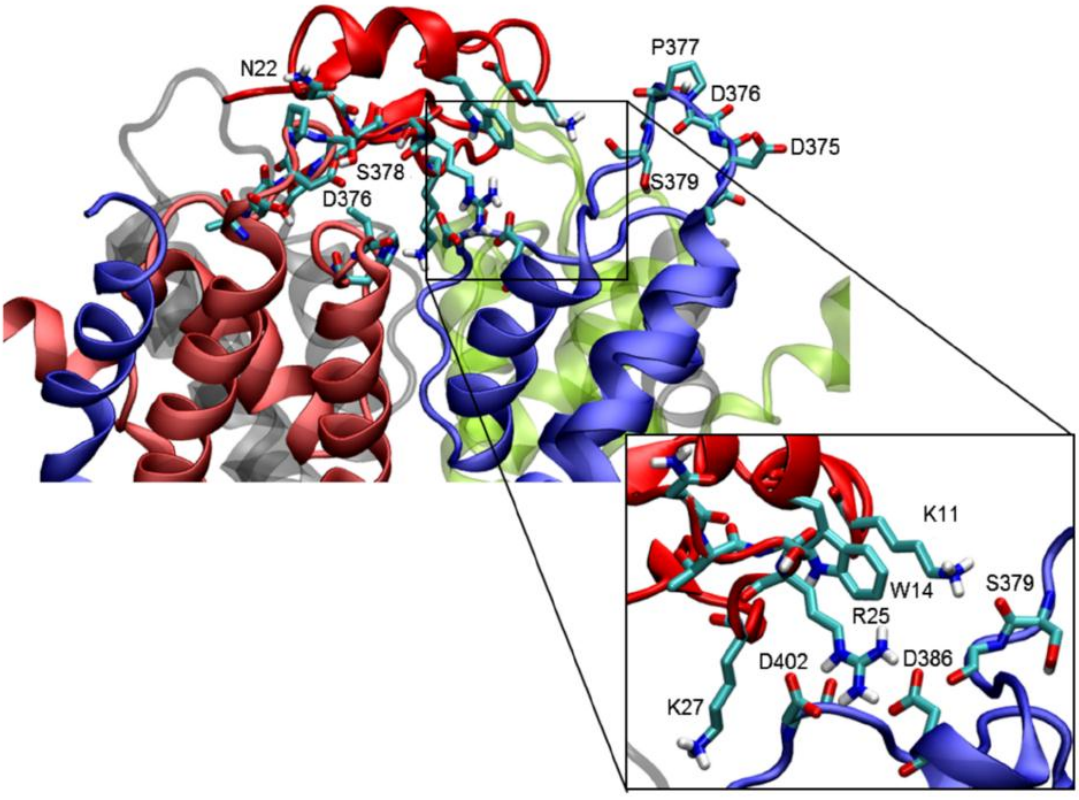

Figure 3.17. Key interactions between ChTX and Kv1.3. The magnified cubic box highlightens the electrostatic interaction of R25 with D386 and D402 and of K11 with S379.

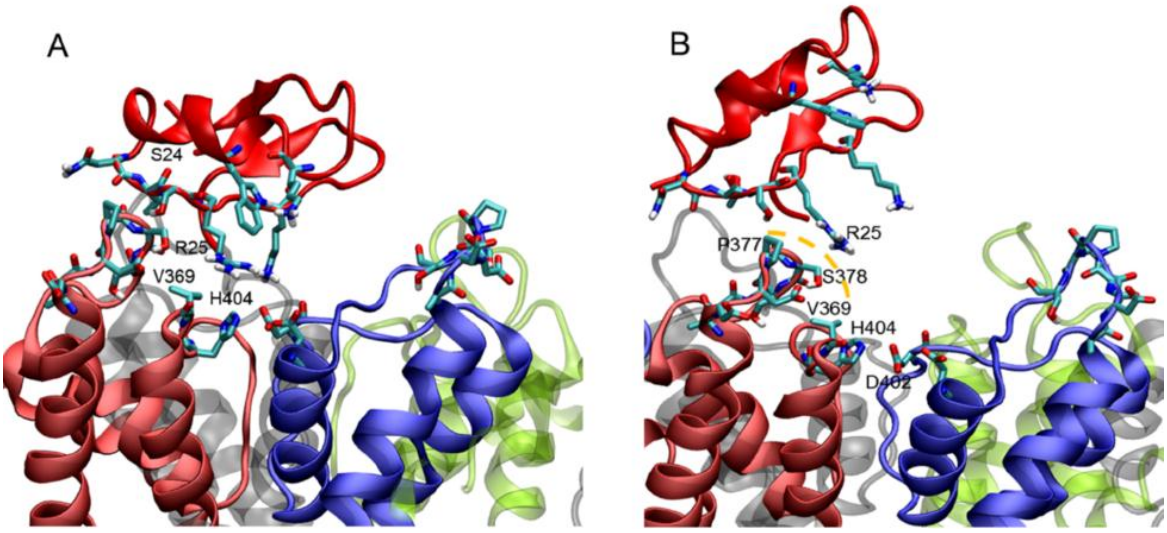

Figure 3.18. ChTX after the loss of short-range electrostatic interaction with the channel. Only hydrophobic interactions are left (A). The hydrophobic patch (yellow dash line) which is created by V369, S378 and P377 (B).

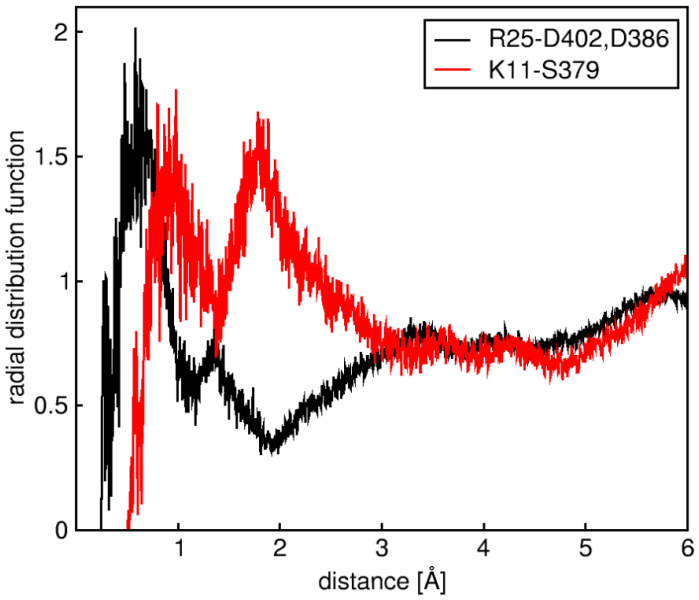

Figure 3.19. Radial distribution functions of K^+ when the toxin is bound to the channel. The RDF is measured around D402 and D386, which are interacting with R25, and around the Ser379 carbonyl oxygen group when interacting with K11. Hereby, the rdf was measured while the ChTX-mKv1.3 complex was solvated by water and ions in the high K^+ concentration in the bulk KCl solution and data were taken from the second umbrella (reaction coordinate 0.5 Å) to monitor the situation when the ChTX-channel interactions are already weakened by the slightly larger distance.

3.3.4 Discussion

The effect of point mutations at positions 388 and 399 in the hKv1.3 structure and their possible effect on the ChTX interaction were investigated by molecular dynamics simulations. Introducing the mutation at position 388 shows that the SF region is becoming more flexible, with larger root mean square fluctuations. The increased flexibility of the selectivity filter is due to the disruption of the network right ”behind' the selectivity filter. This network includes Val388, Trp384, Asp397 from one monomer (for example monomer A) and H399 from the adjacent monomer (then monomer D, if we pick up the example above). The lack of the Val388 methyl group in the hKv1.3_V388C mutant, where the valine is replaced with cysteine, destabilizes the Trp384 indole group, which then finally leads to a loss of the interaction between indole amide group with the Asp397 carboxyl group. Parallel to the observed conformational change of the Trp384 indole group, the Asp397 side change reorients into the bulk solution in all four monomers resulting in a more negative Kv1.3 surface in this region. Interestingly, the introduction of the second mutation at position 399 (histidine to threonine) prevents the structural changes seen in the single mutations, and the channel structure is kept close to the wild type structure. Interestingly, experimental cysteine-scanning mutagenesis implicates pore helix residue Val388 in inactivation of the hKv1.3 channel, enabling partial reactivation by scorpion toxin in whole-cell patch clamp recordings, thus confirming that SF flexibility is directly linked to channel functioning. The second-site mutation His399Thr just beyond the selectivity filter reverts the Val388Cys mutant to a wild type-like inactivation profile in these experiments. Our molecular dynamics simulations thus reveal that Val388, but not Cys388, locks the Trp384 side chain in a conformation compatible with hydrogen bonding to Asp397 of the selectivity filter. This constraint reflects the fact that beta-branched side chains are confined to a single rotamer when the backbone is in helical conformation.

On the other hand, although residue 399 is not in a helical segment, beta-branched Thr399 but not His399 is constrained by steric crowding with the adjacent Pro400, limiting Asp397 to a conformation that enforces its hydrogen bonding with Trp384. These results suggest that the inherent steric limitations of beta-branched residues, which are paradoxically abundant in the transmembrane helical segments of many proteins, play an important role in channel properties.

The comparison of the RMSF between Kv1.3 wild type and mutants shows this stabilizing effect clearly. Additionally, ChTX can be used as a probe to verify our hypothesis, as the peptide toxins prevents the inactivation in the V388C single-mutant channel. In wilde-type ChTX would block the channel, while in the single mutant the orientation of Asp397 creates a hindrance for ChTX when its close enough to block the channel, thus forcing ChTX to sit in a higher position than in wild type, causing a certain tilting of ChTX to one side of the channel. The tilted toxin cannot block the channel completely and is leaving the pore partially open. However, the interactions of the toxin with the channel lead to lower root mean square fluctuations of the selectivity filter, stabilizing the pore in a similar way as the beta-branched residues, and thus partially reactivate the otherwise dead mutant channel. The flexibility and dynamics of the selectivity filter seems to be an important modulator of the channel function, and beta-branched residues are one way the channel assures the “right” dynamics.

In addition to mutation effect, ChTX, binding free energy and the unbinding process of ChTX from the mKv1.3 voltage gated potassium channel was investigated in the absence and presence of external potassium ions. Free energy calculations performed using the PMF method found no difference in free energy of the complex in a solution with low versus high salt concentrations. However, the shape of the free energy curve obtained from PMF calculations shows that there is a difference in the unbinding behavior when comparing low and high ion concentration at a distance of 1-5 Å from the surface of selectivity filter. Considering that the potassium ions occupy the pore region when ChTX is

unbinding, their presence perturbed the ChTX unbinding process by establishing a network of interactions inbetween the ChTX and channel surfaces. However, if error is taken into account for both theoretical and experimental calculations, then the binding free energies found from PMF calculations and experimental measurements in presence and absence of potassium ions are the same. We can conclude that while the presence of potassium ions might have a critical role in the diffusional step of the binding process, however, it does not have an influence on specific binding and the binding free energy.

References:

- Alberts B, Bray D, Lewis J, Raff M, Roberts K, and Watson JD. (1996) Molecular Biology of the Cell Garland Publishing, New York NY.
- Aiyar J, Rizzi JP, Gutman GA, and Chandy KG, (1996) The signature sequence of voltage-gated potassium channels projects into the external vestibule. J Biol Chem, 271:31013–31016.
- Aiyar J, Withka JM, Rizzi JP, Singleton DH, Andrews GC, Lin W, Boyd J, Hanson DC, Simon M, Dethlefs B, Lee C, Hall JE, Gutman GA and Chandy, KG. (1995) Topology of the pore region of a K+ channel revealed by the NMR-derived structures of scorpion toxins. Neuron, 15:1169-1181.
- Aggarwal SK and Mackinnon R. (1996) Contribution of the S4 segment to gating charge in the Shaker K^+ channel. Neuron 16:1169–1177.
- Bernèche S, and Roux B. (2003) A microscopic view of ion conduction through the K+ channel. Proc. Natl. Acad. Sci. USA. 100:8644–8648.
- Bezanilla F. (2000) The voltage sensor in voltage dependent ion channels. Physiol. Rev. 80, 555-592.
- Burg ED, Remillard CV, and Yuan JX. (2006) K+ Channels in Apoptosis. J. Membr. Biol. 209: 3–20.
- Bauer CK, Schwartz JR. (2001) Physiology of EAG K+ channels. J.Membr. Biol. 182: 1–5.
- Bezanilla F (2000) The Voltage Sensor in Voltage-Dependent Ion Channels. Physiol Rev. 80(2):555-592.
- Berendsen HJC, van der Spoel D, and van Drunen R. (1995) GROMACS: A message-passing parallel molecular dynamics implementation. Comp Phys Comm. 91: 43–56.
- Beeton C and Chandy KG (2005) Potassium Channels, Memory T Cells and Multiple Sclerosis. Neuroscientist 11(6):550–562.
- Berger O, Edholm O, Jähnig F. (1997) Molecular dynamics simulations of a fluid bilayer of dipalmitoylphosphatidylcholine at full hydration, constant pressure, and constant temperature. Biophys J. 72(5):2002-13.
- Bruce A.J, Scott P.S, and Joanne M.W. (1994) Determination of the Three-Dimensional Structure of Margatoxin by lH, 13C, 15N Triple-Resonance Nuclear Magnetic Resonance Spectroscopy. Biochemistry, 33:15061–15070.

- Berendsen HJC, Postma JPM, van Gunsteren and Hermans WFJ. (1981) Interaction models for water in relation to protein hydration. In: Intermolecular Forces. Reidel Publishing Company Dordrecht, 331–342.
- Carey J, Benoff B, Harish B, Yuan L, and Lawson CL. (2011) Environment-dependent long-range structural distortion in a temperature-sensitive point mutant, submitted to structure journal
- Capener, C. E., and M. S. P. Sansom. 2002. MD Simulations of a K channel model—sensitivity to changes in ions, waters and membrane environment. J. Phys. Chem. B. 106:4543–4551.
- Choi KL, Aldrich RW, and Yellen G. (1991) Tetraethylammonium blockade distinguishes two inactivation mechanisms in voltage-activatedKC channels. Proc.Natl. Acad. Sci. USA 88:5092–5095.
- Chung SH, Anderson OS, Krishnamurthy VV. (2006) Biological membrane ion channels: dynamics, structure, and applications Springer, 1 edition.
- Chen X, Wang Q, Ni F, Ma J. (2010) Structure of the full-length Shaker potassium channel Kv1.2 by normal-mode-based X-ray crystallographic refinement. Proc Natl Acad Sci U S A. 107(25):11352-7.
- Catterall WA, (1979) Binding of scorpion toxin to receptor sites associated with sodium channels in frog muscle. Correlation of voltage-dependent binding with activation. J. Gen. Physiol, 74:357.
- Catterall WA. (1995) Structure and function of voltage-gated ion channels. Annu Rev Biochem. 64:493-531.
- Choe S. (2002) Potassium channel structures. Nat Rev Neurosci 3:115-121.
- Chandy KG, DeCoursey TE, Cahalan MD, McLaughlin C, and Gupta S (1984) Voltage-gated potassium channels are required for human T lymphocyte activation. J Exp Med 160:369–385.
- Cordero-Morales JF, Cuello LG, Zhao Y, Jogini V, Cortes DM, Roux B, Perozo E (2006) Molecular determinants of gating at the potassium-channel selectivity filter. Nat Struct Mol Biol.13(4):311-318.
- Cordero-Morales J F, Jogini V, Lewis A, Vásquez V, Cortes DM, Roux B , Perozo E (2007) Molecular driving forces determining potassium channel slow inactivation. Nature Structural & Molecular Biology, 14(11):1062–1069.
- Cuello LG, Jogini V, Cortes DM, Perozo E. (2010) Structural mechanism of C-type inactivation in K(+) channels. Nature.466(7303):203-8.
- Cordero-Morales JF, Jogini V, Chakrapani S, Perozo E. (2011) A multipoint hydrogen-bond network underlying KcsA C-type inactivation. Biophys J. 100(10):2387-93.
- Chodera, J.D., Swope,W.C., Pitera, J.W., Seok, C.,Dill, K.A. (2007) Use of the weighted histogram analysis method for the analysis of simulated and parallel tempering simulations, J.Chem.Theo.Comput. 3(1), 26–41.
- Chothia C. (1984) Principles that determine the structure of proteins. *Ann. Rev. Biochem.* 53:537–572.
- DeCoursey TE, Chandy KG, Gupta S, and Cahalan MD (1984) Voltage-gated K channels in human T lymphocytes: a role in mitogenesis? Nature (Lond) 307:465–468.
- Doyle DA, Morais JC, Pfuetzner RA, Kuo A, Gulbis JM, Cohen SL, Chait BT, and MacKinnon R. (1998) The structure of the potassium channel: molecular basis of k+ conduction and selectivity. Science, 280(5360):69–77.

- De Biasi M, Hartman HA, Drewe JA, Taglialatela M, Brown AM, Kirsch GE (1993) Inactivation determined by a single site in K+ pores. Pflugers Archiv 422(4): 354—363.
- Dunbrack RL, and Karplus M. (1993) Backbone-dependent Rotamer Library for Proteins: Application to Side-chain prediction. J. Mol. Biol. 230:543-574.
- Essmann U, Perera L, and Berkowitz ML. (1995) A smooth particle mesh Ewald method. J Chem Phys , 103: 8577-8592.
- Freedman BD, Price M. and Deutsch C. (1992) Evidence for voltage modulation of IL2 production by human blood lymphocytes. J. Immunol, 149:3784–3794.
- Furini S, Domene C. (2009) Atypical mechanism of conduction in potassium channels. Proc Natl Acad Sci U S A. 106(38):16074-7.
- Grissmer S., Nguyen A. N. and Cahalan M. D. (1993): Calciumactivated potassium channels in resting and activated human T lymphocytes. Expression levels, calcium dependence, ion selectivity, and pharmacology. J. Gen. Physiol., 102, 601–630.
- Gutman GA, Chandy KG, Grissmer S, Lazdunski M, McKinnon D, Pardo LA, Robertson GA, Rudy B, Sanguinetti MC, Stuhmer W, Wang X (2005) International Union of Pharmacology. LIII. Nomenclature and molecular relationships of voltage-gated potassium channels. Pharmacol Rev, 57(4):473–508.
- Hamill OP, Marty A, Neher E, Sakmann B, Sigworth FJ, (1981) Improved patch-clamp techniques for high-resolution current recording from cells and cell-free membrane patches. Pflugers Arch. 391(2):85-100.
- Heginbotham L, Lu Z, Abramson T, and MacKinnon R. Mutations in the k+ channel signature sequence. Biophys J, 66(4):1061–1067.
- Hoshi T, Zagotta WN, Aldrich RW (1990) Biophysical and molecular mechanisms of Shaker potassium channel inactivation. Science 250(4980):533-538.
- Hellgren M, Sandberg L, Edholm O. (2005) A comparison between two prokaryotic potassium channels (KirBac1.1 and KcsA) in a molecular dynamics (MD) simulation study. Biophys Chem. 120(1):1-9.
- Hidalgo P, and MacKinnon R. (1995) Revealing the architecture of a Kchannel pore through mutant cycles with a peptide inhibitor. Science, 268: 307–310.
- Hoshi TWN, Zagotta, and Aldrich RW. (1991) Two types of inactivation in Shaker KC channels: Effects of alterations in the carboxy-terminal region. Neuron, 7:547–556.
- Hille B. (1992) Ionic Channels of Excitable Membranes, 2nd edn. Sinauer Associates, Massachusetts.
- Jäger H, Rauer H, Nguyen AN, Aiyar J, Chandy KG, Grissmer S.(1998) Regulation of mammalian Shaker-related K+ channels: evidence for non-conducting closed and non-conducting inactivated states. J Physiol. 506 :291-301.
- Jan LY, Jan YN. (1997) Cloned potassium channels from eukaryotes and prokaryotes. Annu Rev Neurosci. 20:91-123.
- Jensen MØ, Borhani DW, Lindorff-Larsen K, Maragakis P, Jogini V, Eastwood MP, Dror RO, Shaw DE. (2010) Principles of conduction and hydrophobic gating in K+ channels. Proc Natl Acad Sci U S A. 107(13):5833-8.
- Jiang Y, et al. (2003) X-ray structure of a voltage-dependent K+ channel. Nature 423(6935):33–41.
- Jiang Y, Lee A, Chen J, Cadene M, Chait BT, and MacKinnon R. (2002) Crystal structure and mechanism of a calcium-gated potassium channel. Nature, 417(6888):515–522.

- Jorgensen WL, Maxwell DS, and Tirado-Rives J. (1996) Development and Testing of the OPLS All-Atom Force Field on Conformational Energetics and Properties of Organic Liquids. J. Am. Chem. Soc. 118 (45):11225–11236.
- Kandt C, Ash WL, Tieleman DP (2007): Setting Up and Running Membrane Protein Simulations Methods 41(4): 475-488.
- Krieger E, Koraimann G, Vriend G. (2002) Increasing the precision of comparative models with YASARA NOVA--a self-parameterizing force field. Proteins. 47:3:393-402.
- Krieger E, Darden T, Nabuurs SB, Finkelstein A and Vriend G. (2004) Making optimal use of empiral energy functions: force field parameterization in crystal space. PROTEINS: Structure, Function, and Bioinformatics. 57(4):678-683.
- Kuo A, Gulbis JM, Antcli JF, Rahman T, Lowe ED, Zimmer J, Cuthbertson J, Ashcroft FM, Ezaki T, and Doyle DA. (2003) Crystal structure of the potassium channel kirbac1.1 in the closed state. Science, 300(5627):1922–1926.
- Lewis RS, and Cahalan MD. (1988) Subset-specific expression of potassium channels in developing murine T lymphocytes. Science. 239:771–775.
- Lee SY, Banerjee A, MacKinnon R (2009) Two separate interfaces between the voltage sensor and pore are required for the function of voltage-dependent K(+) channels.PLoS Biol 7(3):0676-0686.
- Lindahl E, Hess B, van der Spoel D. (2001) GROMACS 3.0: A package for molecular simulation and trajectory analysis. J Mol Mod. 7:306–317.
- Leonard RJ, Garcia ML, Slaughter RS. and Reuben JP. (1992) Selective blockers of voltage-gated K+ channels depolarize human T lymphocytes: mechanism of the antiproliferative effect of charybdotoxin. Proc. Nat. Acad. Sci. USA, 89:10094–10098.
- Lodish H, Arnold B, Chris A, Kaiser and Monty Krieger. (2007) Molecular Cell Biology, 6th edition, W. H. Freeman.
- López-Barneo J, Hoshi T, Heinemann SH, and Aldrich RW (1993) Effects of external cations and mutations in the pore region on C-type inactivation of Shaker potassium channels. Receptors Channels. 1(1): 61–71.
- Long SB, Tao X, Campbell EB, and MacKinnon R. (2007) Atomic structure of a voltage-dependent k+ channel in a lipid membrane-like environment. Nature, 450(7168):376–382.
- Long SB, Campbell EB, Mackinnon R. (2005) Crystal structure of a mammalian voltage-dependent Shaker family K+ channel. Science, 309(5736):897-903.
- MacKinnon R, Heginbotham L, Abramson T (1990)Mapping the receptor site for charybdotoxin, a pore-blocking potassium channel inhibitor. Neuron 5(6):767-771.
- Morris, G. M., Goodsell, D. S., Halliday, R.S., Huey, R., Hart, W. E., Belew, R. K. and Olson, A. J. (1998), Automated Docking Using a Lamarckian Genetic Algorithm and and Empirical Binding Free Energy Function J. Computational Chemistry, 19: 1639-1662.
- Marrink SJ, Berger O, Tieleman DP, Jahnig F.(1998) Adhesion forces in lipid membranes. Bioph. J.74:931-943.
- Miller C, Moczydlowski E, Latorre R. and Phillips M. (1985) Charybdotoxin, a protein inhibitor of single Ca2+-activated K+ channels from mammalian skeletal muscle. Nature, 313:316–318.
- Nos´e, S., Klein, M. L. (1983) Constant pressure molecular dynamics for molecular systems. Mol. Phys. 50:1055–1076.
- Panyi G, Sheng Z, and Deutsch C, (1995) C-type inactivation of a voltage-gated K_channel occurs by a cooperative mechanism. Biophys J 69(3):896–903.

- Parsegian A. (1969) Energy of an ion crossing a low dielectric membrane:solutions to four relevant electrostatic problems. Nature. 221:844–846.
- Price M, Lee SC, and Deutsch C. (1989) Charybdotoxin inhibits proliferation and interleukin 2 production in human peripheral blood lymphocytes. Proc. Nat. Acad. Sci., USA, 86:10171–10175.
- Parrinello, M., Rahman, A (1981) Polymorphic transitions in single crystals: A new molecular dynamics method. J. Appl. Phys 52:7182–7190.
- Rauer H and Grissmer S, (1999) Effect of deep pore mutations on the action of phenylalkylamines on the Kv1.3 potassium channel. Br J Pharmacol 127(5)1065-1074.
- Rauer H, Lanigan MD, Pennington MW, Aiyar J, Ghanshani S, Cahalan MD, Norton RS, and Chandy KG (2000) Structure-guided transformation of charybdotoxin yields an analog that selectively targets Ca2-activated over voltage-gated K channels. J Biol Chem, 275:1201 1208.
- Ryckaert, J. P., Ciccotti, G., Berendsen, H. J. C. Numerical integration of the Cartesian equations of motion of a system with constraints; molecular dynamics of n-alkanes. J. Comp. Phys. 23:327–341, 1977.
- Sands SB, Lewis RS, and Cahalan MD. (1989) Charybdotoxin blocks voltage-gated K+ channels in human and murine T lymphocytes. J. Gen. Physiol. 93 (6):1061-1074.
- Seoh SA, Sigg D, Papazian DM. and Bezanilla F. (1996) Voltage-sensing residues in the S2 and S4 segments of the Shaker K^+ channel. Neuron 16:1159–1167.
- Schlegel B. (1982) Optimization of equilibrium geometries and transition structures. J. Comput. Chem, 3:214 – 218.
- Sigworth FJ. (1994) Voltage gating of ion channels. Q Rev Biophys, 27(1):1-40.
- Shieh CC, Coghlan M, Sullivan JP, Gopalakrishnan M. (2000) Potassium channels: molecular defects, diseases, and therapeutic opportunities. Pharmacol. Rev. 52(4):557-594.
- Tang DT, Santarelli LC, Heinemann SH, Hoshi T. (2004) Metabolic regulation of potassium channels. Annu. Rev. Physiol. 66: 131–159.
- Tieleman DP, MacCallum JL, **Ash WL**, Kandt C, Xu Z, Monticelli L. (2006) Membrane protein simulations with a united atom lipid and all atom protein model: side chain transfer free energies and model proteins, *J. Phys. Cond. Matt.* 18, S1221-S1234.
- Wonderlin WF, Strobl JS. (1996) Potassium channels, proliferation and G1 progression. J. Membr. Biol. 154:91–107.
- Wulff H, Knaus HG, Pennington M, and Chandy KG (2004) K channel expression during B cell differentiation: implications for immunomodulation and autoimmunity. J Immunol 173:776–786.
- Yu K, Fu W, Liu H, Luo X, Chen KX, Ding J, Shen J, Jiang H. (2004) Computational simulations of interactions of scorpion toxins with the voltage-gated potassium ion channel. Biophys J. 86(6):3542-55.
- Yu F, Yarov-Yarovoy V, Gutman GA, Catterall WA (2005) Overview of Molecular Relationships in the Voltage-Gated Ion Channel Superfamily.Pharmacol Rev, 57(4): 387–395.
- Yellen G (2002) The voltage-gated potassium channels and their relatives.Nature 419 (6902):35-42.
- Zagotta WN, Hoshi T, Aldrich RW (1990) Restoration of inactivation in mutants of Shaker potassium channels by a peptide derived from ShB. Science 250(4980):568–571.

– Zhou Y, Morais-Cabral JH, Kaufman A, and MacKinnon R. (2001) Chemistry of ion coordination and hydration revealed by a k+ channel-fab complex at 2.0 a resolution. Nature, 414(6859):43–48.